KU LEUVEN

FACULTY OF SCIENCE

FACULTY OF SCIENCES

GHENT UNIVERSITY

Early Weichselian paleoclimate reconstruction using geochemical methods on the Gibraltar speleothem from the Père Noël cave (Belgium)

Jef DECUYPERE

Supervisor: Prof. Dr. Philippe Claeys
Vrije Universiteit Brussel

Mentor: Stef Vansteenberge
Vrije Universiteit Brussel

Thesis presented in fulfillment of the requirements for the degree of Master of Science in Geology (Ghent – Leuven)

Academic year 2016-2017

PREFACE

From watching nature documentaries on National Geographic when I was little, to starting with my studies in geology, nature and the workings of our planet have always fascinated me. Our planet looks simple at the surface, but looks can be deceiving and the complexity of all processes and feedbacks which have created living conditions for such a wide variety of species, including our own, is simply mind-boggling. One topic which has always triggered my curiosity is climate change. Humans play an important role in the present-day climate change, but even before humans inhabited this planet, it underwent several drastic climatic changes. Understanding why natural climate change occurs and how it influences the different processes in the atmosphere, biosphere, cryosphere, hydrosphere and geosphere, is essential to predict future climatic change and protect the species living on this planet.

This is the reason why I was incredibly happy to have the opportunity to work on a topic about paleoclimatic change. This thesis proposes a paleoclimatic reconstruction of the early Weichselian climate in Belgium and is at this point the first Belgian continental record for this specific timeframe. On the following pages the used methodology and results are discussed, but first I would like to express my gratitude towards a number of people.

In the first place, I would like to thank my promoter, Prof. Dr. Philippe Claeys, head of the Analytical, Environmental and Geochemistry (AMGC) research unit at the Vrije Universiteit Brussel (VUB) for giving me the chance of working on a subject which really sparked my interest. Although, coming to another university to work on a thesis is no obviousness, he welcomed me with open arms, gave me confidence and always believed in me, even at the more difficult times. Secondly my mentor Stef Vansteenberge deserves a special word of gratitude. Without his help, especially with the construction of the age model and measurements of the stable isotope and trace elements, this thesis could not have been made.

I would also like to thank the very friendly people working at the AMGC unit: Prof. Steven Goderis for his time and help with the trace element measurements, but also Dr. Christophe Snoeck, Dr. Koen Stein, Matthias Sinnesael and Niels de Winter, for helping me find my way around the lab and answering my questions.

Finally, I would like to thank my parents, brother and sister. Not only for proofreading this thesis, but also for their everlasting patience, encouragement and support.

Jef Decuypere – Moorslede – June 2017

ABSTRACT

A paleoclimatic reconstruction of the continental early Weichselian climate in Belgium is proposed in this thesis. For this reconstruction, a core (PNG-01) was drilled the Gibraltar speleothem from the Père Noël cave. This cave is part of the karstic system of Han-sur-Lesse, situated in the southern part of Belgium. The PNG-01 core was first morphologically described and scanned before U/Th ages were derived from 13 samples. These ages allowed for the construction of an age-depth model and based on this model, growth rate variation of the speleothem was estimated over time. Using a tungsten carbide drill bit, 197 samples were collected along the growth axis of the speleothem and analysed for their oxygen and carbon isotopic signature using IRMS. Of these 197 samples, 94 samples were analysed with HR-ICP-MS to obtain trace element records for Sr, Ba, Mg, U, Zn, Pb, Y and Ca.

Based on the different proxies retrieved from the PNG-01 speleothem, the following interpretations are proposed. The PNG-01 speleothem formed between around 103,6 and 93,8 ka, combined with the total length of the speleothem (1015 mm), this results in average growth rate of around 0,104 mm/year. A good positive correlation between the oxygen and carbon isotope records and changes in the Sr/Ca and Mg/Ca-ratios points towards the presence of kinetic fractionation processes influencing the records, most likely prior calcite precipitation (PCP). The chance of PCP increases when residence times are higher for example during drier climates. In this speleothem, both the stable isotope and trace element records unfortunately not completely reflect changes in paleotemperature, but rather correspond with changes in water excess or effective precipitation.

The PNG-01 proxies point towards, at least in comparison with today, a relatively warm and wet climate with continuous speleothem deposition. At the start of speleothem formation (± 103,6 ka) and between around 100 and 97 ka, the climate was distinctly wetter than in the other section of the speleothem. The younger section of the speleothem shows signs of a climate gradually becoming drier. The start and end of speleothem formation can potentially be linked with the transition from Greenland Stadial 22 towards Greenland Interstadial 23 and the transition from Greenland Interstadial 23 towards Greenland Stadial 23 respectively. However, more research is necessary to confirm the different hypotheses proposed in this thesis.

ABBREVIATIONS

AMGC	Analytical, environmental and geochemistry research unit
BP	Before present
Dft	Distance from top
ELSA	Eifel laminated sediment archive
GI	Greenland interstadial
GS	Greenland stadial
HR-ICP-MS	High resolution inductively coupled plasma mass spectrometry
IRMS	Isotope ratio mass spectrometry
ka	kilo annum (1000 years)
MIS	Marine isotopic stage
NALPS	Northern European Alps stalagmite chronology
NGRIP	North Greenland ice core project
PCP	Prior calcite precipitation
PNG-01	The core from the Gibraltar speleothem studied in this thesis
U/Th	Uranium-thorium (dating)
VPDB	Vienna Pee Dee Belemnite
VUB	Vrije Universiteit Brussel

TABLE OF CONTENTS

1 INTRODUCTION

It is almost impossible to unfold the paper, watch television or casually browse the internet without coming across a reference to a topic which has, already today, an influence on the daily lives of almost all species on this planet. No, this is not a reference to recent elections in the United States, but to climate change. However, in the scientific world there is consensus that climate change is real (IPCC, 2013). In order to protect not only our own specie from the potential dangers connected to a global increase in temperature, understanding the mechanisms behind climate change is crucial. Scientific research covers many aspects of climate change. Geologists have a specific interest in how climate has changed throughout the history of our planet. Therefore, they use a multitude of different proxies that record the signals of ancient climatic change. Ice core and marine records are well known, but more recently also cave deposits, speleothems, are more and more studied as paleo-archive.

Speleothems are valuable climate archives because they can, like ice core and some pollen records, be independently dated and because they contain different proxies. Speleothem morphology, variation in growth rate of the calcite layers, stable isotope signals and trace element variations throughout its formation all highlight different aspects of climate change occurring at the surface above the cave. Another important benefit of speleothems is that they form on the continent, where the availability of paleoclimatic archives is, aside from pollen and lake records, rather limited.

This thesis studies the PNG-01 speleothem collected from the Père Noël cave, which is part of the Han-sur-Lesse karstic system, situated in the southern part of Belgium. This specific speleothem grew probably almost continuously during the early Weichselian from around 103,6 to 93,8 ka, a timeframe that correlates with the warmer Greenland Interstadial 23 described in the NGRIP ice core record (NGRIP Members, 2004) and is equivalent with Marine Isotopic Stage 5c in the marine record (Shackleton, 1976). It is a period dominated by relative stable climatic conditions and a slow but gradual cooling trend towards Greenland Stadial 23 (see chapter 2.4). For this time-frame no other Belgium speleothem records have already been studied.

“Did the continental climate in Belgium during the early Weichselian experience similar climatic change as observed in other paleoclimatic proxies (e.g. NGRIP, NALPS and ELSA; discussed in section 2.4)?”

This is the main question this thesis proposes to answer. In other words, what can, but equally as important, cannot be learnt from the different paleoclimatic proxies stored in the PNG-01 speleothem archive. Did the PNG-01 stalagmite precipitate in isotopic equilibrium? Are the stable isotope and trace element signals mainly controlled by temperature or by effective precipitation? How do the results of this study compare with other research? These are three other important questions discussed throughout this thesis.

This thesis starts with a state-of-the-art in the use of speleothems as paleoclimatic archives (chapter 2). Stable isotopes measurements form the basis of all speleothem research, therefore a short overview of what stable isotopes are and how they are influenced by processes like fractionation, forms the first topic of this chapter. Secondly an overview is given of what speleothems are, where they can be found and how they can be used as paleoclimatic archives. The location of the Père Noël cave and its geological history is the next topic of this section and finally, an overview of the early Weichselian climate concludes this chapter.

Chapter 3 highlights all the methods used to study the PNG-01 speleothem, the results of this work are discussed in chapter 4. First the speleothem had to be dated, which made it possible to construct an age-depth model, secondly growth rate variation was assessed, and finally samples were analysed for their stable isotope signal and trace element concentrations. Chapter 5 concludes this thesis and tries to answer the main research question of this study.

2 STATE-OF-THE-ART OF SPELEOTHEM RESEARCH

Before discussing the methods used to reveal the different proxies stored inside the PNG-01 speleothem, it is important to have an idea about the current state-of-the-art of speleothem research. What are speleothems? Where can they be found? Which type of proxies are stored inside a speleothem and how can these be used to reconstruct paleoclimatic change? Where was the PNG-01 speleothem deposited? What can we learn from other proxies about the climate during the formation of the PNG-01 speleothem? These are only some of the questions answered in this chapter, but first the general concepts of stable isotope geochemistry are discussed.

2.1 STABLE ISOTOPES

(after Hoefs, 2015)

2.1.1 Introduction

In this section, some basic concepts of stable isotopes and stable isotope geochemistry are discussed. The focus will be on the stable isotopes of carbon and oxygen, as these are the most commonly used proxies used in speleothem paleoclimate reconstructions.

2.1.2 Isotopes

Everything in our world, every solid, liquid, gas or plasma, is made of atoms. These small building blocks consist of protons carrying a positive charge, electrons carrying a negative charge and neutrons carrying no charge at all. Protons and neutrons make up the nucleus and the electrons are bound to this nucleus (see figure 1). The number of protons in an atom is unique for every chemical element and defines the atom number Z, which equals the number of electrons in case of a neutral atom. Protons and neutrons make up the majority of mass in an atom, which explains why the mass number A is defined as the sum of the number of protons and neutrons (A=Z+N). Each specific element X can be described as a combination of an atom number Z and a mass number A.

$$^{A}_{Z}X$$

Isotopes are atoms with the same number of protons (Z), which inherently means that they are the same chemical element, but with a different number of neutrons and thus

a different mass (A). The number of neutrons is A-Z. The term isotope originates from the Greek roots 'isos' (equal) and 'topos' (place), referring to the fact that all isotopes of a specific element can be found on the same place in the periodic table.

For example, carbon-12 or ^{12}C, the most common isotope of carbon, has 6 protons and 6 neutrons. The atomic number subscript is often omitted because the chemical element already defines the atomic number or the number of protons. This also implies that the carbon-13 isotope has a larger mass due to the presence of an extra neutron.

The atomic mass and abundance of all isotopes of a specific chemical element defines the relative atomic mass of that element. Finally, the term nuclide refers to all atoms with the same number of protons (Z) and neutrons (A-Z), which implies that nuclides of one element are isotopes.

2.1.3 Stable isotopes

Isotopes can be stable or unstable (experiencing radioactive decay), however the term stable is deceiving because radioactive decay also occurs in stable isotopes, but the rate of this decay is so small that it is almost impossible to measure. Stability of the nuclides depends on the neutron-to-proton ratio N/Z. For nuclides with a low atomic number, this ratio is close to 1, but in nuclei with a larger number of protons the electrostatic Coulomb repulsion of the protons increases rapidly, which means that more neutrons need to be incorporated in the nucleus to maintain stability. Consequently, the N/Z-ratio for stable nuclides deviates away from 1 with increasing atomic number and reaches a maximum value of around 1,5 for the heaviest known stable nuclei. Aside from the N/Z-ratio, nuclides with an even number of protons are also more abundant than those with odd numbers.

Some elements, for instance beryllium and phosphorus, only have one stable isotope and are therefore referred to as pure elements. Yet, most elements in the periodic table have at least two isotopes. In lighter elements, such as oxygen and carbon, one isotope is predominant and the others are only present in trace amounts. Stable isotopes of an element are therefore present in varying abundances (see table 1). The three different isotopes of carbon are visualised in figure 1.

Stable isotope concentrations are commonly represented with the isotope ratio R, which is the ratio of the second most common isotope of a certain element over the most abundant one. For example, the ^{18}O concentration of a sample is represented by

the $^{18}O/^{16}O$-ratio and the ^{13}C concentration by the $^{13}C/^{12}C$-ratio. In the end, it is the variation in these two specific ratios that form the scientific foundation for the paleoclimatic reconstructions conducted in this thesis. In practice, absolute isotopic ratios are avoided and isotopic ratios are expressed as a relative change with respect to an internationally accepted standard. This expression results in values that are more manageable and these so called δ-values are expressed in per mille (‰).

$$\text{For example, } \delta^{13}C = \frac{\left(\frac{^{13}C}{^{12}C}\right)_{sample} - \left(\frac{^{13}C}{^{12}C}\right)_{standard}}{\left(\frac{^{13}C}{^{12}C}\right)_{standard}} * 10^3 \text{ ‰}$$

In paleoclimate studies, the international standard for $\delta^{18}O$ and $\delta^{13}C$ values is the PDB standard (Pee Dee Belemnite). However, this standard is exhausted now and the currently used standard is NBS19 expressed as Vienna PDB (Friedman et al., 1982).

A positive δ-value indicates that the sample is enriched in the heavier isotope (e.g. ^{18}O) with respect to the standard. In contrast, a negative δ-value means that the sample is depleted in the heavier isotope with respect to the standard. In other words, in the second case the sample has a 'lighter' signature than the standard.

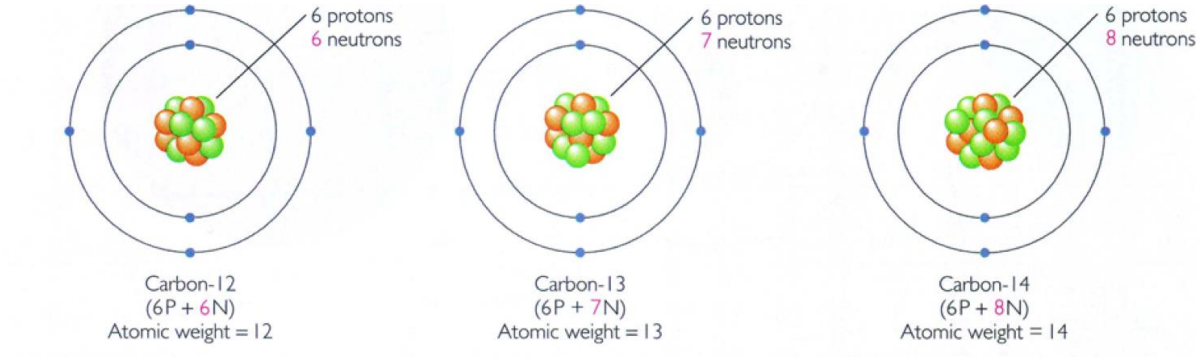

Figure 1 - The different isotopes of carbon (Scienceblogs, 2017)

Element	Isotope	Average natural abundances (%)
carbon	^{12}C	99,8952
	^{13}C	0,0148
	^{14}C	Negligible ($T_{1/2}$ = 12,26 a)
oxygen	^{16}O	99,757
	$^{17}0$	0,038
	^{18}O	0,205

Table 1 – Average natural abundances of carbon and oxygen isotopes (Hoefs, 2015)

2.1.4 Fractionation

Mass variations between isotopes result in differences in their physical and chemical properties. These differences are called 'isotope effects' and can lead to a preferential separation of an element's stable isotopes during physical (e.g. evaporation) or chemical processes (e.g. calcite precipitation). This separation is better known as 'isotope fractionation'.

During isotope fractionation, isotopes are partitioned between two substances (or two phases of the same substance) with different isotope ratios. Isotopic fractionation between substances A and B is quantified using the (unitless) fractionation factor alpha (α):

$$\alpha = \frac{R_A}{R_B}$$

with R_A the stable isotope ratio of substance A and R_B the stable isotope ratio of substance B. The isotope effects mentioned above are the result of quantum mechanical effects. Firstly, because the kinetic energy of a molecule (see equation below) only depends on its temperature, isotopes have the same kinetic energy at a certain temperature.

$$kT = \frac{mv^2}{2} = E_{kin\ molecule}$$

with k = the Boltzmann constant, T = absolute temperature, m = molecular mass and v = average velocity of the molecule. However, if their kinetic energy is the same, isotopes with a higher mass will move at a lower velocity. This decreases the chance of 'bumping' into other molecules and makes heavy isotopes less reactive than lighter isotopes of the same element.

Secondly, molecules with heavier isotopes form stronger bonds than molecules containing lighter isotopes. This can be explained as follows. The distance between two atoms forming a molecule depends on both the gravitational attraction and the electrostatic repelling forces and defines the potential energy of a diatomic molecule (see figure 2). The energy of a such a molecule is restricted to certain discrete energy levels. The lowest of these energy levels is not the minimum of the curve visible on the figure, but is situated right above it with an amount of 1/2 hv, with h the Planck's constant and v the vibrating frequency of the atoms in the molecule. This implies that

even at a temperature of absolute zero, the molecule contains a certain 'zero-point energy'. This zero-point energy depends on the vibration frequency of the atoms in the molecule. In its turn, this vibrating frequency is inversely correlated with the mass of the isotopes, or in other words, the heavier the isotope, the lower the zero-point energy of the molecule formed with this isotope.

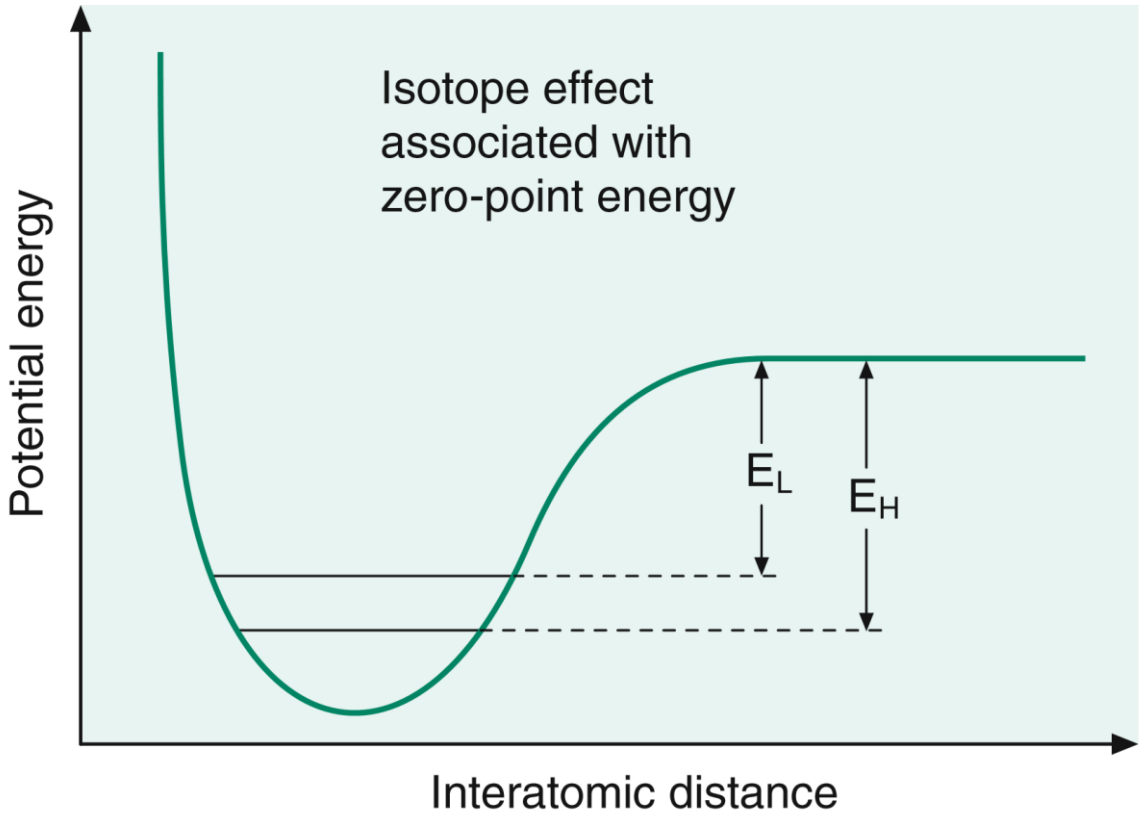

Figure 2 – Potential energy curve for the interaction of two atoms in a stable molecule (Hoefs, 2015)

In figure 2, the 'dissociation' energy of a light (EL) and a heavy (EH) molecule is indicated. This dissociation energy is an energy interval between the zero-point energy level and the 'continuous' level. The figure illustrates that molecules with heavier isotopes, and lower zero-point energies, have a higher dissociation energy than those composed out of lighter isotopes. This means that the bounds formed by heavy isotopes are stronger and require more energy to break than the ones formed by lighter isotopes.

To conclude, at a certain temperature, heavy isotopes are, in comparison with light isotopes, less reactive and the bounds formed within a molecule by these heavier isotopes require more energy to break.

2.1.4.1 Fractionation processes

The two most important processes causing fractionation of stable isotopes are isotope exchange reactions (*equilibrium fractionation*) and kinetic processes (*kinetic fractionation*).

2.1.4.1.1 Equilibrium fractionation

During an isotope exchange reaction, only the isotope distribution changes between different substances, phases or individual molecules, meaning that no net reaction takes place. Isotope exchange reactions are reversible reactions and in fact a special case of chemical equilibrium. Often the fractionation factor α is used to describe these types of reactions instead of the equilibrium factor K. In an exchange reaction where only one atom is exchanged, K equals α. An example of such an exchange reaction that is crucial in the geochemistry of cave environments is the exchange of ^{18}O and ^{16}O between cave waters and freshly precipitated speleothem $CaCO_3$. When $\alpha > 0$, $\delta^{18}O$ of $CaCO_3$ is enriched compared to the cave water. In contrast, when $\alpha < 0$, $\delta^{18}O$ of $CaCO_3$ is depleted with respect to the cave water.

$$H_2{}^{18}O + \frac{1}{3}CaC^{16}O_3 \leftrightarrow H_2{}^{16}O + \frac{1}{3}CaC^{18}O_3$$

The value of the fractionation factor α depends on physical and chemical parameters such as temperature, pressure, chemical composition and crystal structure. In the case of oxygen, the effect of temperature on α is however the most important (Kendall & McDonnell, 1998).

2.1.4.1.2 Kinetic fractionation

Kinetic fractionation occurs during kinetic reactions, which are, unlike equilibrium reactions, irreversible and unidirectional reactions. Examples of kinetic reactions are evaporation and diffusion. Kinetic reactions tend to result in depleted stable isotope ratios because of the faster reaction rates of lighter isotopes. This is in contrast with equilibrium reactions, which can produce products that have enriched or depleted stable isotope ratios.

For example, large pCO_2 gradients between the dripwater and the cave atmosphere can trigger fast degassing of CO_2 and may result in an enrichment in ^{18}O-signature of speleothems (Lachniet, 2009). Other processes influencing the stable isotope signatures of speleothems are discussed in the following section.

2.2 SPELEOTHEMS

2.2.1 Introduction

Speleothems or cave deposits such as stalactites, stalagmites and flowstones are crystalline deposits, which are formed in a solution cave after the creation of the cave itself. They are mostly composed of calcium carbonate ($CaCO_3$) that originates from the surrounding limestone rocks, which are dissolved by percolating groundwater. When this water, saturated in calcite, reaches the cave, CO_2 is released and this reduces the capacity of the groundwater to contain calcite in solution. This drives calcite deposition and speleothem formation. The growth rate of speleothems depends on a multitude of factors like the flowrate or the CO_2-content and can ultimately be used as a proxy for climate (Van Rampelbergh, 2014), one of the main objectives of this thesis. This section will briefly explain the main processes controlling the formation speed, the stable isotope and trace elemental signature of speleothems. But first, a short overview of karst and karstic regions in Belgium is presented here because the existence of karst defines where speleothems can be found.

2.2.2 Karst

Karst landscapes are the result of the excavating effects of underground water on soluble limestone and develop all around the globe where limestones and dolomites crop out and where sufficient water for dissolution weathering is available (Frisia and Borsato, 2010). The name originally refers to a limestone dominated region in Slovenia, but is now commonly used to indicate all regions with similar features. Key for karst development is the presence of a dense well jointed limestone situated close to the surface, a humid climate with intense rainfall and good circulation of groundwater. Slightly acidic rainwater can percolate through these joints and cracks, making them gradually wider due to dissolution of the limestone until finally the cave systems and underground streams typical for karst regions are developed (Van Rampelbergh, 2014). Karst regions also play an important role in the carbon cycle because dissolution and precipitation of carbonates in karst regions transports carbon from the surface to the subsurface zone. This carbon flux is controlled by the amount of water and the CO_2-concentration, dissolution is positively correlated with both of these parameters and subsequently depends on changes in temperature, rainfall and vegetation cover (Frisia and Borsato, 2010).

2.2.2.1 Karst development

Meteoric water containing CO_2 dissolves surface and shallow subsurface carbonate rocks. These dissolved carbonates provide the bulk of the material for the speleothem deposits found in caves. The subsurface can be divided in different zones based on their saturation level, the unsaturated vadose zone on top and the saturated phreatic zone below the water table. The vadose zone itself consists of the soil, the epikarst zone and the transmission zone, in the vadose zone most ions are mobilized, transported and again precipitated. The soil provides the bulk of the CO_2 necessary for the carbonate dissolution, but for example in arid regions a soil can be absent and then all CO_2 originates directly from the atmosphere. The epikarst zone right below the soil reaches depths up to 30 m and can store large volumes of water due to the presence of a high secondary porosity. Most of the flow in the epikarst is horizontal, this is in contrast with the transmission zone below where less water is stored and the dominant flow direction is vertical. In other regions, the water table forms the boundary between the unsaturated vadose and saturated phreatic zone. In karstic regions, the situation is more complicated: a new fluctuating zone characterised by intermittent flooding in which properties of both the vadose and phreatic zones is defined the epiphreatic zone. This intermediate zone is where most cave developments occur and its level is ultimately controlled by sea-level. Finally, the endokarst zone is the deepest zone of the karstic system situated in the solid limestone rocks (Frisia and Borsato, 2010; Grimes, 1999; Williams, 2008). An overview of these different zones in karstic regions and their dominant flow direction is given on figure 3.

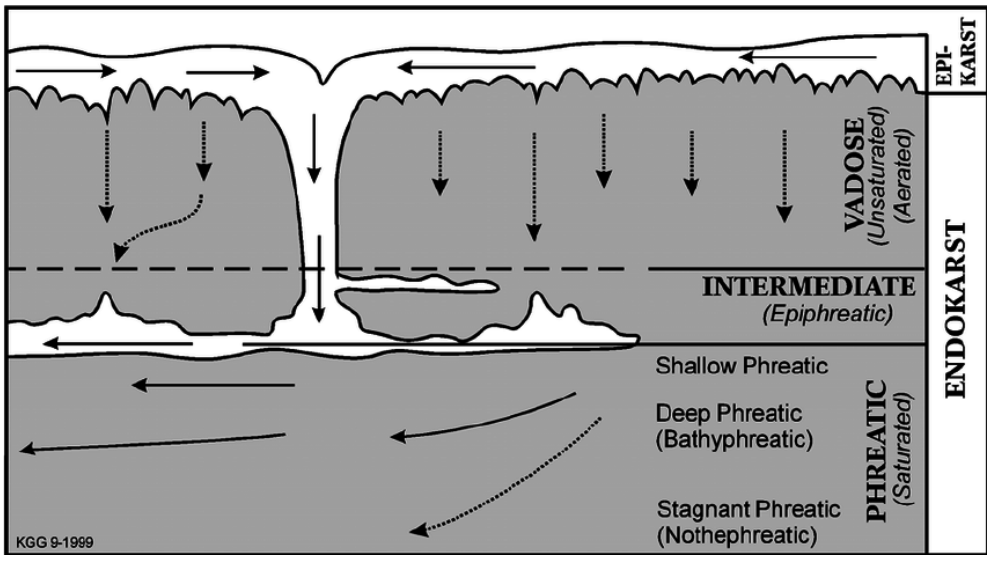

Figure 3 - Hydrological zones and flow directions in a typical karst system (Grimes, 1999)

Carbonate dissolution in the epikarst is possible due to the **dissolution of CO_2** in the meteoric water, which forms carbonic acid and then further dissociates and releases two protons according to the following three reactions:

$$CO_{2\,(g)} + H_2O_{(l)} \leftrightarrow H_2CO_{3\,(aq)} \ (\mathbf{1})$$

$$H_2CO_{3\,(aq)} \leftrightarrow HCO^-_{3\,(aq)} + H^+_{(aq)} \ (\mathbf{2})$$

$$HCO^-_{3\,(aq)} \leftrightarrow CO^{2-}_{3\,(aq)} + H^+_{(aq)} \ (\mathbf{3})$$

Because the dissociation constant of the second equation is higher than for the third reaction, the bicarbonate ion is the dominant carbonate ion and the largest contributor of H^+ in karstic waters. An increase of H^+ ions decreases pH levels, because pH is defined as the negative logarithm of the H^+ ion concentration. Dissolution of CO_2 in water increases at lower temperatures, this explains why karst dissolution is also possible in colder climates and at high altitudes where soils can be absent. Of course, presence of soils is preferred for karst dissolution because vegetation captures CO_2 from the atmosphere (photosynthesis) and then release a large part of that CO_2 back in the soil when no sunlight is available (respiration). Root activity of plants increases when temperatures rise which leads to more acidic soil waters when temperatures are higher. This implies that at mid-latitudes the amount of CO_2 in the soil will show a strong seasonal pattern, high CO_2-concentrations in warmer periods (up to 10 000 ppm) and much lower values in colder periods (about 1000 ppm). Higher availability of soil CO_2 during warmer temperatures has a larger effect than the decrease of CO_2 solubility at increasing temperatures (Frisia and Borsato, 2010).

Carbonate dissolution in karstic regions is described by the following two equations:

$$CaCO_{3\,(s)} + CO_{2\,(g)} + H_2O_{(l)} \leftrightarrow Ca^{2+}_{(aq)} + 2HCO^-_{3\,(aq)} \ (\mathbf{4})$$

$$CaCO_{3\,(s)} + HCO^-_{3\,(aq)} + H^+_{(aq)} \leftrightarrow Ca^{2+}_{(aq)} + 2HCO^-_{3\,(aq)} \ (\mathbf{5})$$

At 25°C, the solubility of calcite ranges from 10 to 50 mg/l depending on the amount of CO_2 present in the soil. Looking at equation 5, it should be clear that dissolutions of calcite consumes H^+ and thus increases the pH values (Frisia and Borsato, 2010).

After dissolution of calcite, water with dissolved calcite is transported downwards and when this water reaches a cavity, **reprecipitation of calcite** occurs according to the

following reaction, which is in fact the inverse reaction of the carbonate dissolution reaction (reaction 4):

$$Ca^{2+}_{(aq)} + 2HCO^{-}_{3\,(aq)} \leftrightarrow CaCO_{3\,(s)} + CO_{2\,(g)} + H_2O_{(l)} \quad (\mathbf{6})$$

Karstic water should be above the saturation value for calcite for this reaction to take place. However, to initiate calcite deposition nucleation should first occur, which is mostly triggered by an increase in supersaturation of the karstic water with respect to calcite. Supersaturation in the karstic water can be reached by outgassing of CO_2, which moves reaction 6 to the right. This also underlines the importance of the partial pressure of CO_2 in the cave where the calcite is precipitated, the lower this partial pressure the more favourable the conditions for calcite precipitation (Fairchild et al., 2006; Frisia and Borsato, 2010).

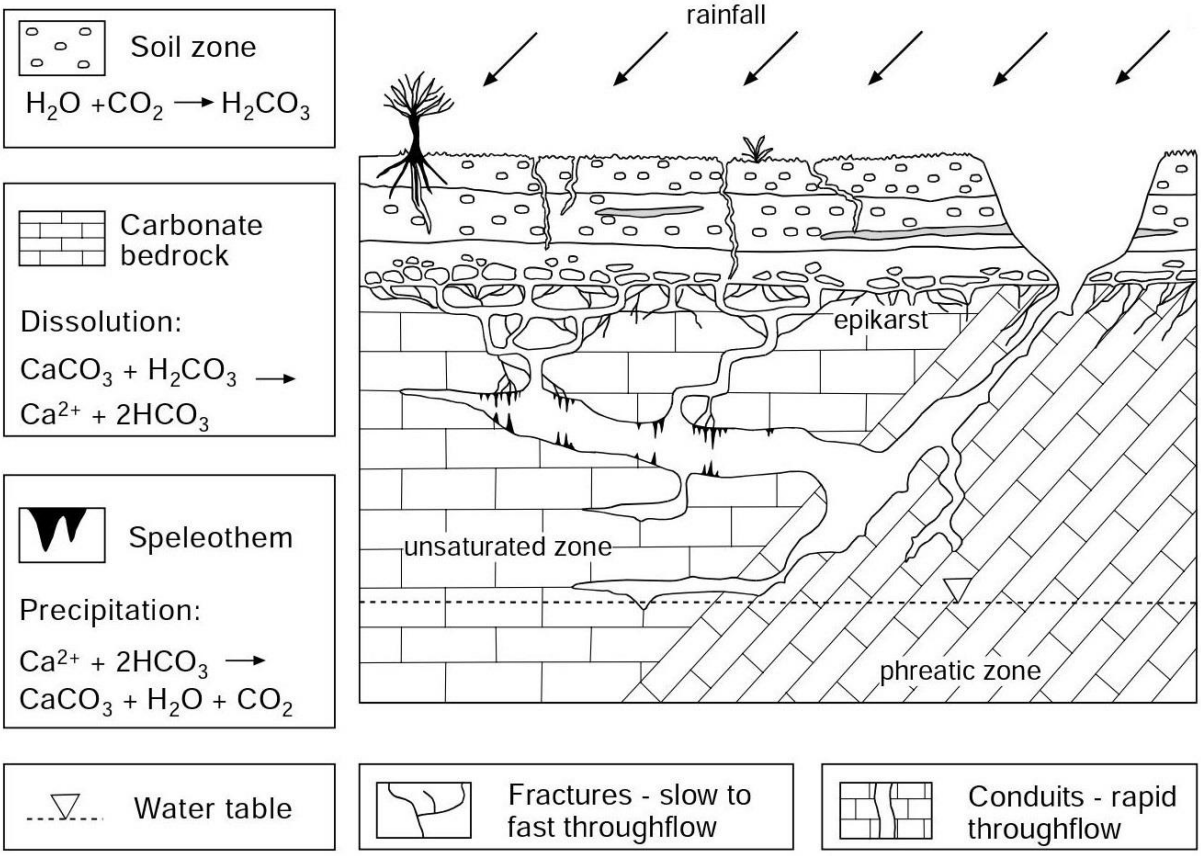

Figure 4 – An overview of the karst development process and the import reactions involved (Fairchild et al., 2006)

Figure 4 gives a schematic overview of the different steps in karst development; first meteoric water is enriched with CO_2 from the atmosphere and the soil lowering the pH of the water, this is then followed by a dissolution of carbonate rocks and transport of karstic water enriched in these carbonates and finally calcite precipitation in the cave

triggered by CO_2 outgassing. All these steps will influence growth rate of speleothems. The longer water resides in the epikarst, the higher the concentration of dissolved calcite and the faster a state of supersaturation will be reached. Speleothem growth rate will also increase with increasing discharge. Finally, a higher difference in partial CO_2 pressure between the drip water and the air of the cave will result in faster CO_2 degassing and subsequently also faster speleothem growth. In cool and temperate climates speleothem growth rates vary between 10 and 100 µm per year, however growth rates of up to 2 mm are no exception (Fairchild et al., 2006; Frisia and Borsato, 2010; Genty and Quinif, 1996). In the end, the deposited calcite layer forming the speleothem reflects the geochemical composition of the meteoric water, the soil and the overlying limestone host-rock.

2.2.2.2 Karst in Belgium

Approximately 10% of the Belgian surface is covered in carbonate rocks and almost all of these carbonate rocks are situated in the southern part of Belgium. Limestones in which karst could develop are mainly of Devonian or Carboniferous age. The presence of E-W oriented limestone bands intercalated with non-carbonate rocks can be explained by the geologic history of the area, where a tectonic pulse coming from the south folded the area during the Variscan orogeny (see also the part on the tectonic history of Belgium and the Ardennes region). The karst in Belgium is a typical *'karst barré*' or in other words a 'blocked karst'. This refers to the fact that non-carbonate rock layers can obstruct the flow towards deeper limestone layers. The most well-known caves of Belgium all developed in a specific Givetian limestone band, which runs 150 km, from west to east, across the southern part of Belgium, the 'Calestienne' (see also figure 8). The Han-sur-Lesse cave system and consequently also the Père Noël cave, are both part of this specific limestone band (Verheyden & Delaby, 2012; Verheyden, 2014).

2.2.3 Speleothems

Speleothems or cave deposits form in karstic regions and exist in many shapes and sizes, but the most used forms for paleoclimatic research are stalagmites, stalactites and flowstones. The main differences between these forms are that stalactites hang on the roof of the cave, while stalagmites are fed by a single drip and grow upwards from the cave floor. Flowstones finally are fed by several drips or a spring and can be

found in the inner passages of a cave (Frisia and Borsato, 2010). The studied PNG-01 speleothem is a stalagmite, so the of this section will be on stalagmites.

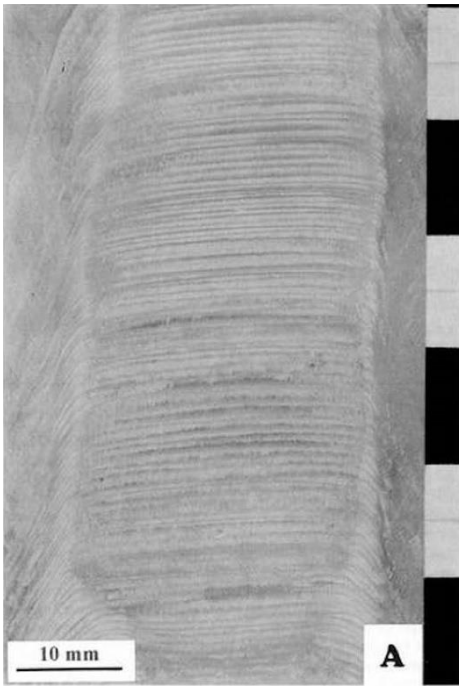

Figure 5 - PNst4-speleothem from the Père Noël cave with clear alternations between dark-compact and the white more porous laminae (Genty and Quinif, 1996)

Stalagmite morphology can vary, from cylindrical to more conical forms (Fairchild et al., 2006), but maybe more important is the control of climate on the stalagmite morphology. For example, drip rate, which is related to rainfall, has a strong influence on the stalagmite diameter, in wetter periods the stalagmite diameter increases. The growth axis of a stalagmite is perpendicular to the substrate and often laminations can be observed in stalagmites, which are interpreted to reflect changes in drip water composition. For example, Genty and Quinif (1996) described the PNst4-speleothem (figure 5) of the Père Noël cave and interpreted the fine couplets of dark compact calcite and white more porous calcite as the result of seasonal variation in supersaturation and drip rate. This illustrates why stalagmites have an excellent potential as paleoclimatic archives (Fairchild et al., 2006; Frisia and Borsato, 2010).

2.2.4 Dating of speleothems

The possibility of accurate and precise dating of speleothems and thus the ability to construct an independent chronology is one of the reasons why speleothems are studied more and more as paleoclimatic archives in recent years. Annual layer counting, radiometric and radiocarbon dating are the most used speleothem dating

techniques. Layer counting techniques are straightforward and inexpensive, but hiatuses in the speleothem growth could go unnoticed and the often-false assumption is made that the speleothem grew until the present day. Radiometric dating techniques overcome these problems as they provide scientists with absolute ages. The most common radiometric dating technique relies on the uranium-thorium disequilibrium series (U/Th) and is also the technique used in this thesis research (Fairchild and Baker, 2012).

For U/Th-dating, small amounts of speleothem material are collected at specific intervals along the growth axis and these samples are then analysed with multi-collector inductively coupled plasma mass-spectrometry (MC-ICPMS). The U/Th-dating method is based on the principle that during speleothem formation, small amounts of uranium from the aqueous solution are incorporated in the carbonate while the insoluble thorium can only be incorporated in the non-carbonate phases of the speleothem. After the deposition of a calcite layer, ^{234}U starts to decay to ^{230}Th. The half-life of this decay is around 245 000 years and speleothems with ages of up to 500 000 can be dated with this technique. Analytical precision of 100 years or less was achieved for samples of more than 120 000 years old. However, when samples contain original detrital thorium (^{232}Th), corrections are necessary and the errors on the ages increase significantly. Finally, radiocarbon dating can be used for younger samples, but the relevance of this technique is limited by the amount of dead carbon incorporated during growth (Cheng et al., 2009; Fairchild et al., 2006: Fairchild and Baker, 2012). This method is not applicable to the PNG-01 speleothem.

Radiometric dates are expensive, so commonly only a limited number of growth layers are dated with this technique. In a next step, an age model is constructed, which defines an age for every distance along the growth axis of the speleothem. Age models can be linear, but nature is often more complex and differences in growth speed and the possible presence of hiatuses and age-inversions need to be taken into account when constructing an age model (Fairchild and Baker, 2012). More on the specifics of the construction of an age model can be found in section 4.3, which discusses the age model obtained for the PNG-01 stalagmite.

2.2.5 Speleothems as paleoclimatic proxies

Speleothems contain different proxies for paleoclimate (figure 6), examples are growth rate, Mg concentration and maybe more importantly the $\delta^{18}O$ and the $\delta^{13}C$ signatures. Changes in these proxies over time can be used to reconstruct environmental or climatic change. However, because these signals are generated or influenced by processes in the atmosphere, soil, epikarst, and also during and after speleothem formation(diagenesis), these reconstructions are not always straightforward. In other words, understanding the contribution of all these processes and how they can influence the final signals measured in the speleothem is essential to understand what the measured values really represent. Stable isotopes are the most used proxies in speleothems, but trace elements like Mg or Sr provide valuable extra information on what processes influenced the stable isotope signals. Finally, the time-scale of change also plays a major role in the interpretation, annual-scale changes can be controlled by completely different processes then changes on a millennial scale.

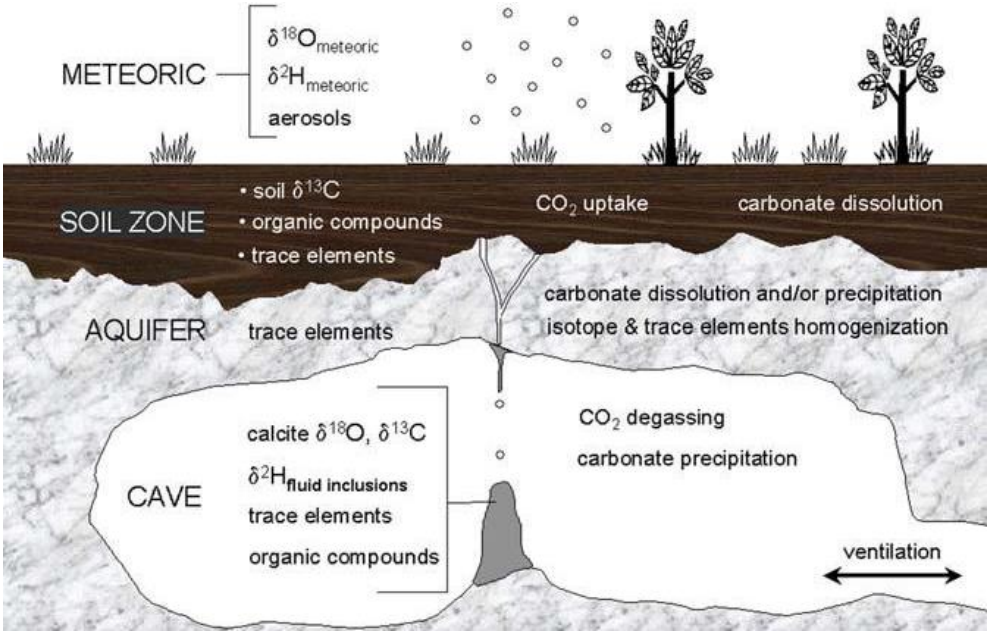

Figure 6 – An overview of the most important proxy records in speleothems (Frisia and Borsato, 2010)

2.2.5.1 Stable isotopes

The ratio of oxygen and carbon isotopes in the speleothems are mostly a reflection of processes happening in the soil ($\delta^{13}C$) and atmospheric change ($\delta^{18}O$). A multitude of processes influences the variability of these isotopic signals. In this section, a summary of these processes is given for both the carbon and oxygen stable isotopes.

2.2.5.1.1 Carbon isotopes

In theory, the $\delta^{13}C$ signal observed in speleothems reflects the $\delta^{13}C$ value of the dissolved inorganic carbon (DIC) in the drip water responsible for speleothem formation. However, this is only the case when the drip water to calcite fractionation occurred in isotopic equilibrium. Kinetic fractionation can significantly alter this signal and needs to be assessed before the $\delta^{13}C$ signal is interpreted. Changes in the $\delta^{13}C$ signal of DIC can be explained by climate-driven vegetation shifts at the surface between C3 and C4-type vegetation. The C3-type vegetation like trees and temperate grasses will respire CO_2 in the soil with a lighter signature (between around -26 and -20‰) than C4-type vegetation like grasses found in drier climates (typical values are in the range of -16 and -10‰) because C4-plants use a different pathway for carbonate fixation. If speleothems are formed in equilibrium with the respired CO_2, expected $\delta^{13}C$ values of the calcite range between -14 to -6‰ for C3 and between -6 and +2‰ for C4 vegetation. However, the lack of natural C4 vegetation in temperate regions makes the interpretation of the carbon isotope signal in these regions difficult. Furthermore, aside from kinetic fractionation other processes can influence the $\delta^{13}C$ signal. For example, incomplete equilibration between the CO_2 in the soil and the percolating water can result in higher than expected $\delta^{13}C$ values. If that is the case, higher $\delta^{13}C$ values correspond with wetter periods because the time for contact between water and the soil is shorter. Also, prior degassing of CO_2 in the vadose zone above the cave causing deposition of calcite (prior calcite precipitation or PCP) can result in elevated $\delta^{13}C$ values. Genty et al. (2003) also observed higher $\delta^{13}C$ values during the colder late glacial period compared to the Holocene values. They attributed this difference to the fact that during colder periods the production of CO_2 in the soil (generating carbon with a light signature) can be limited or almost zero, implying that the relative importance of atmospheric (heavy) carbon increased and the $\delta^{13}C$ signature became higher. Trace elements like Sr, Ba and Mg (see section 2.2.5.2) can possibly be used to rule-out some of these processes and try to determine the dominant process influencing the $\delta^{13}C$ value (Baker et al., 1997; Fairchild et al., 2006; Frisia and Borsato, 2010; McDermott, 2004).

2.2.5.1.2 Oxygen isotopes

Assuming isotopic equilibrium, the $\delta^{18}O$ signal reflects the $\delta^{18}O$ of the drip waters and subsequently also the $\delta^{18}O$ of the precipitation at the surface (in semi-arid and arid

regions the $\delta^{18}O$ signal is mainly controlled by changes in evaporation of the meteoric water prior to infiltration). The present-day variation in the $\delta^{18}O$ signal of precipitation is generally quite well understood and depends on a multitude of factors or 'effects' like latitude, altitude, air temperature, distance from the sea (continentality effect) and the amount of precipitation (see figure 7). Problem is that not many speleothems are deposited in perfect isotopic equilibrium which implies that the $\delta^{18}O$ signal is altered and not exactly represents the meteoric $\delta^{18}O$ signal. If $\delta^{18}O$ is constant along a growth line while $\delta^{13}C$ varies and if there is no correlation between $\delta^{18}O$ and $\delta^{13}C$ from the same growth layer, isotopic equilibrium can be assumed. The tests used to determine if speleothems are indeed deposited in isotopic equilibrium are the so-called 'Hendy tests' (Hendy, 1971; Frisia and Borsato, 2010; McDermott, 2004; Mickler et al., 2006).

Temperature dependence of the $\delta^{18}O$ of atmospheric precipitation is highly variable and site dependent. On average the modern-day relationship between the $\delta^{18}O$ of precipitation and temperature is 0.6‰ per °C, higher atmospheric air temperatures thus correspond with higher $\delta^{18}O$ values. On the other hand, the calcite-water fractionation in equilibrium is approximately -0.24‰ per C°. Because temperatures normally have less influences on the calcite-water fractionation, a positive correlation between temperature and the $\delta^{18}O$ signal in the speleothem can be expected (Fairchild et al., 2006). However, these relationships between the $\delta^{18}O$ signal and temperature could have been different in the past and on a longer timescale, other factors like changes in continental ice volume and the amount of precipitation, extreme precipitation depletes the $\delta^{18}O$ signal (Dansgaard, 1964), could have caused variations the $\delta^{18}O$ signal. This illustrates why additional proxy information is necessary to strengthen the interpretation of the $\delta^{18}O$ signal in stalagmites (McDermott, 2004).

In the case of kinetic fractionation (recognisable by a positive correlation between $\delta^{18}O$ and $\delta^{13}C$) for example due to fast degassing (whereby the lighter isotopes of both oxygen and carbon are preferentially removed from the drip water), the development of transfer functions that allow for the interpretation of oxygen isotope trends in function of temperature or the amount of precipitation becomes even more complex. Most scientists nowadays agree that $\delta^{18}O$ stored in speleothems should not be used as a direct proxy for changes in air temperature, but rather that $\delta^{18}O$ shifts can be used as a chronological control on major climatic changes like changes in atmospheric circulation or the Dansgaard-Oeschger of the last glacial observed in other records like

for example the Greenland ice cores (see 2.4.2.2.3). Still, even if there is a positive co-variation of the oxygen and carbon isotope record, speleothem records can still provide valuable paleoclimate proxies. For example, evapotranspiration and prior calcite precipitation are both linked to climatic parameters and result in positive co-variation between $\delta^{18}O$ and $\delta^{13}C$. Direct measurements of the $\delta^{18}O$ signal in fluid inclusions of the speleothem could potentially also decrease the amount of uncertainty in the interpretation of the $\delta^{18}O$ signal (Fairchild et al., 2006; Frisia and Borsato, 2010; Krüger et al., 2011; McDermott, 2004).

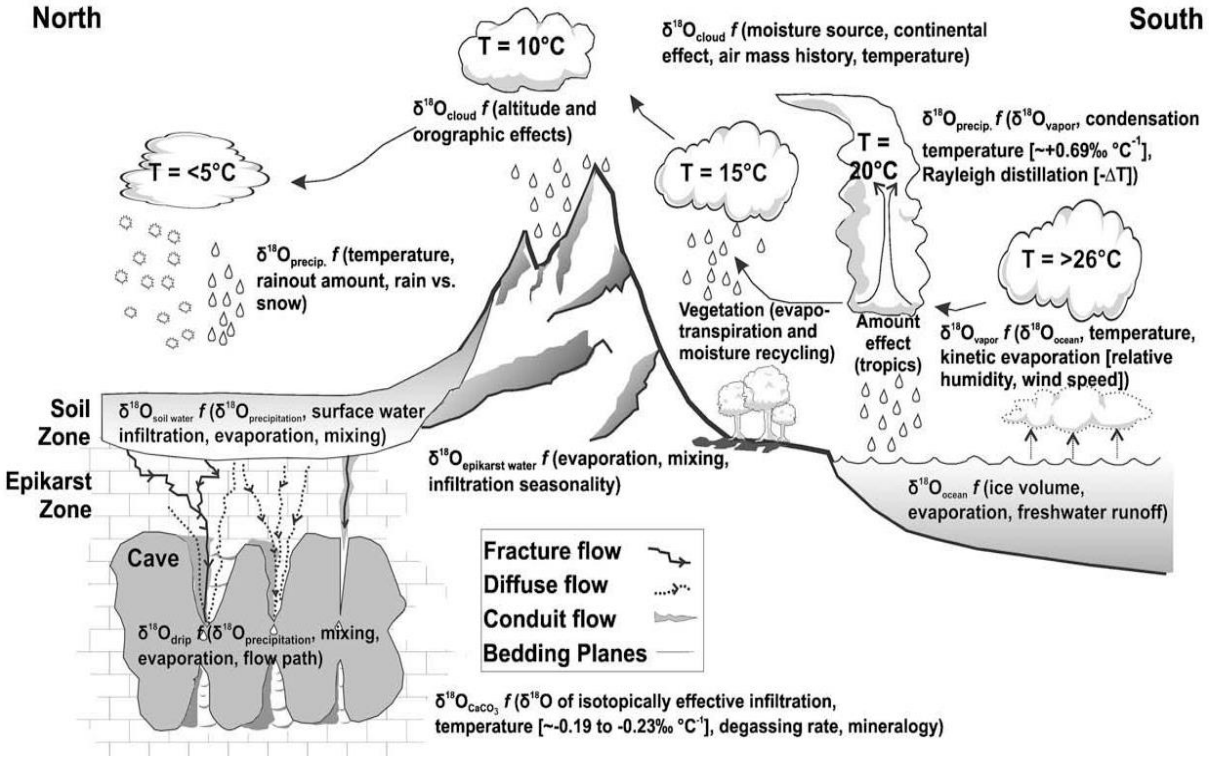

Figure 7 – Overview of the processes controlling the $\delta^{18}O$ signal in speleothems (Lachniet, 2009)

2.2.5.2 Trace elements

Variations in the trace element record can be used to further enhance or clarify the interpretations of the stable isotope signals. Trace elements in speleothems can be divided in three different groups. The most studied group of elements are the elements, which can substitute for Ca or CO_3 in calcite or aragonite like Sr, Ba, U, Mg and SO_4. The partition coefficient K for these type of reactions is defined as follows:

$$\frac{Tr}{Cr_{CaCO_3}} = K \frac{Tr}{Cr_{solution}}$$

with Tr the trace element in question and Cr the carrier of the trace element (Ca or CO_3). K depends on temperature, growth kinetics and other factors like the crystallographic form. A second group of elements are the elements that are incorporated interstitially on a molecular scale in $CaCO_3$ like PO_4, Na and F. These types of elements are generally incorporated at growth defects. A third group of trace elements, like Na or Cl, can be found in the solid or fluid inclusions inside the carbonate (Fairchild and Treble, 2009; Fairchild et al, 2006).

Trace elements are influenced by atmospheric input, the karstic aquifer, vegetation, primary speleothem growth and secondary alteration (Fairchild and Treble, 2009). Trying to understand the relative contribution of all these different factors on the final trace element values is, similar to the interpretation of the stable isotope records in speleothems, not straightforward.

There are different sources for the trace elements found in the speleothem carbonate, but in contrast with the stable isotope records, the host-rock and the overlying regolith are the main sources for most trace elements in speleothems. Meteoric water, which infiltrates in the host-rock moves from a dissolution to a precipitation regime when encountering a gas phase with lower partial CO_2 pressure. This prior calcite precipitation removes cations from the water into calcite and because partition coefficients for these types of reactions are usually lower than 1, the ratio of the trace element to Ca in solution increases. PCP is enhanced during drier climatic periods because karst waters are able to degas. In other words, significant PCP leads to an enrichment in trace elements like Sr and Mg compared to the host-rock compositions and this enrichment can be used as a proxy for drier climates. This also implies that strong co-variance between Sr and Mg records can be a sign of PCP and, like discussed before, PCP will also result in higher $\delta^{13}C$ values (Fairchild and Treble, 2009).

Under typical karstic conditions, the partition coefficient of Mg largely depends on temperature. Scientists tried to use the Mg record in speleothems as proxy for paleotemperature (e.g. Gascoyne, 1983), but newer research mainly emphasizes on the importance of palaeohydrology on the Mg signal (e.g. Roberts et al., 1998). Mg can be useful as a proxy for effective rainfall (actual rainfall – evapotranspiration) and be correlated with trends in the $\delta^{13}C$ and $\delta^{18}O$ record. The Mg/Ca ratio, which is also related to PCP, can be used as an indicator of dilution or water excess created by high

drip water flow or changes in the dominant flow path of karstic water. If water volumes are high, residence time in the vadose zone decreases and the Mg concentration in the karstic water drops. In this respect speleothem Mg concentrations are lower during wetter periods. While Mg is an indicator of effective water excess, the $\delta^{18}O$ signal on the other hand is assumed to largely reflect changes in rainfall amount. Also, Sr is incorporated in larger quantities if precipitation rates are high. However, like for Mg, this relationship is not observed in all studied speleothems. This indicates why Sr is, also like Mg, mainly used as a palaeohydrological indicator due to the impact of PCP on the Sr signal. Finally, Ba often show a positive correlation with Sr, pointing towards similar process influencing these trace elements (Fairchild and Treble, 2009; Verheyden et al., 2000). One of the main conclusions derived from the trace element and stable isotope measurements conducted by Verheyden et al. (2000) on a Holocene speleothem from the Père Noël cave (same cave as the PNG-01 speleothem) was that PCP seemed to be the dominant process controlling the Mg and Sr records of that speleothem. This shows why trace elements can be a useful tool when trying to interpret stable isotope signals. One of the targets of this thesis research is to check if PCP was also a dominant process during the formation of the PNG-01 speleothem.

The previous paragraphs focused on the first group of trace elements, which can substitute for Ca or CO_3 in the speleothem carbonate and are mainly host-rock derived elements. However, more recently Borsato et al. (2007) also looked at other elements like Y, Zn, Cu, Pb, P and Br, which can be adsorbed by the growing calcite or aragonite crystals. These elements have distinct properties, but all have the tendency to show strong sorption behaviour in soils, which explains why they are referred to as soil-derived elements. The variation of these elements in the cave calcite was related to the annual rhythm of the studied cave. Peaks in these elements corresponded with thin darker calcite layers which are related to high levels of water infiltration at the turn of the hydrological year (autumn). This suggests that this high-water flux flushed organic colloids from the soil and brought higher volumes of these trace elements inside the cave, which was confirmed with present-day water analyses of drip water in the cave. Of all these elements, Y appears to be most sensitive to these changes in water infiltration and is said to be related to behaviour of other rare earth elements (REE). Peaks in soil-derived elements can thus be linked with periods of high water

infiltration, at least on annual scale. At this point in time, the behaviour of these elements on a longer time-scale is not yet fully understood (Borsato et al., 2007).

To summarize, trace elements in speleothems can be divided in two important groups. Host-rock derived elements like Sr, Ba and Mg can be used as a proxy for effective precipitation, with peaks in the trace element record corresponding with drier periods. Together with the stable isotope records they can also be used to estimate the relative importance of processes like PCP. Peaks in soil-derived elements like Y, Zn and Pb can, at least at an annual scale, be used to estimate periods of high infiltration.

2.3 THE PÈRE NOËL CAVE

2.3.1 Introduction

The studied speleothem core (PNG-01) was drilled in the Gibraltar speleothem from the Père Noël cave. A group of cavers discovered this cave in 1964 during Christmas time which explains the peculiar name (the French Père Noël translates to Santa Claus). The cave is part of the karstic cave system of Han-sur-Lesse (Verheyden et al., 2008). The geological and geographical context, but also the conditions inside in the cave all have a major impact on the isotopic and trace-element values, which makes it important to have a closer look at these different aspects before interpreting the measurements conducted for thesis. The part on the contemporary cave conditions is mainly based on the work of Sophie Verheyden (Verheyden et al., 2008).

2.3.2 Geographical and geological context

2.3.2.1 Geography

Situated in the province of Namur in the southern part of Belgium (50.1°N, 5.2°E, around 230 m a.s.l.), the climate of the Père Noël cave, which is situated only around 200 km inland, is like the rest of Belgium and most of northwest Europe influenced by the presence of the North Sea and the Atlantic Ocean. The Han-sur-Lesse cave system and the Père Noël cave are formed in the Calestienne limestone-belt, which crosses Belgium from west to east and is labelled on figure 8.

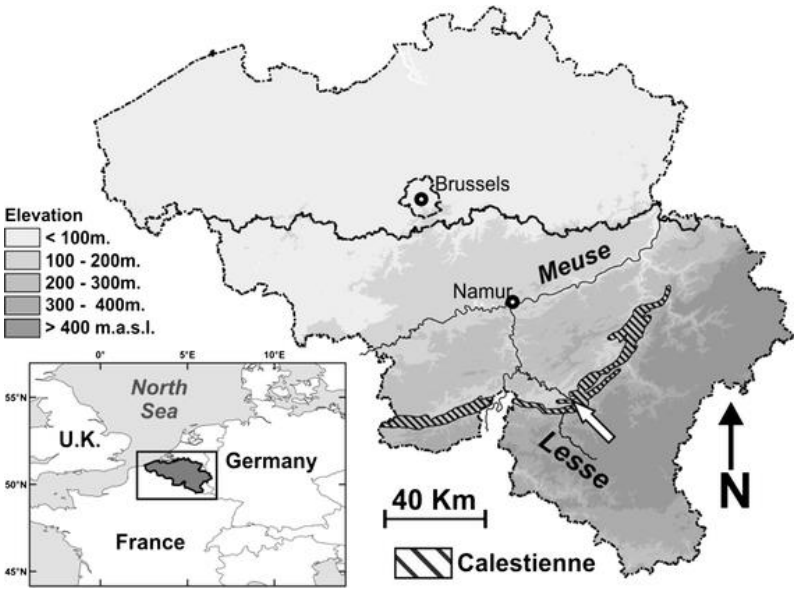

Figure 8 – Geographical location of the Han-sur-Lesse cave system and the Père Noël Cave (Poulain, 2015)

2.3.2.2 Climate

The Köppen-Geiger climate classification for this region, Cfb, translates to a temperate climate without a dry season and a warm summer, which in practice means that at least 4 months have an average temperature of more than 10°C and the average temperature of the hottest month is below 22°C (Peel et al., 2007).

In Belgium, weather and climate data is collected and processed by the Royal Meteorological Institute and made available at municipality level for the period between 1981 and 2010. Because Han-sur-Lesse is part of the larger Rochefort municipality, the climate data of Rochefort is discussed here.

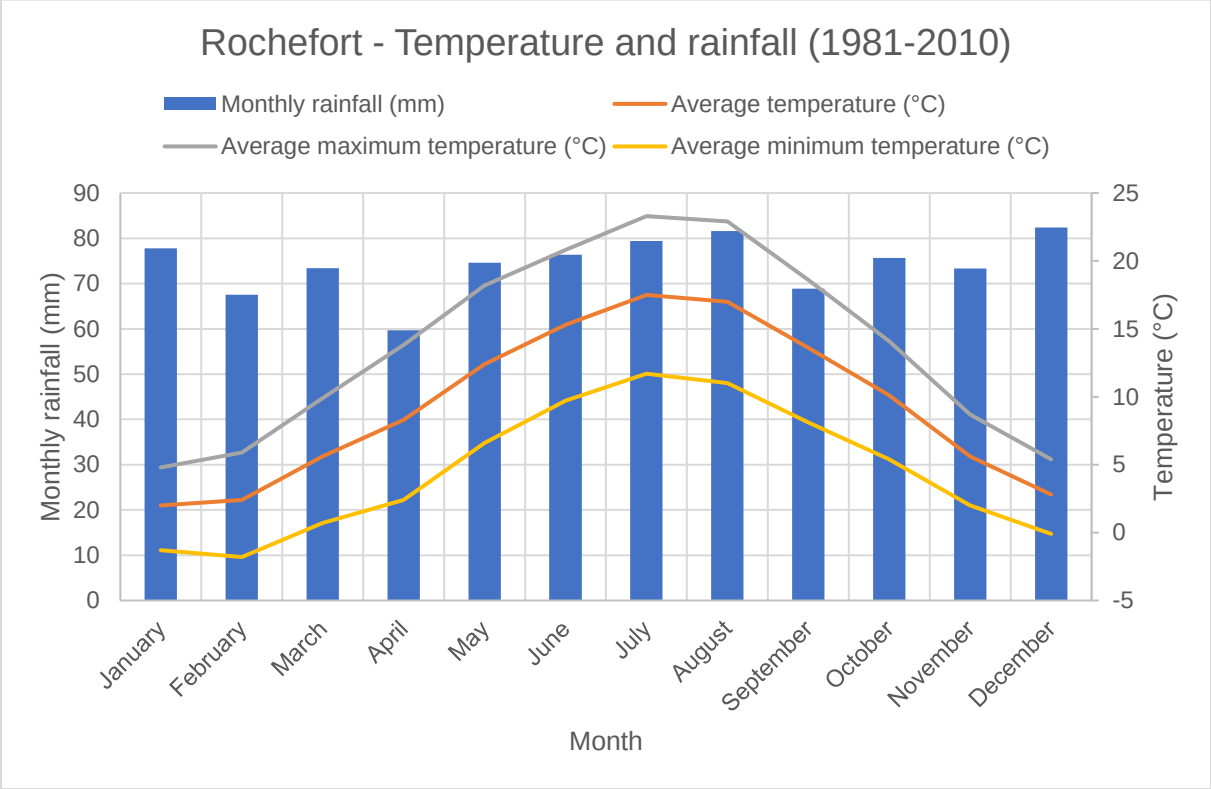

Figure 9 – Climate data for the Rochefort municipality between 1981 and 2010 (original data: KMI)

According to the dataset visualised in figure 9, the average temperature in this period was 9,4°C, while the average maximum and minimum temperature were 13,8 and 4,5°C respectively. January is with an average temperature of 2°C the coldest month, July on the other hand is the warmest with an average temperature of 17,5°C. These values confirm that the climate in this region does not really experience extreme temperatures in summer and winter and is thus considerate temperate. Looking at the rainfall amounts, the average annual rainfall in this 30- year period is 891 mm. The individual months show some slight variation, the winter and summer months are a bit

wetter, but in general the differences between the months are not pronounced. On average, every year has 144 days of rain, with a day of rain defined as a day with more than 1 mm of rainfall (KMI, 2017). To summarize, temperatures show a clear seasonal pattern, while the rainfall amounts are rather homogeneous throughout the year.

2.3.2.3 Vegetation

The bedrock above the cave is covered with C3 type of vegetation, more specifically a mixed-leaf forest with hazel, oak and beech trees. The soil, which is around 40 cm thick, is heavily rooted and consists of loose brown earth with some limestone fragments and residual clays. Also important is that the area above the cave is protected from direct human influence due to the fact that the cave is property of the natural touristic caves of Han (Verheyden et al., 2008).

2.3.2.4 Tectonic evolution of the Ardennes

(after Sintubin, 2004)

This section gives a concise overview of the tectonic evolution of Belgium and more specifically of the Ardennes region, in which the Père Noël cave is situated. Unless stated otherwise, the reference used for this section is Sintubin, (2004). As can be seen on figure 10, the Père Noël cave is situated in an area of Middle Devonian and Carboniferous age, at the northern border of the High Ardenne slate belt. More specifically, the cave developed in limestone of Givetian age (Delvaux de Fennfe in Verheyden, 2008). The Givetian is the youngest stage of the two stages of the Middle Devonian and lasted from 387,7 to 382,7 Ma (ICS, 2017). This section tells the background story on why carbonates of this age can be found in this specific region of Belgium.

In the early Ordovician (485 - 475 Ma) the Avalonia microplate, which now accommodates the Benelux, England, Newfoundland, Avalon and parts of Germany, France and Ireland, started to drift away from Gondwana and moved in northern direction towards Laurentia and Baltica. This movement continued throughout the Ordovician and at the end of the Ordovician (around 450 Ma), Avalonia collided with Baltica, which triggered the start of the Ardennes orogeny.

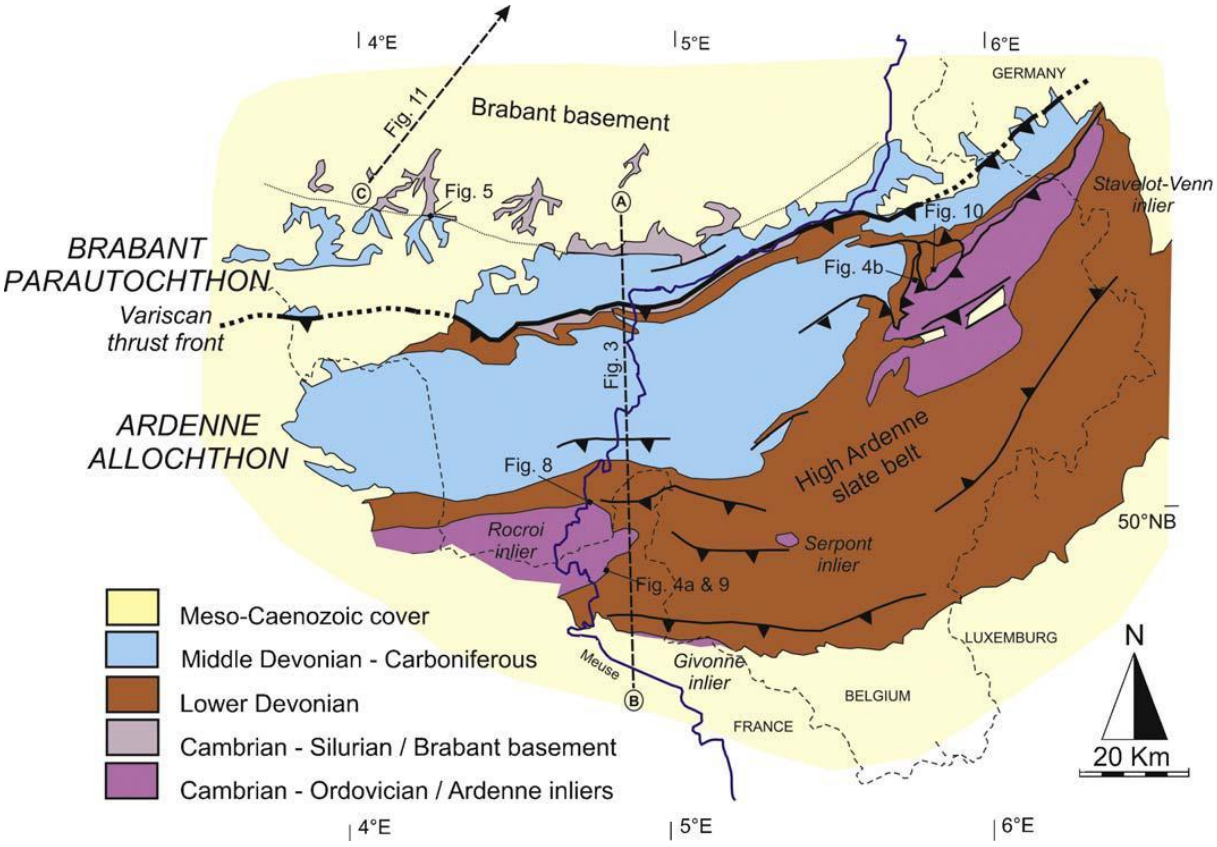

Figure 10 - Simplified geological map of the Brabant-Ardenne region with indication of the main tectonostratigraphical entities (Sintubin et al., 2009)

Around 425 Ma, the early Silurian, Baltica collided with Laurentia, which closed the Northern Iapetus Ocean and formed the Caledonian mountain range. This collision also created the new continent Laurussia, made up out of Baltica and Laurentia. In the next 30 million years the Western Iapetus Ocean, situated between Laurentia and Avalonia, slowly closed. This tectonic pulse uplifted the Caledonian massifs of the Ardennes and created a minor supercontinent consisting out of Baltica, Laurentia and Avalonia, the Old Red Continent. In the early Devonian, the Caledonian orogeny slowly comes to an end and the Rheic Ocean closes when Armorica bumps into Avalonia. Almost immediately after Armorica colliding with Avalonia, a new sedimentary basin was created in which the erosion material of the Old Red Continent accumulated, the Rhenohercynic sea. However, already in the Middle Devonian (around 390 Ma), the Rhenohercynic sea started to close again under the influence of a new phase of convergence, the Variscan orogeny. This orogeny started because the Gondwana supercontinent collided with the southern margin of Armorica. The Variscan orogeny ultimately took around 90 million years to completely develop and at the end (around 290 Ma) a new supercontinent Pangea saw the light of day.

This geological story, which spans from Cambrian, over Ordovician, Silurian and Devonian to Carboniferous, is summarized in figure 11.

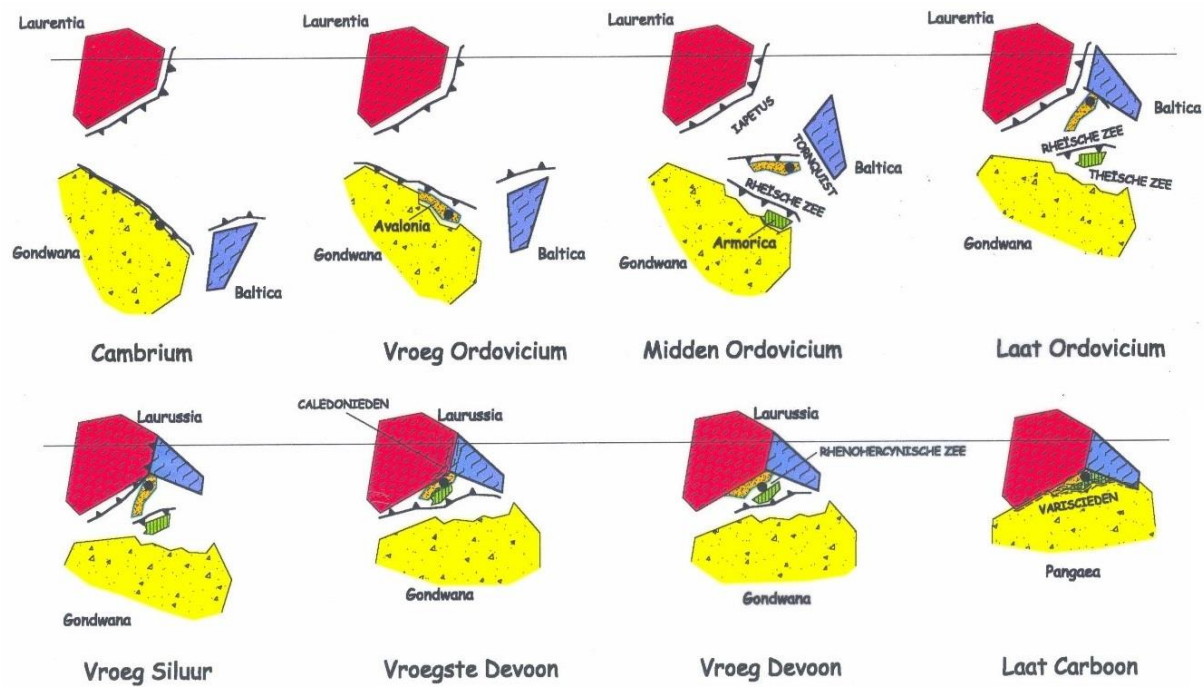

Figure 11 - Tectonic evolution of the Ardennes from Cambrian to Carboniferous (Sintubin, 2004)

In the region of the Ardennes specifically, the early Devonian sedimentation was controlled by rift-basins on the northern margin of the Rhenohercynic sea. In the remainder of the Devonian and in the early Carboniferous period, the Ardennes region was characterised by typical post-rift shelf sedimentation and development of carbonate platforms. Ultimately, in these carbonate platforms the caves of Han-sur-Lesse and thus also the Père Noël cave developed.

2.3.2.5 Cave geology

As discussed in the previous paragraphs, the Père Noël developed in Givetian limestones. These limestones contain partly dolomitised beds and the overlying host rock reaches thicknesses of up to 70 m and has a southwards dip of approximately 45° (Vandersleyen in Verheyden et al., 2008; Verheyden et al., 2014). Presence of large pebbles (10 to 20 cm in diameter) in the Salle du Bivouac (see figure 13) are a hint that this cave was formed by a meander of the Lesse river cutting of the Lesse through the Massif de Boine. However, nowadays and for at least 150 000 years (Quinif & Bastin in Verheyden, 2008), the water entering the cave is only local rain, which seeps directly through the overlaying limestone bedrock and a small water flow from unknown origin (Verheyden et al., 2008).

Figure 12 shows a geological cross section through the Père Noël cave area. The cave developed in an anticlinal structure because the Givetian limestone of the Père Noël cave can be found below the younger Frasnian shales and above the older the Eifelian formations.

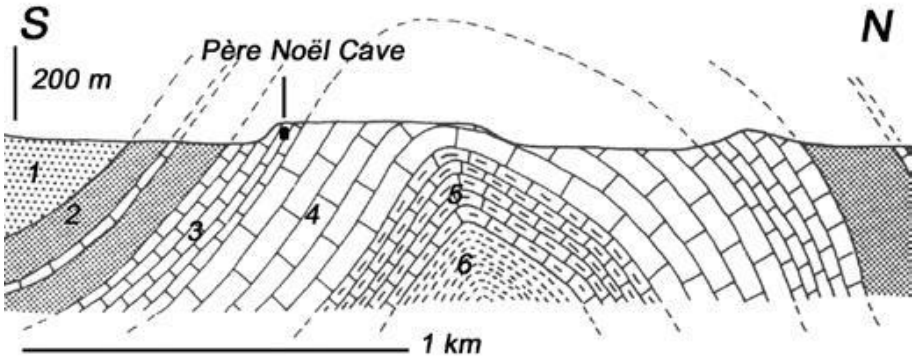

Figure 12 – Geological cross section of the Père Noël cave area (Verheyden et al., 2008)

2.3.2.6 Cave morphology

The Père Noël cave consists out of different connected rooms (see figure 13). After entering the cave through a narrow entrance, a small descend of around 25 m leads towards a first small room. The biggest room of the cave, the Salle du Bivouac, can be reached after another descend of around 20 m. This room is around 200 m long, 50 m large and 30 m high. A narrow passage in this room, the *Chambre à coucher*, is the place where the automatic sampling of the cave conditions, discussed in the next section, took place. Candle shaped calcite stalagmites are the most common speleothems in the Père Noël cave, but there can also huge columns, rounded stalagmites and draperies to be found in the cave (Verheyden et al., 2008).

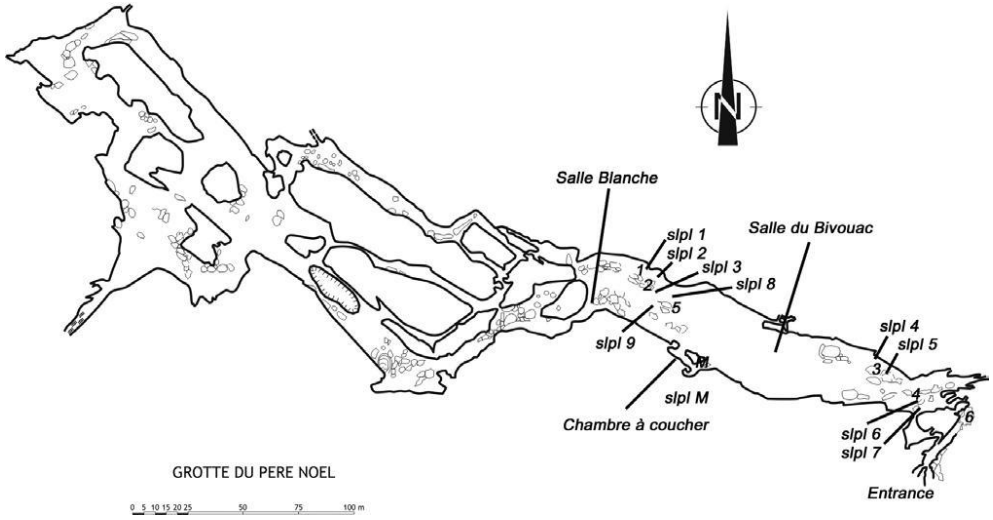

Figure 13 - Map of the Père Noël cave (Verheyden et al., 2008)

2.3.3 Cave conditions

The study of Verheyden (2008) focused on the monitoring of the Père Noël cave climatology (air and water temperature, PCO_2), hydrology (drip rate and conductivity) and geochemistry of water and calcite deposits ($\delta^{18}O$, $\delta^{13}C$, Mg/Ca and Sr/Ca ratios) in an effort to better estimate the effect of these parameters on the isotopical and trace element signatures of speleothems. Therefore, both automated and manual sampling techniques were used (Verheyden et al., 2008). The results of these measurements and the interpretations suggested by the authors are summarized in the following paragraphs.

2.3.3.1 Cave climatology

The air temperature in the largest room of the cave was measured every two or three months in the period between October 1995 and August 1998 and varied between 8,5 and 9,3°C with a mean of 9°C, but no clear seasonal variation was observed (Verheyden et al., 2008). This mean temperature is only a bit lower than the mean temperature measured at Rochefort, 9,4°C (period between 1981 and 2010), which shows that there is clear correlation between the air temperature above and inside the cave.

However, it is important to keep in mind that the reference period for this two values is clearly not the same and because only the average climate data of Rochefort in the period between 1981 and 2010 is publicly available, a request was made at the Royal Meteorological Institute of Belgium to obtain the specific data for the period in which the temperatures were measured inside the cave (1995-1998). These data show an even better correlation between the temperature in- and outside the cave. The average temperature on the surface between October 1995 and August 1998 was 8,8°C and the average temperature over the three complete years, which is probably a better value to compare with as it contains both the warm and cold months, was 9,1°C. Thus, within the margin of error, the temperatures in- and outside the cave are exactly the same. This gives value gives confidence in using speleothem data to reconstruct the paleoclimate of this region.

The seepage water on the other hand, was in general slightly warmer than the air temperature inside the cave, with a mean temperature of 9,2°C and a minimum and maximum value of 8,8 and 10,2°C respectively in the same sampling period. The CO_2

pressure, showed the largest (seasonal) variation. The lowest values were measured at the end of winter, minimum values reached 350 ppmv, while at the end of summer values from 650 to, albeit occasionally, 1000 ppmv were reached (Verheyden et al., 2008). An explanation for this variation could be the seasonal production of CO_2 by vegetation and bacterial activity in the soil, which then enters the cave through fractures and degassing (Gewelt & Ek in Verheyden et al., 2008). Compared to other caves in Belgium, these values are rather low, which lead to the interpretation that exchange between air in and outside the cave is probably rather important. The relative humidity finally, varied between 95 and 98%, but maybe due to low accuracy of the measurements at high humidity levels, no seasonality could be found (Verheyden et al., 2008).

2.3.3.2 Cave hydrology

Installed in 1991, the automated drip monitoring installed in the Père Noël cave was one of the first in the world (Genty and Deflandre, 1998). Placed right below a soda-straw stalactite, the drip rate was measured with electroluminescent diodes. Aside from the drip rate also the water volume, air temperature, air pressure, pH, conductivity and the number of drops were measured automatically every 10 minutes in the period between 1991 and 1999 (Verheyden et al., 2008).

Genty and Deflandre studied the results of this automatic monitoring and wrote their findings in a paper published in 1998 (see references). Their most important conclusions are summarized below.

- The variation in drip and flow rate shows a clear seasonal pattern and they found three stages in these rates: first there is an abrupt increase in flow rate in late autumn or early winter, the winter itself then has a high flow rate regime and finally, from March to November the flow rate decreases before the cycle starts over again in late autumn. According to the authors these variations in drip rate might explain the presence of seasonal laminae often observed in stalagmites.
- During the flow rate increase in late autumn, the conductivity increases at the same time as the drip rate, meaning that water rich in minerals or organic matter is brought into the karst by the late autumn flush. These waters could have been in the epikarst since the last flow rate increase. This can be important when interpreting geochemical seasonal signals in speleothems.

- There appears to be a good correlation between water excess (rainfall minus evapotranspiration) and the annual flow rate of the stalactites, which illustrates that the amount of water feeding a stalactite is controlled by the annual rainfall.
- During some periods in the year, an anti-correlation between the drip rate and air pressure was observed, which was explained by the fact that the air pressure could influence the diameter of the pathways used by the water moving through the host rock. Some oscillations superimposed to the seasonal flow variations were found when the flow rate reached a certain threshold during wetter periods.
- The drop volume was almost constant at 0.14 ml, only for extreme drip rates the drop volume varied significantly. For example, at high drop rates the drop volume could maybe decrease due to the formation of satellite drops.

2.3.3.3 Geochemistry of seepage water and calcite deposits

The drip rate shows seasonal variation, but is never zero, which implies that some of the drip water must originate from some kind of reservoir. Knowing that the stalactite drip rate is controlled by the water excess (correlated to rainfall), it is important to have an idea if the drip water forming the stalactite is from rainfall of the same year or if the water is mixed with older reservoir water. One possible explanation could be that water is stored in the epikarst for a certain period and then is flushed out in the late autumn, which fits with the conductivity measurements (Genty & Deflandre, 1998; Verheyden et al., 2008).

2.3.3.3.1 Seepage waters

The $\delta^{18}O$ signal of the seepage water inside the cave was compared with rainwater samples of Han-sur-Lesse. The signal of the seepage water itself varied between -8,0 and -6,8‰ with a mean value of -7,51‰ (± 0,2‰) using the VSMOW-standard as reference in the 1995 to 1998 sampling period. This mean value is, within uncertainty, similar to the mean rainwater signature of -7,3‰, however the main difference is that the seasonal signature of the seepage water is much less pronounced than that of the rainwater. This implies that mixing takes place in the vadose waters, but not enough to mix the waters of an entire year (Verheyden et al., 2008).

Because the isotopic signals of the seepage and drip water were in antiphase, the lowest values for the seepage water were reached in the summer, while for the rainwater winter showed the lowest values, Verheyden et al. (2008) indicated that there

might be a time lag of around 6 months before rainwater enters the cave and starts the formation of a speleothem. All of this suggests that the drip rate increase observed in late autumn pushes out water with a still visible summer signature, which was stored in the layers above the cave and only underwent partial mixing, into the cave to start the formation of speleothems (Verheyden et al., 2008).

Aside from the isotopic signature of the seepage waters, also the concentrations of certain trace elements were sampled, more specifically the ratios of Mg and Sr to Ca concentrations (in ppm). The 1000Mg/Ca and 1000Sr/Ca ratios were 324 and 2,32 respectively, but these ratios showed an important temporal and spatial variability. The same ratios for the host rock were 12,1 and 0,99 for calcite minerals and 313,8 and 0,71 for dolomite minerals, which shows that the seepage water is enriched in both Sr and Mg. Like the isotopic signals, there are seasonal trends to be observed, but the highest values are not the same for every sample location (Verheyden et al., 2008).

At all sample locations, a positive relationship was found between the Sr/Ca and Mg/Ca ratios, which suggests that signal of the seepage water depends on the residence time; the longer the water stays in the vadose zone, the more it becomes enriched in both Sr and Mg (Fairchild et al., 1998). Residence time is linked to the drip rate because the residence time depends on the water recharge. This relationship between drip rate and the Sr/Ca ratio was very strong, but less clear for the Mg/Ca ratio (Verheyden et al., 2008).

2.3.3.3.2 Calcite deposits

Not only the seepage waters were analysed, but also present-day calcite was collected and analysed. The $\delta^{18}O$ and $\delta^{13}C$ signals varied between -6,0 and -3,8‰ and between -9,0 and -2,6‰ respectively, all values are expressed with correspondence to the VPDB standard (Verheyden et al., 2008). These authors suggested that these wide ranges in the isotopic signals of present day calcite, definitely compared to the range of isotopic values in the seepage waters and the expected range in temperature, are a sign for the presence of non-equilibrium processes occurring when the calcite is precipitated. If calcite is deposited in isotopic equilibrium, oxygen isotopes of the seepage water and calcite can be used to calculate the calcite precipitation temperature. When isotopic equilibrium was assumed, the reconstructed temperatures varied between -4,8 and 13,6°C. To reach temperatures close to the present-day

temperature in the cave, the lowest value for the seepage water and calcite had to be used. Aside from the oxygen isotopic signal, also the range in the $\delta^{13}C$ signal was larger than what could be expected from the presence of a dense C3 vegetation. Not only was the range of the isotopic signals in the calcite higher than expected, both the $\delta^{18}O$ and $\delta^{13}C$ signals became less negative in the deposited calcite. There was also a good positive correlation between the $\delta^{18}O$ and $\delta^{13}C$ signal, indicating that these signals are controlled by the same or related processes. All these signs combined, the conclusion was that calcite in the Père Noël cave is influenced by some non-equilibrium processes (Verheden et al., 2008).

Two processes that could possibly control the fractionation that occurs when seepage water is used to form a speleothem are evaporation of the water and fast CO_2 degassing (Fornaca-Rinaldi et al. and Gonzales & Lohmann in Verheyden et al., 2008). Both processes favour the removal of the lighter isotope of oxygen and carbon, which means that calcite precipitated from fast dripping waters has a more negative or lighter signature because there is less degassing and evaporation. Because the PCO_2 in the cave is relative low, fast CO_2 degassing is possible, but due to the high humidity, important fractionation by evaporation seems much less likely in this case. Measurement on other recent calcite and a Holocene stalagmite from the Père Noël cave lead to the hypothesis that calcite deposited over a longer period is precipitated in and influenced by similar conditions and processes as the present-day calcite.

2.3.4 Conclusions

Verheyden et al. (2008), made the following conclusions concerning the conditions in the Père Noël cave:

- the climatology (temperature and humidity) in the cave is rather constant
- only slight variations were observed in the isotopic composition of the seepage water
- both the drip rate and chemical composition of the seepage water as well as the isotopic and chemical composition of the calcite show spatial and seasonal trends
- observed variations in the $\delta^{18}O$ and $\delta^{13}C$ signal are linked with the drip rate and consequently also with rainfall

- the Mg/Ca and Sr/Ca rations in the seepage water and calcite are dependent on the residence time of the water
- the processes controlling the fractionation during the calcite precipitation are most likely very similar for recent history and Holocene period

2.4 THE EARLY WEICHSELIAN CLIMATE

2.4.1 Introduction

Preliminary dating of the PNG-01 speleothem indicated that the stalagmite formed during the early Weichselian (from around 103 ka to around 92 ka). By definition, the Weichselian starts at the end of the Eemian (see figure 15), at around 115 ka, and lasts until 11,7 ka, the start of the Holocene period (Mangerud et al., 2011; NEEM Members, 2012). The German name of the Vistula river in Poland, 'Weichsel', gave in the 1930's its name to this period (Oxford Dictionaries, 2017). The Weichselian is not an official stage in the International Chronostratigraphic Chart (see figure 14), but together with the Eemian it forms the Upper Pleistocene stage (ICS, 2017).

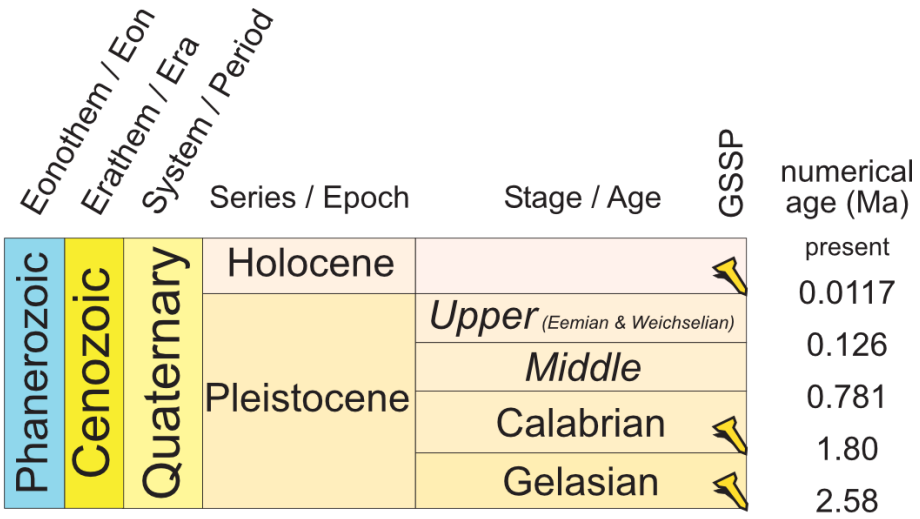

Figure 14 – The Upper Pleistocene stage, International Chronostratigraphy Chart (adapted from ICS, 2017)

The Weichselian corresponds to the most recent glacial period in north-west Europe or the last major incursion of the continental ice sheets during the Pleistocene (2,58 Ma – 11,7 ka). This same cold stage corresponds with the Würm glaciation in central and south Europe. During the Weichselian period, the Fennoscandian ice sheet dominated north-west Europe, creating an environment with polar desert conditions and widespread permafrost. However, throughout the Weichselian temperatures rose at quasi-regular intervals, which lead to different pulses of ice build-up and ice retreat.

These periods of climate ameliorations are called interstadials and the warmest ones occurred during the early Weichselian, the Brørup and Odderade interstadials (see figure 15) in the Netherlands and northern Germany or the equivalent Saint Germain I and II interstadials in France (Bell & Walker, 2005).

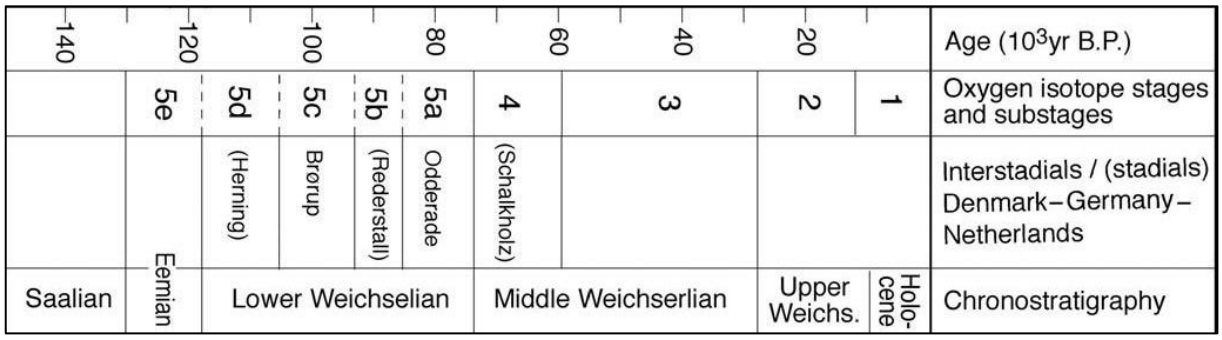

Figure 15 – Chronostratigraphy of the Weichselian (Mangerud et al., 2011)

The early or lower Weichselian is an informal subdivision of the Weichselian and represents the European continental equivalent of Marine Isotope Stages (MIS) 5d to 5a (see figure 15). From preliminary U/Th dates, the PNG-01 speleothem appears to have an MIS 5c equivalent age. The MIS 5c stage corresponds with the continental early Weichselian Brörup/Saint Germain I interstadial which has an age of around 100 ka BP (Bell & Walker, 2005). At this point, no continental records for that timeframe are available in Belgium, providing further motivation for this thesis research.

Marine Isotope Stages go back to Arrhenius who created the first subdivision of climatic change throughout the Quaternary based on changes in calcium carbonate precipitation (Arrhenius, 1952). In 1955, Cesare Emiliani used the same subdivision when he reconstructed ocean temperatures through time with the aid of oxygen isotopes from planktonic and pelagic foraminiferal species in deep marine cores (Emiliani, 1955). However, Shackleton later reassessed the work of Emiliani and concluded that the changes in the oxygen isotope record of Emiliani were mainly representations of terrestrial glacial events rather than oceanographic events. Reasoning behind this conclusion was that he observed that fluctuations in the oxygen record of benthic foraminifera living in the deep-sea, which is much less influenced by temperature variations, were very similar to the fluctuations in the planktonic record. According to Shackleton, this meant that both the planktonic and benthic foraminifera were influenced by the same process, changes in the continental ice volume (Shackleton, 1967; Shackleton, 1969).

Nevertheless, changes in the oxygen isotope records from marine cores can be used to create a global stratigraphic framework. The MIS chronostratigraphic scale is divided in different stages, counting from the top downwards, which means that smaller numbers reflect younger periods. Conventionally, even numbers mark colder, glacial periods while odd numbers represent warmer, interglacial periods (Shackleton et al., 2003). Because marine cores always have some kind of local signature, scientists have created standard curves by stacking the records from different cores above each other and statistically calculating an 'average curve', prime examples are the SPECMAP-curve (see figure 16) by Imbrie et al. (1984) and the LR04-curve (see figure 19) of Lisiecki & Raymo (2005).

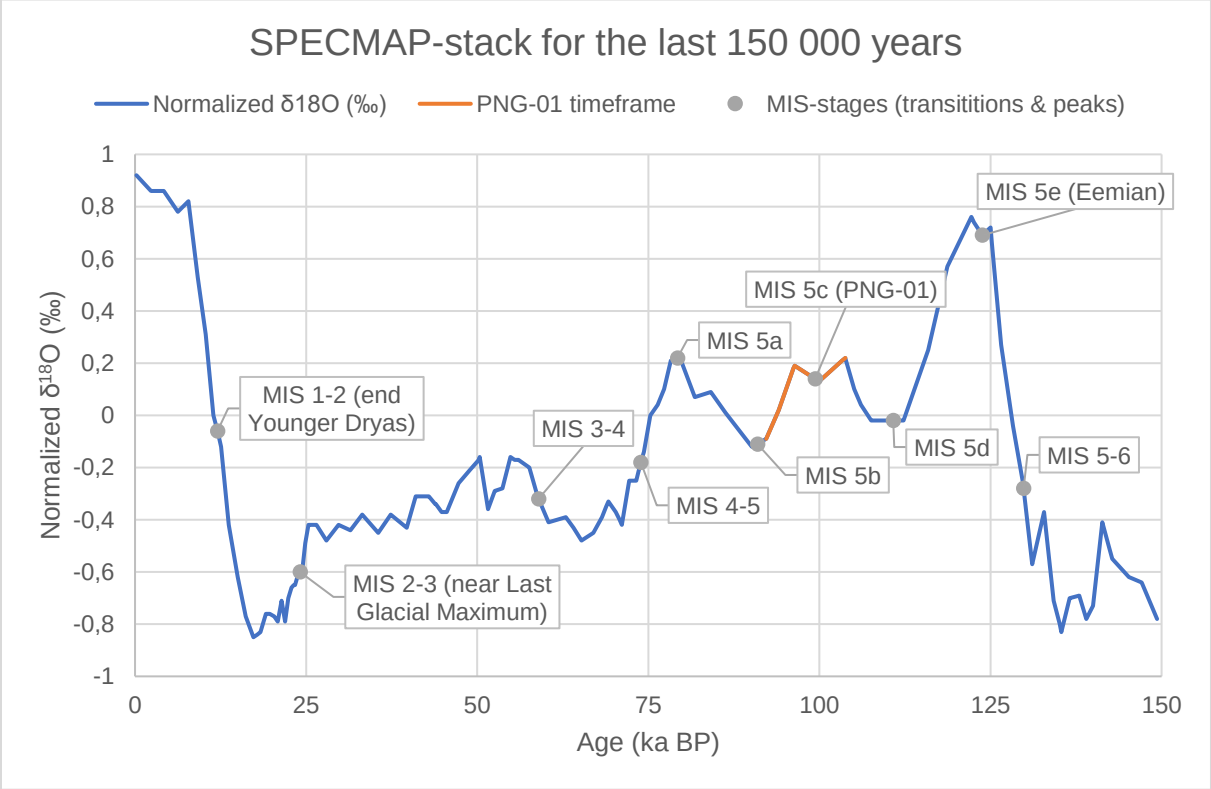

Figure 16 – SPECMAP-curve for the last 150 000 years (original data: Martinson et al., 1987)

On the SPECMAP-curve (figure 16), transitions between the different MIS-stages for the last 150 000 years are indicated. For example, the 'MIS 5-6'-transition correlates with the transition from the Middle Pleistocene towards the Upper Pleistocene period. Exceptions are the MIS 5 sub-stages (5a, 5b, 5c, 5d and 5e), which are presented as peak events. Aside from the MIS-stages, also the timeframe in which the PNG-01 stalagmite was formed is shown, the MIS 5c peak event (around 99 ka on this curve) is situated almost in the middle of the stalagmite formation. Important climatic events

like the Last Glacial Maximum (around 24,5 ka), a period in which the ice sheets were at their maximum extent, and the end of the Younger Dryas, which marks the end of the last glacial pulse and subsequently also the start of the Holocene (11,7 ka), are presented on the curve. Also note that the $\delta^{18}O$-values on this SPECMAP-curve are normalized, in this case lower values represent periods with advancing ice sheets and thus colder climatic conditions (Martinson et al., 1987).

In general, the quality of the proxies used for paleoclimatic research decreases when going back further into time because the resolution of many proxies lowers and every proxy only has a limited usable range. The MIS 5c stage is a relatively recent period in geological history, ensuring that the amount and quality of the available proxies is good (Wohlfarth, 2013). The Eemian interglacial to Weichselian glacial transition, set at 117.5 ka in Belgium (Vansteenberge et al., 2016), was and is still part of many research projects because it is the most recent interglacial-glacial transition in earth's history. A gradually decreasing solar insolation triggered a series of feedback processes, which together moved the climate of the earth below a certain threshold temperature, the start of the last glacial period (Wohlfarth, 2013).

Trying to understand the dynamics of such transitions is very important, but looking at the SPECMAP-curve (figure 16) it is also clear that after this rather abrupt change in climate, it takes around 100 ka for the climate system to reach its coldest conditions (the Last Glacial Maximum). At first sight, this cooling trend appears to be rather gradual, but looking closer to the curve it becomes obvious that Earth’s climate system cannot be described by simple mathematical formulas. The Weichselian cooling trend is interrupted by relatively short millennial-scaled, but rather abrupt warming events. These shifts are interstadial periods like for example the Brørup interstadial which correlates with the MIS 5c stage. Understanding how the Earth’s climate system evolved during these warmer intervals is one of the main research goals for this thesis research.

2.4.1.1 Records and proxies

These important climatic and environmental shifts are recorded in a multitude of archives, retrieved from different environments. Examples are marine archives such as sediment cores and terrestrial archives including lake cores, speleothems and ice cores. Each record or paleoclimatic archive provides another perspective on these

climatic and environmental changes, but of course each type of archives has its own strengths and limitations.

Ice cores hold information on the changes in the atmosphere and can be used as a proxy for temperature, but have also an important local component (NGRIP Members, 2004; NEEM Members, 2012). Sea surface and deep-sea temperatures and changes in salinity are stored in marine records (Shackleton, 2003). In contrast, terrestrial records are mostly used to study changes in vegetation patterns (Woillard, 1978; de Beaulieu and Reille, 1992). However, speleothems for example, also yield information on relative temperature and precipitation changes (Fairchild et al., 2006). Each proxy in the above-mentioned archives records various effects of climate change, for example $\delta^{18}O$ in Greenland ice cores provides information on absolute temperature changes whereas the dust content can be used as a proxy for aridity (NGRIP Members, 2004). In order to get a better understanding of the climate system, which is one of the main objectives of all paleoclimatic studies, it is important to compare different archives with each other. However, this implies that for each archive a good and independent chronology can be constructed, which is often problematic (Govin et al. 2015). The accurate and independent chronology potentially provided by speleothem records illustrates why these records are so valuable for continental paleoclimate reconstructions (Wohlfarth, 2013).

2.4.2 An overview of the early Weichselian climate

2.4.2.1 Last interglacial – glacial climate transition

It is believed that changes in solar insolation at high northern latitudes are a major driver in orbital-scale climate change and could have triggered a cooling that caused the climate, due to series of subsequent feedback mechanisms, to gradually shift from warm interglacial to colder glacial conditions. First signs of a changing climate are observed as changes in vegetation cover in the northern latitudes as early as 120 ka (Helmens, 2014; Wohlfarth, 2013). However, these records are poorly constrained in time making it hard to mark this as the Eemian-Weichselian transition. Contributing to this complexity, is the fact that the Eemian is defined based on the occurrence of temperate trees. Consequently, the Eemian will last longer in southern Europe than in northwestern Europe. In Belgium for example, the Eemian lasted until 117,5 ka (Tzedakis et al. 2003; Vansteenberge et al., 2016).

Although many scientists have worked and are still working on this import climatic transition, the exact order and magnitude of all mechanisms creating this abrupt climatic shift is still unknown. For example, ice sheets could already have started to form at the end of the Eemian period as a response to lower summer insolation values. In turn, this could have created changes in vegetation in the higher latitudes (forests are being replaced by grasses as the treeline moves southwards). This change in vegetation would then have increased the albedo, which lead to decreased land surface temperatures (Schurgers et al., 2007). This is a good example of a positive feedback mechanism; the formation of ice sheets has a positive effect on the growth of the ice sheets itself. Another example of such a positive feedback mechanism is brine rejection during the formation of sea ice, which influences the circulation pattern of the Atlantic Ocean brings more moisture towards the higher latitudes and has a positive effect on the growth of the ice sheets. Both feedback mechanisms become gradually stronger with an increasing sea ice cover (Wohlfarth, 2013).

2.4.2.2 Dansgaard-Oeschger climate variability during the early Weichselian

As discussed before the Weichselian cooling towards the Last Glacial Maximum was definitely not a gradual cooling event, but was marked by a multitude of different abrupt warming pulses, these pulses are better known as the Dansgaard-Oeschger events and have shaped the climate during the last glacial period. Evidence for this climate variability can be found in a multitude of different marine and terrestrial records. In the following paragraphs these different types of records are discussed and particular attention will be given to the timeframe in which the PNG-01 stalagmite was formed, the Brørup interstadial, which is equivalent with the MIS 5c stage in marine records, and to the mechanisms explaining this Dansgaard-Oeschger millennial scale climate variability.

2.4.2.2.1 Orbital forcing and solar insolation

Shifts between glacial and interglacial periods on earth are controlled by changes in the different orbital parameters of the earth (precession, obliquity and eccentricity, all having a specific recurrence interval) because these parameters control the amount of solar radiation received on earth and subsequently the activity of a large amount of feedback processes in every component (atmosphere, hydrosphere, cryosphere, lithosphere and biosphere) of the climate system (Köhler et al., 2009).

Figure 17 shows the computed values of June insolation for three latitudes in the Northern Hemisphere for the last 150 000 years. The original data was obtained from Berger and M. F. Loutre (1991). To render the interpretation of these curves more straightforward, the ages of the SPECMAP MIS-stages as defined by Martinson et al. (1987) are also indicated. The MIS-stages seem to correlate very good with the changes in solar radiation. For example, the Last Glacial Maximum appears to correspond with a minimum in solar radiation, while the start of the Eemian (MIS 5-6 transition) is probably linked with a maximum in solar radiation. This is one of the main reason why scientists believe that changes in solar insolation are most likely the trigger for orbital-scale climate change. The exact insolation values also depend on the latitude, nevertheless the general trends are almost exactly the same (Berger & Loutre, 1991).

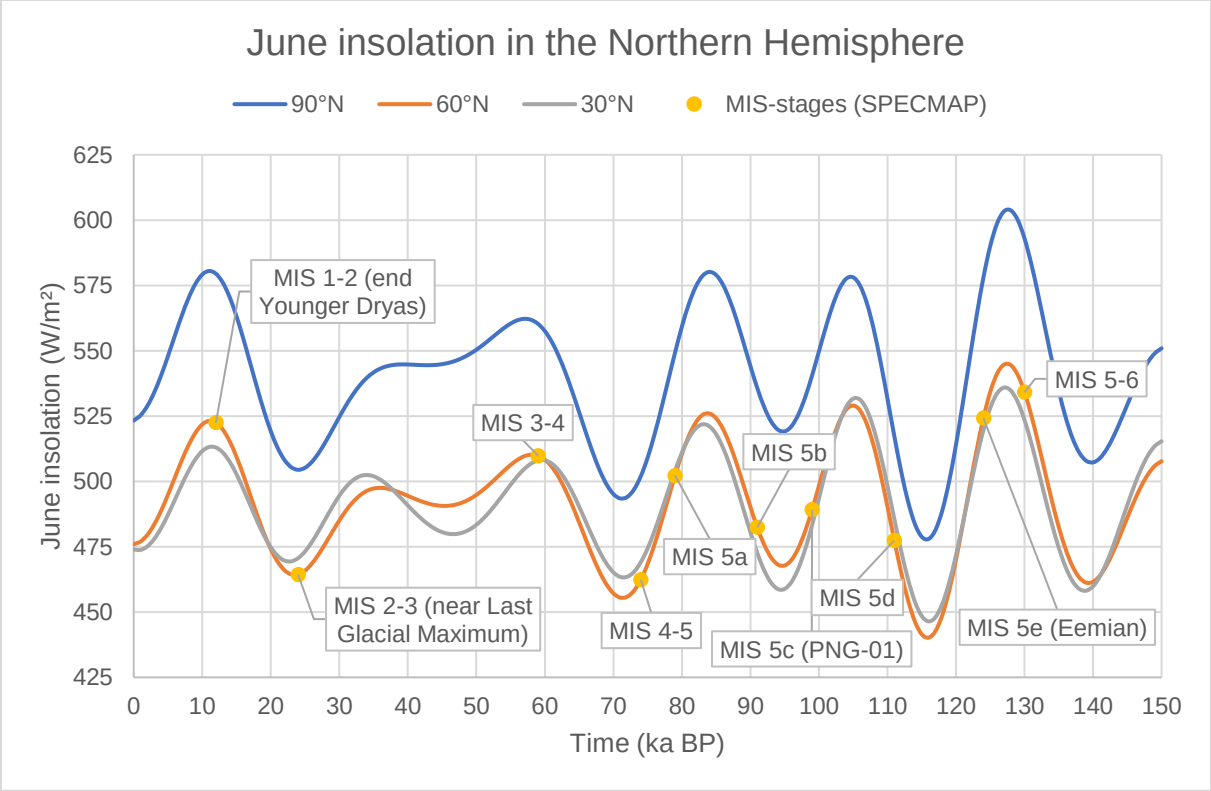

Figure 17 - June insolation computed for 30, 60 and 90°N for the last 150 000 years (original data: Berger et al., 1991)

At around 127 ka June insolation started to decrease and a minimum in insolation was reached at around 114 ka. This minimum corresponds with the MIS 5e-5d transition in northern Europe. After reaching this minimum, insolation started to increase again until at around 104 ka a new maximum is reached, which corresponds to MIS 5d-5c transition. A next minimum was reached at around 94 ka (MIS 5c-5b transition).

Considering the preliminary dating of the PNG-01 speleothem, the period of stalagmite formation almost exactly corresponds with the continuous decrease in solar insolation observed from 104 to 94 ka. Nevertheless, there was speleothem formation during a solar minimum (94 ka). Knowing that liquid water is required for speleothem formation, this could be an indication that the Fennoscandian ice sheet did not cover Belgium at that time or it could indicate that a minimum in solar insolation is only a precursor for a minimum in temperature. In other words, this solar minimum could have been the trigger for different feedback mechanisms leading to an even stronger decrease in temperature.

2.4.2.2.2 Changes in sea level and ice volume

Lambeck et al. (2002) reconstructed relative sea-level fluctuations for the past three million years. However, only for the last 130 000 years, direct, accurate and high-resolution observations for past sea levels, radiometrically dated corals combined with stratigraphic evidence, exist. Going back further in time oxygen isotopes in foraminiferal assemblages from marine cores can be used as proxy for sea-level because these oxygen isotopes reflect changes in continental ice volume, which is linked with sea-level change (Lambeck et al., 2002).

The relative sea-level curve (figure 18) seems to correlate with the insolation changes. In general, lower insolation values correspond with lower relative sea-levels although the two curves do not line up perfectly. Relative sea-levels reached values of up to -70 m during the Weichselian glaciation when compared to the present-day levels and during the Eemian interglacial, the sea-levels were even higher than the present levels. Please note that this curve has the oldest ages on the left side of the graph in contrast with all the other figures used throughout this section. The dataset of this curve is not publicly available, which explains why the curve from the original paper is presented instead.

During the MIS 5c stage, the relative sea-level curve shows a gradual decrease from around -20 to around -50 m, which is then followed by smaller scale increase of the relative sea-level of around 10 m at the end of the stage. This gradual decrease at the first half of the stage seems to correspond with the decrease in solar insolation observed in the previous figure. However, the minor sea-level rise in the second half of the MIS 5c stage is difficult to correlate with the insolation curve because insolation

levels were still at a minimum at that point in time (around 94 ka). This seems to suggest that ice-volume changes also depend on some other sub-orbital climate fluctuations (Wohlfarth, 2013).

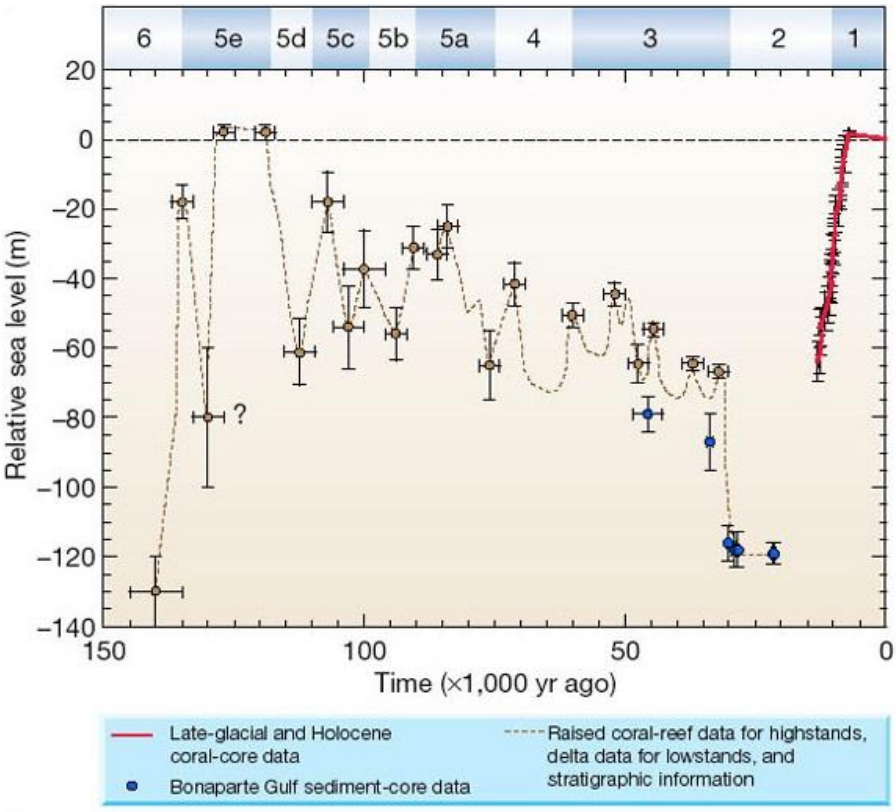

Figure 18 – Relative Sea-level curve between for the last 150 ka, based on U/Th and 14C dated corals and other stratigraphic evidence (Lambeck et al., 2002)

Changes in ice volume are, like long scale sea-level trends, based on oxygen isotope values of foraminiferal assemblages in marine cores. Both benthic and planktonic foraminifera can be used, but benthic foraminifera are preferred because they are, like discussed earlier, less influenced by changes in sea surface temperatures. The SPECMAP-stack is probably the best-known example of a long-scale benthic $\delta^{18}O$ stack (Martinson et al., 1987), but more recently Lisiecki and Raymo (2005) developed the LR04 stack, which spans the last 5,3 Ma and uses 57 globally distributed benthic $\delta^{18}O$ records. On the following page (figure 19) a correlation between both the SPECMAP and LR04 stacks and the benthic MD95-2042 core from the Iberian margin (Shackleton et al., 2000) is made. Note that every curve uses a slightly different age model, so direct correlation is not entirely possible, but because the graph spans 150 ka, the differences between the curves should be rather small. Also, a moving average filter was applied on the oxygen isotope values of the MD95-2042 core to average out

some smaller scale fluctuations. The LR04 stack and MD95-2042 core provide absolute $\delta^{18}O$-values, while the SPECMAP $\delta^{18}O$-values are normalized. Values near the bottom of the graph represent periods with higher ice volumes.

In an ideal world, trends observed in both stacks should be very similar and the core values should also follow the trends of both stacks, keeping in mind that the core has also a small local component. However, some small differences exist between both stacks even though the general trends are rather similar. For example, at around 78 ka the SPECMAP stack shows a local maximum while the LR04 stack has a local minimum at that time, the opposite is true at around 84 ka. This could be the consequence of the fact that both stacks use a different age model, however, more pronounced minima and maxima, for example at 18 and 135 ka, do line up quite well in both curves. Other explanations for the differences between both stacks could be the fact that the SPECMAP curve has less data points and thus a lower resolution or that more recent techniques and methods simply deliver other and maybe better results. This last explanation could then also explain the better correlation between the MD95-2042 core and the LR04 stack which are both more recent than the SPECMAP stack. Of course, none of these explanations completely rule out the other ones. It should also be noted that due to the differences between the LR04 and SPECMAP stack, they both define slightly different definitions of the different MIS-stages.

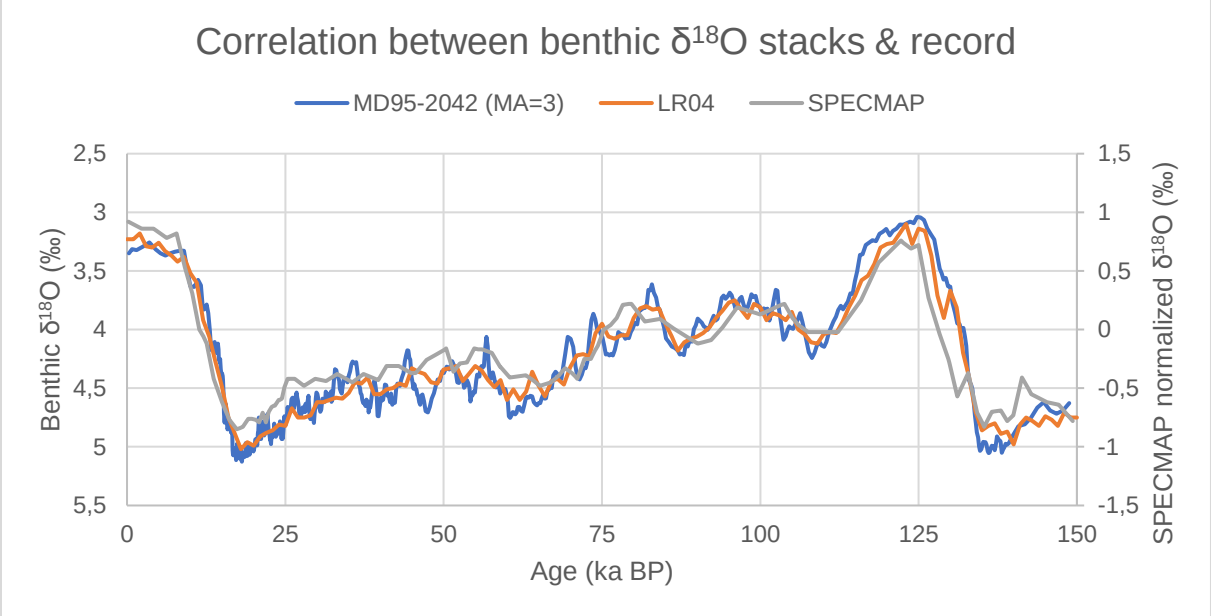

Figure 19 – Correlation between different benthic stacks and a benthic record from the Iberian Margin for the last 150 000 years (Original data: Lisiecki and Raymo, 2005; Martinson et al., 1987 and Shackleton et al., 2000)

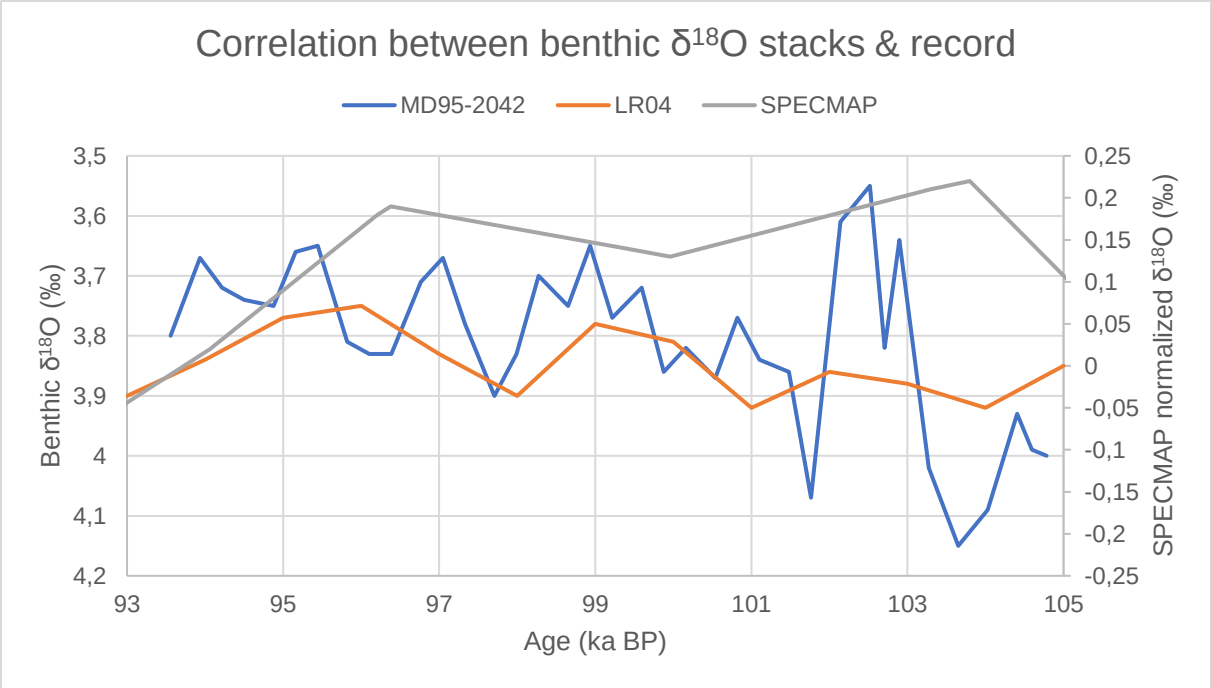

Figure 20 – Correlation between different benthic stacks and a benthic record from the Iberian margin for the PNG-01 timeframe (Original data: Lisiecki and Raymo, 2005; Martinson et al., 1987 and Shackleton et al., 2000)

Looking more specific at the MIS 5c timeframe (figure 20), it appears that differences between the stacks and record are quite significant, but keep in mind that the scales on the y-axis are different compared to the previous graph. In general, all three curves suggest a quite stable and relatively warm climate with relatively low changes in continental ice volumes. Only the SPECMAP curve seems to fit with the changes in insolation and relative sea-level previously observed, both of which suggested a cooling trend with build of ice sheets, however the differences between the curves are quite small, so it is hard to tell how different these records really are.

2.4.2.2.3 Ice core records

Ice cores are unique paleoclimatic records as they contain a continuous record of the oxygen and hydrogen isotopes of rain falling onto the ice sheets. Because fractionation of these isotopes is mainly controlled by temperature, variations of the isotope ratios reflect global climate fluctuations. In that respect ice core records are similar to marine isotope records. The main benefit of ice core records is that they provide scientists with an independent chronology (Bell & Walker, 2005) by using for example incremental dating methods like layer counting. Ice cores are valuable as paleoclimatic records because they also contain information on a multitude of other parameters of our climate system. For example, air bubbles trapped inside the ice can provide a record of past atmospheric conditions and windblown dust and ashes settled on the ice can be used

as proxies for wind patterns (Riebeek, 2005). However, a discussion on these other type of proxies is beyond the scope of this thesis.

The record obtained by the North Greenland Ice Core Project (NGRIP) is visualised on figure 21 and covers the Holocene, the entire last glacial period and a part of the Eemian period (up to 123 000 years BP) and confirmed the existence of the abrupt climatic shifts during the last glacial already discovered in other records (NGRIP Members, 2004), the so-called Dansgaard-Oeschger events. Figure 21 displays the $\delta^{18}O$-record obtained from the NGRIP ice core (lower $\delta^{18}O$-values correspond with the lower temperatures). The timeframe in which the PNG-01 stalagmite developed is also indicated.

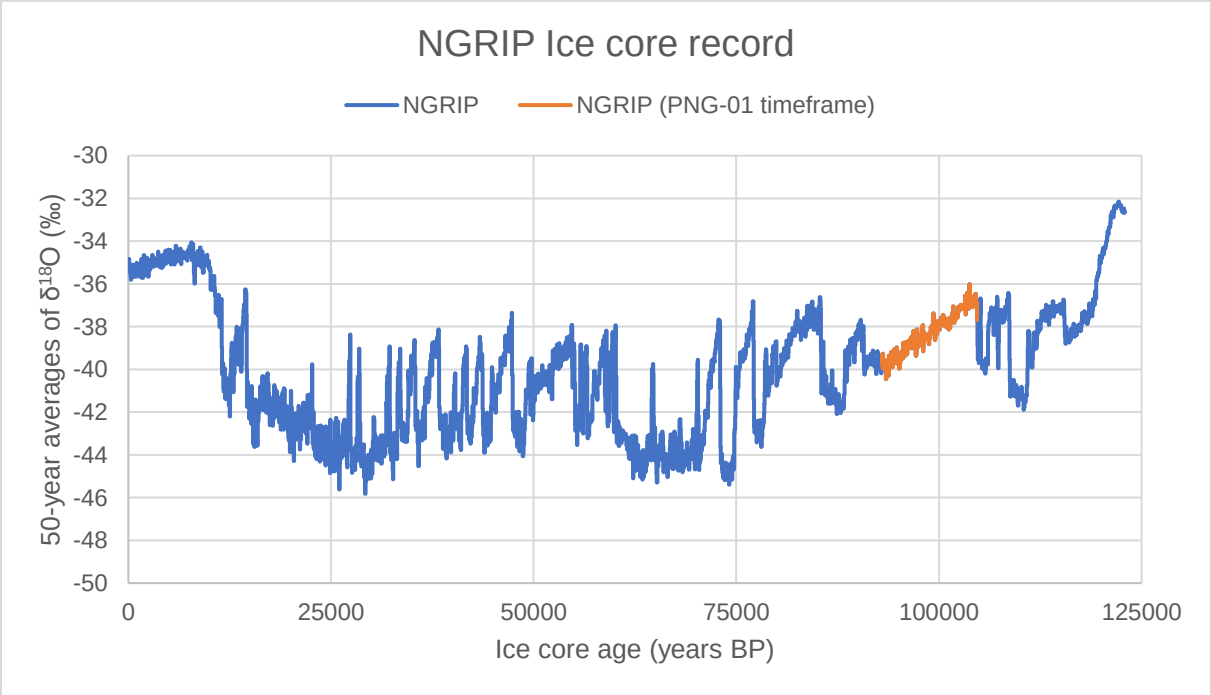

Figure 21 – NGRIP Ice core record for the last 123 000 years (original data: NGRIP Members, 2004)

Although the NGRIP record shows large-scale fluctuations during the Weichselian glaciation, the gradual decrease observed during the time of speleothem formation is immediately apparent. This almost linear decrease (R^2 is close to 1) of the $\delta^{18}O$-signal points towards a gradual decrease in atmospheric temperature, which closely corresponds with the gradual decrease in solar insolation observed during this timeframe. Also, the change in relative-sea level, based on dated corals, correlates quite good with this curve.

The NGRIP curve is of large scientific importance because it was used to better understand the mechanisms behind the climate fluctuations in the Weichselian. Like other records, the NGRIP record shows different relatively warm and cold periods. Stadial and interstadial periods defined with Greenland ice cores are called Greenland Stadials and Greenland Interstadials (abbreviated GS and GI). Even though these periods closely correlate with the terrestrial stadial and interstadial periods, they should not be mixed up. Figure 22 gives on overview of the different Greenland Stadial and Interstadial periods between 60 and 123 ka. The period of speleothem formation corresponds with Greenland Interstadial 23 (GI23), which is confined between GS24 (around 105 ka) and GS23 (around 92 ka).

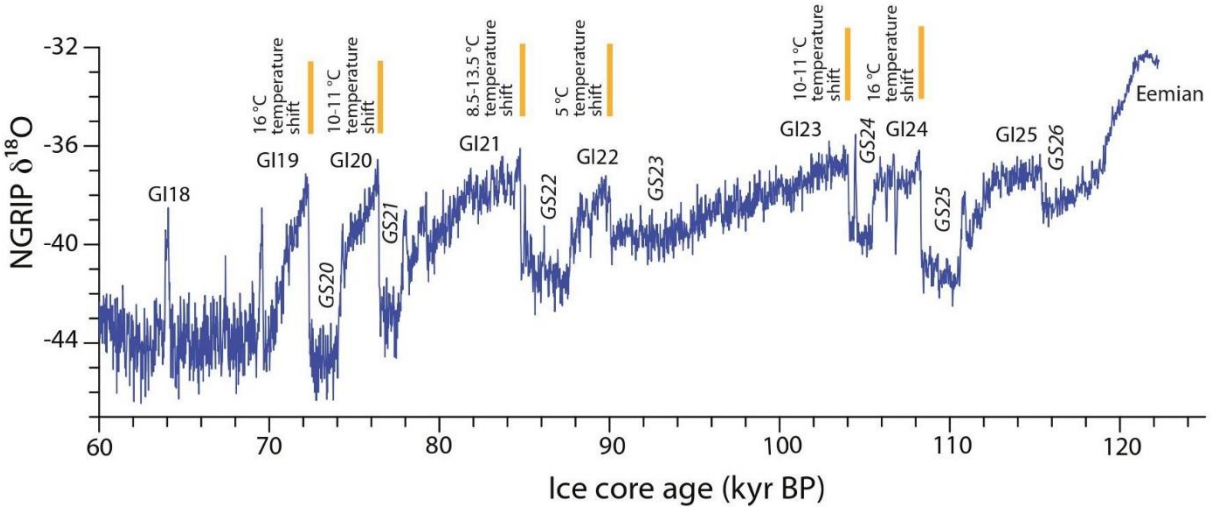

Figure 22 – δ18O record from the NGRIP ice core between 60 and 123 ka (NGRIP Members in Wohlfarth, 2013)

On the NGRIP record Greenland stadial to interstadial transitions appear to be different from Greenland interstadial to stadial transitions. At the end of each stadial, there is an abrupt warming phase which corresponds with a temperature shift between 5 and 16°C (see figure 22). This warming pulse is then followed by a gradual cooling towards the next interstadial. These cycles are better known as Dansgaard-Oeschger or D-O events and during the last glacial period 24 of these events have been counted, using ice core records like this one. The exact causes for these events are complex and still part of ongoing research, but they are most likely linked to changes in the Atlantic Ocean circulation patterns. A possible trigger for these changing circulation patterns could have been the influx of a large volume of fresh water. When ice sheets continuously grow, they can become unstable under their own weight and break up,

bringing large volumes of icebergs, build up out of fresh water, towards the North Atlantic Ocean, the so-called Heinrich events (Bond, 1999; Stocker & Johnsen, 2013).

The NGRIP ice core curve can also be correlated with marine cores (figure 23). In this case, the MD95-2042 core was selected because the MD95-2042 dataset already contained ages on the GRIP-timescale, making correlation more straightforward. A moving average filter was applied on both datasets. Looking closely at the two curves they represent a similar long-term trend and although there is correspondence between the stadial and interstadial ages, the peeks do not line up perfectly. On average, there is a shift of around 1 to 2 ka between the peeks of both curves, in this case NGRIP ages of corresponding events are older than the D95-2042 ages. This could imply that atmospheric changes influence ice volumes and not the other way around.

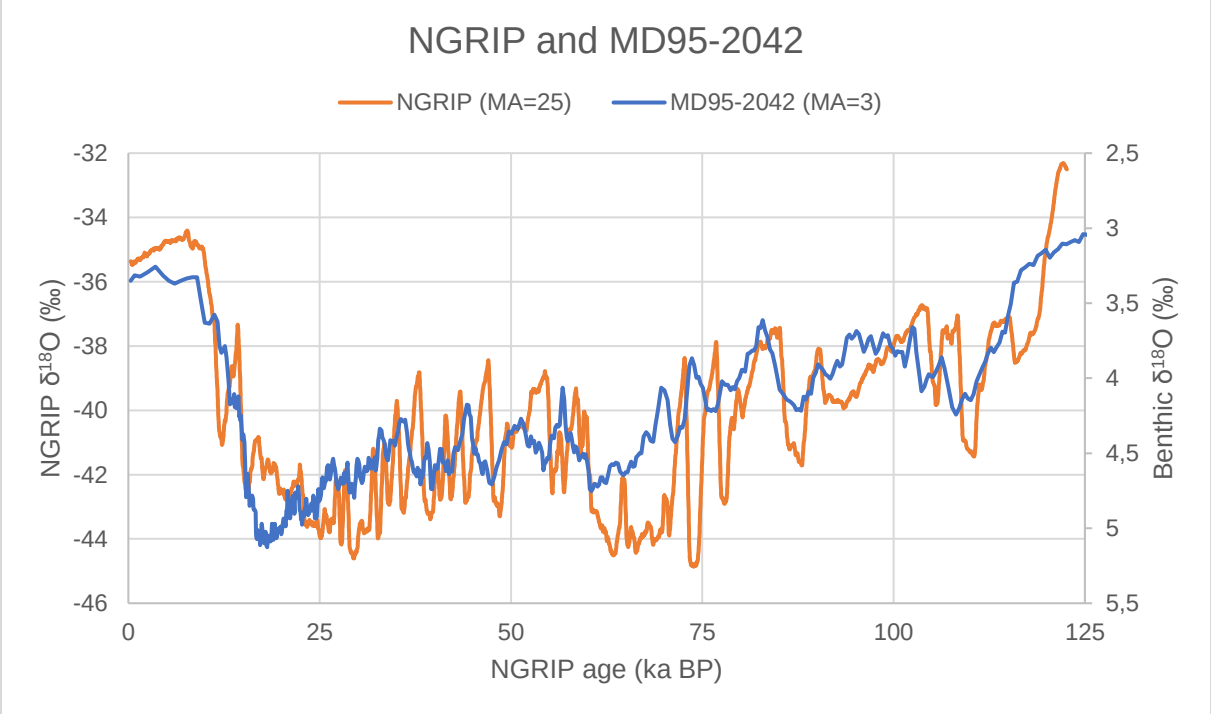

Figure 23 – Correlation between the NGRIP ice core and the MD95-2042 marine core (benthic) from the Iberian Margin (Original data: NGRIP Members, 2004 and Shackleton et al., 2000)

Zooming in on the timeframe of speleothem formation (figure 24), the trend of both curves looks opposite to each other, but keep in mind that the observed differences in the $\delta^{18}O$ signal are relatively small. Like discussed earlier, ice volume appears to be rather stable during this period of gradual cooling and decreasing solar insolation. A major increase of ice volume is only observed at around 93 ka.

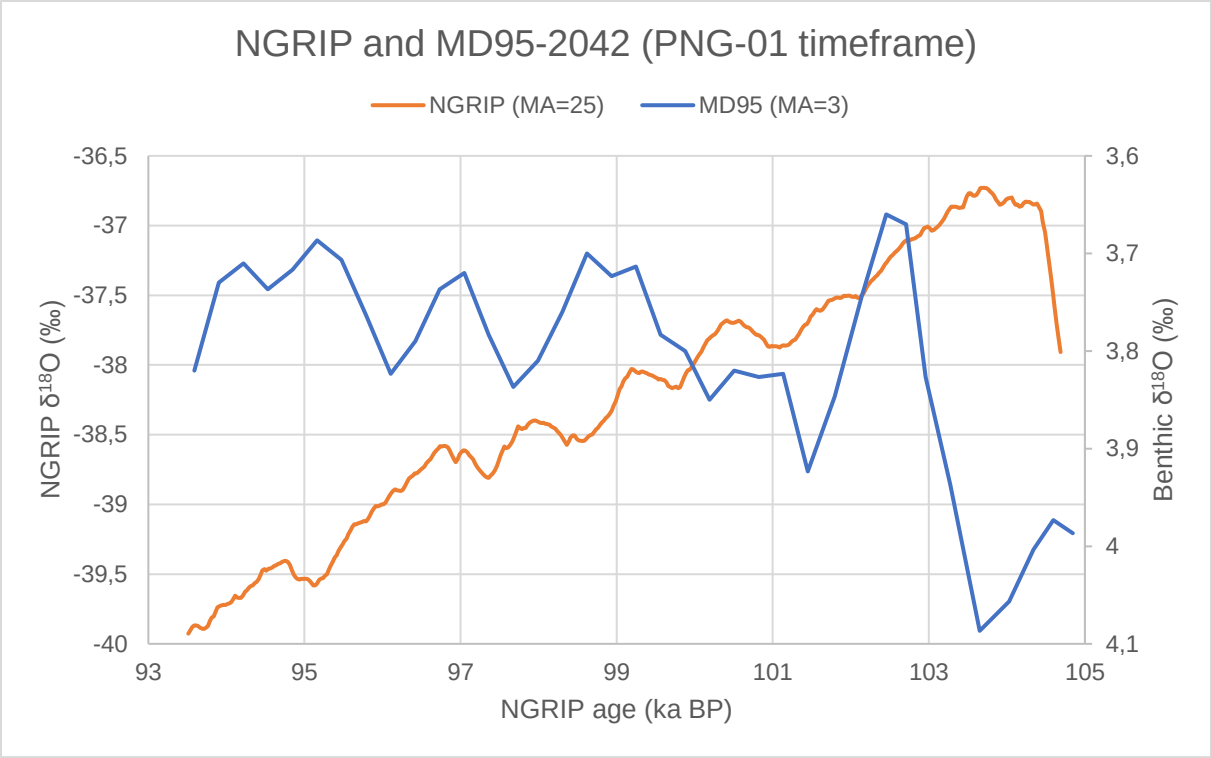

Figure 24 – Correlation between the NGRIP ice core and the MD95-2042 marine record for the PNG-01 timeframe (Original data: NGRIP Members, 2004 and Shackleton et al., 2000)

2.4.2.2.4 Sea surface temperatures of the North Atlantic Ocean

Planktonic foraminiferal assemblages and the possible presence of Ice Rafted Debris (IRD - an indicator of the presence of icebergs) in marine sediments can be used to reconstruct sea surface temperatures (SST). Figure 25 shows the reconstructed temperatures for the North Atlantic Ocean between 60 and 120 ka. According to this specific curve, the MIS 5c period is interrupted by two marine cold events, C22 and C23 (Oppo et al., 2006). However, to some other authors these cold events define the boundaries of the MIS 5c stage, in that case the C23 cold event can be assigned to the MIS 5d-5c transition and the C22 event to the MIS 5c-5b transition (Chapman et al., 2000; Wohlfarth, 2013).

Different studies tried to link and compare the planktonic and ice core records with each other to verify if Greenland interstadials correspond with higher sea surface temperatures and stadials with decreasing SST-trend. Because both records have an independent chronology, such a comparison is possible and is presented in figure 26. Looking at this comparison, it is clear that each of the sea surface cooling events observed in the planktonic marine record can be correlated with a Greenland Stadial from the NGRIP record, for example Cold Events 22 and 23 correspond with Greenland

Stadials 23 and 24 (Wohlfarth, 2013). The good correlation between these cold events and stadials gives more confidence in using these events as markers for the MIS 5c period.

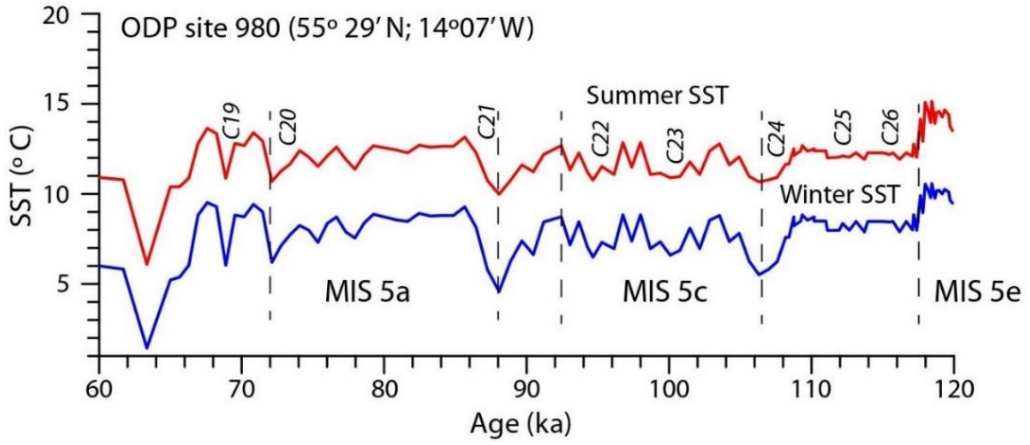

Figure 25 – North Atlantic sea surface temperature reconstructions based on planktonic foraminiferal assemblages (Oppo et al. in Wohlfarth, 2013)

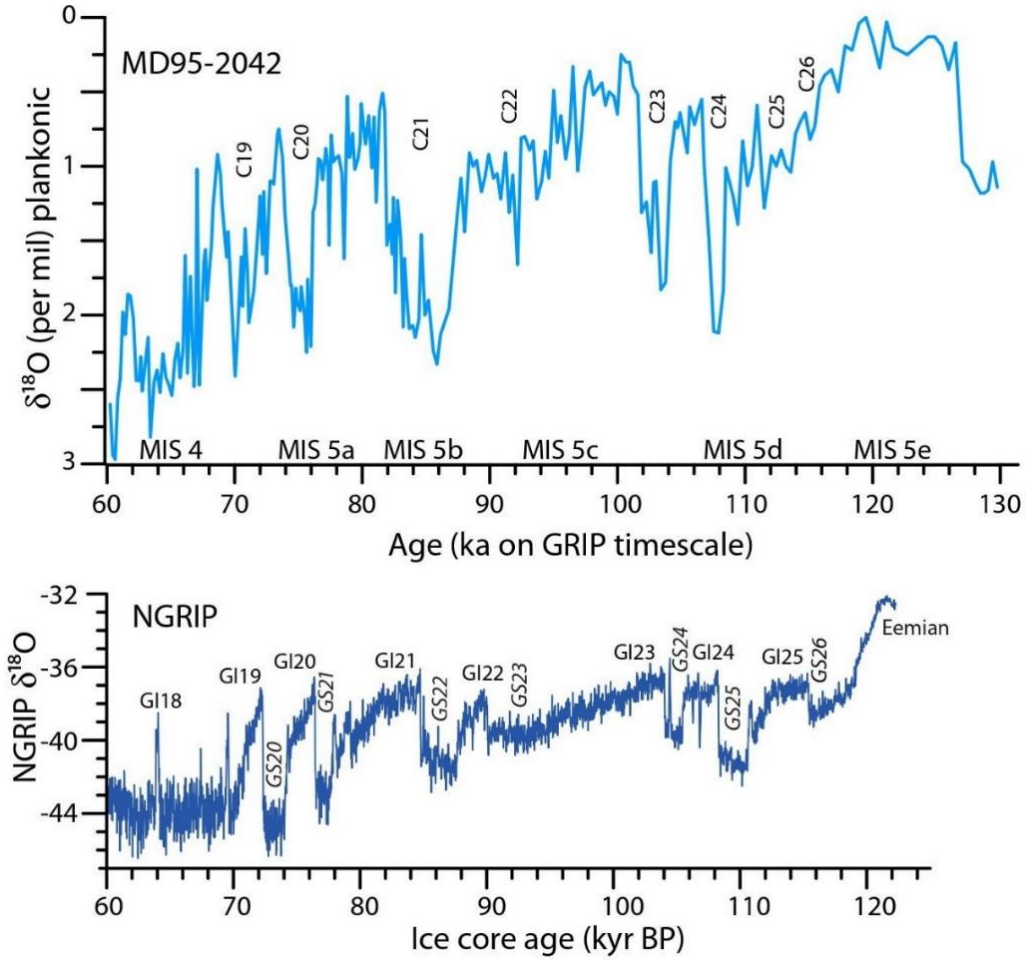

Figure 26 – Comparison between the planktonic and NGRIP oxygen record, clearly indicating the North Atlantic Sea surface cooling events (C26 to C19, upper part) and the Greenland Stadials (GS) and Insterstadials (GI) on the lower part of the figure (Wohlfarth, 2013)

2.4.2.2.5 Pollen records

Pollen grains are derived from seed producing plants and transported by wind, water or animals before they become incorporated in peats or lake sediments where they can be preserved if the conditions remain anaerobic. Because the composition of pollen assemblages reflects the regional vegetation cover, pollen records can, -if they are long and continuous-, serve as a proxy for vegetation and environmental or climatic change. By creating a pollenstratigraphy, they can also be used to reconstruct glacial-interglacial sequences, plant migrations or sea-level changes through time. Indicator species, of which the climatic requirements can be quantified, are in that respect crucial for the interpretation of pollen records (Bell and Walker, 2005). To be able to draw conclusions from these type of records, construction of a good chronology is key. Sometimes optically stimulated luminescence dating of sediments (OSL) or the presence of tephra layers in the sediments (Sirocko et al., 2005) can help in the construction of such a chronology, other times pollen records first need to be tuned to other records which have an independent chronology, for example ice cores (Wohlfarth, 2013).

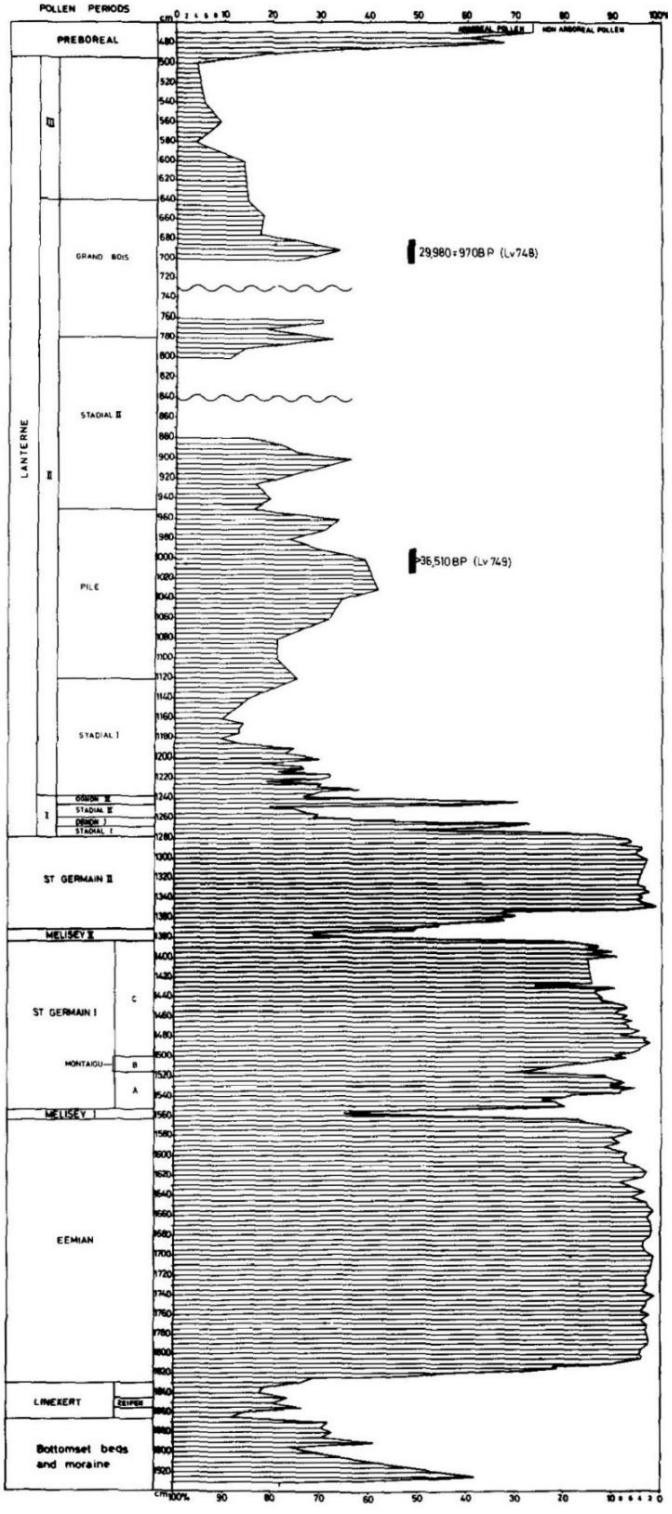

Figure 27 – Palynological sequence of the La Grande Pile peat bog (Woillard, 1978)

2.4.2.3 La Grande Pile peat bog

A pollen record in close proximity to the Père Noël cave is the record of La Grande Pile (figure 27, previous page). It is situated in north-eastern France (47°44′N, 6°30′14″E) at an altitude of 330 m and is located at a distance of only 290 km from the Père Noël cave. The La Grande Pile record was the first record spanning the last climatic cycle in western Europe, it goes back to 140 ka BP, and lead to a revision of the chronology of the last glacial (de Beaulieu and Reille, 1992; Woillard, 1978). A multitude of scientific studies already covered the La Grande Pile cores, which can give an indication of the quality and resolution of these peat bog cores.

The pollen record describes two interstadial periods, Saint Germain I and II, after the Eemian interglacial period. These interstadials correspond with the Brørup (MIS 5c equivalent age) and Odderade (MIS 5a equivalent age) interstadials discussed in the introduction of this chapter. The Saint Germain interstadials are separated by two colder phases, the Melisey I and II stadials (MIS 5d and 5b equivalent ages). The Saint Germain interstadials are characterized by a vegetation evolution from very cold forests to climax forests, followed by a return of cold forests. More specifically there is transition from tundra to taiga, to mixed forest and acid forest and then back to tundra via taiga, which can be interpreted as an important warming event followed by a (gradual) cooling. The Melisey stadial periods on the other hand are marked by the development of steppe species and the presence of subarctic and subalpine species, which are all indicative of a dry and cold climate. During these cold periods, the forests were destroyed and replaced with an open landscape, ready to be recolonized in the next interstadial period (Woillard, 1978).

These changes in vegetation are visualised in figure 27 on the previous page. According to this palynological sequence (Woillard, 1978), arboreal or forest cover was on average at least 80% during the Saint Germain I interstadial period, which corresponds with the period of speleothem formation. After a small drop during the Mointagu cold event, peak values of more than 90% forest cover are reached before the arboreal cover shows a decreasing trend towards the end of the interstadial when the Melisey I stadial destroys a large part of the forest cover.

2.4.2.4 Eifel Maar deposits

Maar (crater lake) deposits in the German Eifel region contain another detailed record of the vegetation changes in north-western Europe during the last glacial cycle. These records are interesting because the Eifel region is situated close to the Père Noël cave at a distance of around 150 km. A multitude of cores were collected from different dry maar lakes to create different stacked records, the ELSA (Eifel Laminated Sediment Archive) project. One of the research goals of this project was to get a better understanding of the Eemian-Weichselian transition and the subsequent glaciation in Europe (Sirocko, 2016; Sirocko et al., 2005).

The ELSA greyscale stack, is one of these ELSA records and indicates how light or dark varve layers of a core are on a scale from 0 to 1 (the lighter the varve, the closer the value to 1). Varve sediments become darker when the amount of organic carbon is high, indicating warm climates with a vegetation cover, and lighter when the amount of silt-sized quartz grains in the sediment increases, which points towards colder and drier climates. This explains why the greyscale stack can be used as a proxy for paleoclimatic change (Sirocko et al., 2005).

On the figures on the next page (figures 28 and 29), the ELSA greyscale stack, which has been dated with a multitude of different dating techniques like radiocarbon, luminescence and radionuclide dating, is compared to the NGRIP record. In general, the similarity between the two curves is quite good. However, during the Holocene and the last interglacial period similarity is lower because the interglacial laminae consist of both dark organic carbon-rich layers and light calcite and diatom layers (Sirocko et al., 2005). Looking at the graph showing the same comparison for the timeframe of speleothem formation (figure 29), the ELSA stack shows more variation than the NGRIP record, which implies that there were some distinct shifts in vegetation cover. In general, the climate was relatively wet and warm because the maar deposits contain a good amount organic matter (the ELSA greyscale values are mostly between 0,4 and 0,6). These shifts do not completely line up with the observations in the benthic marine and ice core records discussed earlier.

Of course, it would be an oversimplification to assume that vegetation above the Père Noël at that time completely corresponded with the vegetation in these parts of Germany and France, but knowing that both regions have the same Köppen-Geiger climate classification as Belgium, Cfb (Peel et al., 2007), and the distances between

these regions and the Père Noël cave are relatively small, the observed vegetation patterns would have been probably very similar. Pollen records throughout Europe all show a very similar pattern of two cold stadials with steppe vegetation and two warmer interstadials with expansion of forests and woodlands after the Eemian-Weichselian transition (Wohlfarth, 2013). In conclusion, for the timeframe of interest, pollen records point towards a relatively warm and wet interstadial climate dominated by (boreal) forests and with some shifts in vegetation.

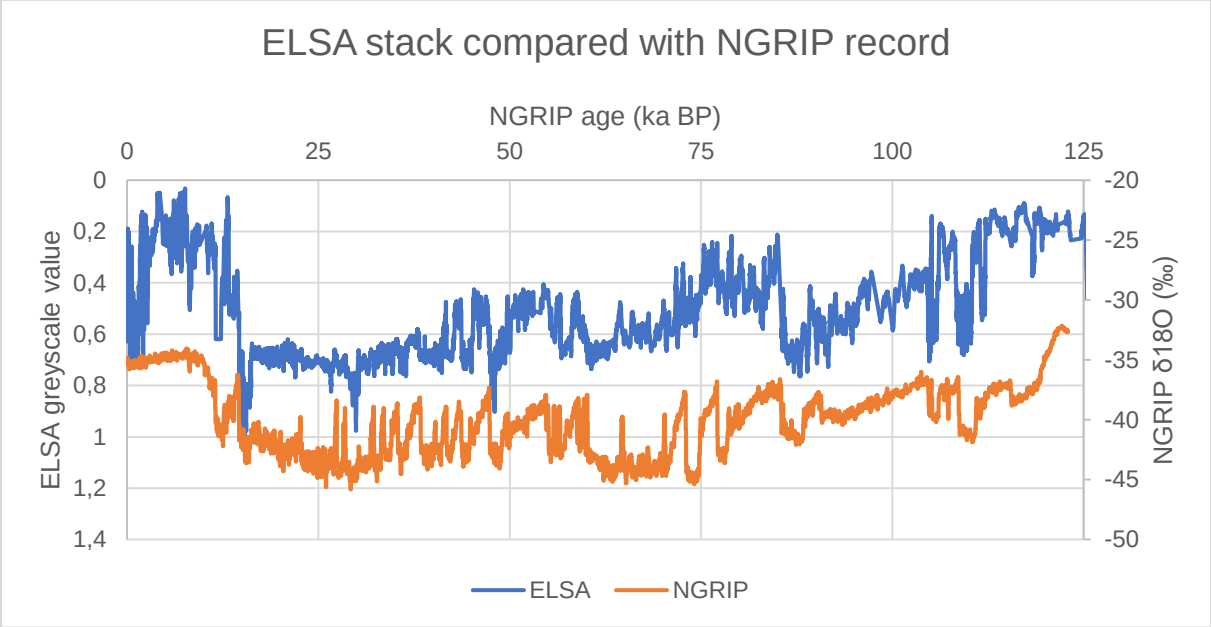

Figure 28 – Comparison between the ELSA greyscale and the NGRIP records for the last 125 ka (original data from NGRIP Members, 2004 and Sirocko et al., 2005)

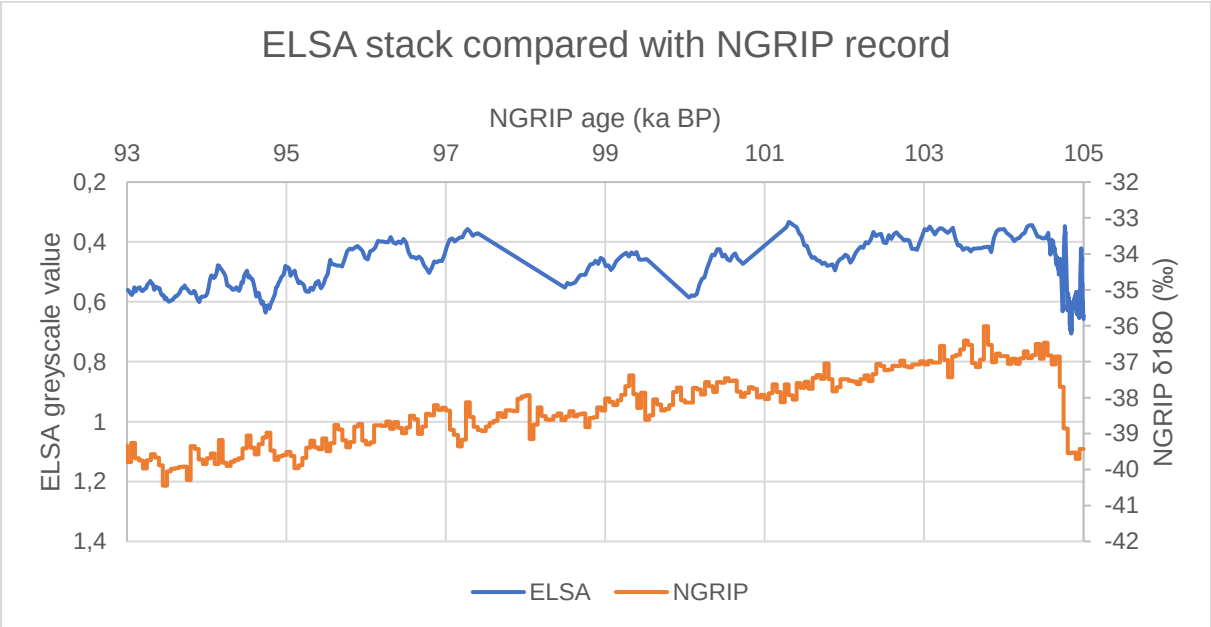

Figure 29 – Comparison between the ELSA greyscale stack and the NGRIP records for the timeframe of speleothem formation (Original data from NGRIP Members, 2004 and Sirocko et al., 2005)

2.4.2.4.1 Speleothems

Like ice core records and some pollen archives, speleothems are one of the few paleoclimatic records with a completely independent chronology. Boch et al. (2011) described a speleothem dataset based on seven different speleothems situated in the northern Alps, the NALPS record. In the Alps, the oxygen isotopic composition of regional meteoric precipitation, which ultimately forms the speleothems, is strongly connected with temperature, higher $\delta^{18}O$-signals correspond with higher the temperatures. Figure 30 shows a comparison of the NALPS record with the NGRIP record. The dashed lines connect the mid-points of major D-O transitions or isotopic maxima and the Greenland interstadials are indicated with grey numbers. In the early Weichselian, the NALPS chronology closely corresponds with the NGRIP chronology, but between ca. 106 and 60 ka the NALPS record suggests slightly younger ages of the stadial and interstadial transitions and also a longer duration of the stadial following Greenland Interstadial 22 (Boch et al., 2011). Nevertheless, there appears to be a good correlation between the Greenland ice cores and the Alpine speleothems.

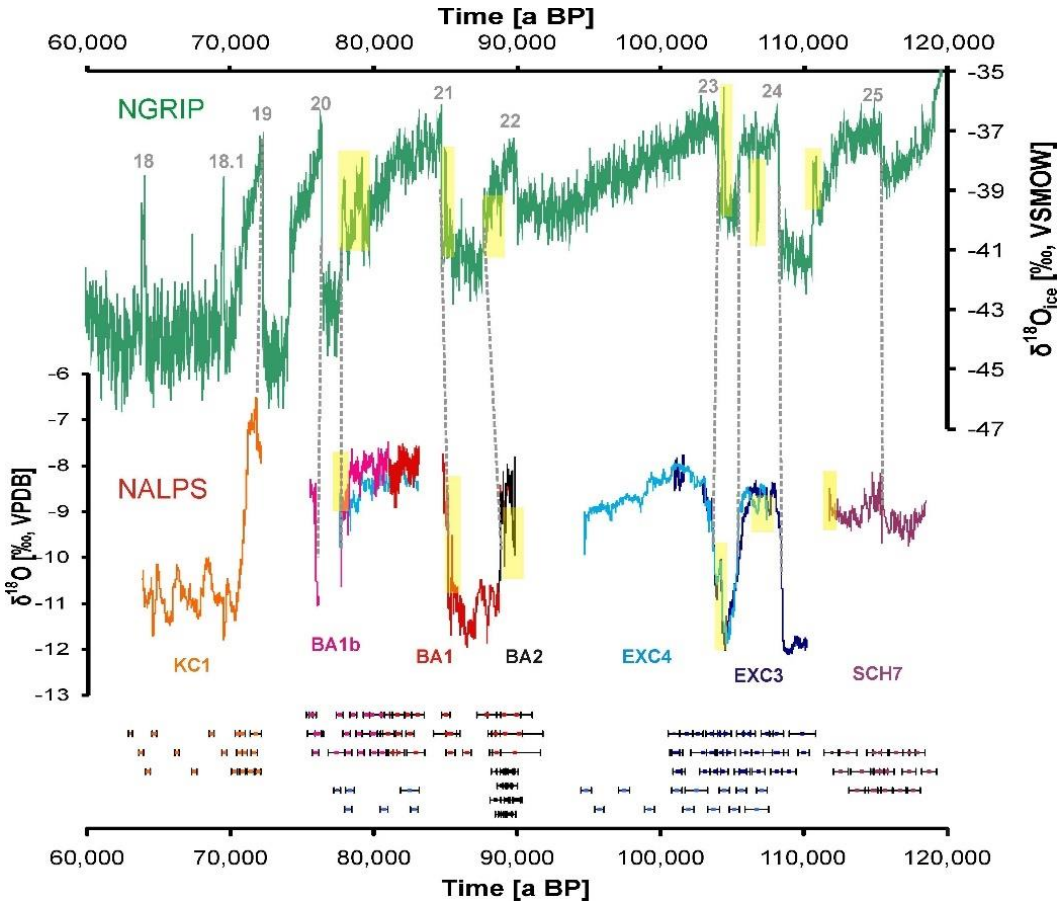

Figure 30 – The Complete NALPS record compared to the NGRIP ice core record (Boch et al., 2011)

On figure 31, a subset of the NALPS dataset is shown, more precisely the record of the EXC4-speleothem, which covers the timespan of interest for this thesis research. Taking only the section between 94.5 and 103 ka into account, the EXC4-record shows decrease in temperature over time. This matches the decreasing trend observed in the NGRIP record, which suggests a close correlation between these two records. Note that the rate of change is higher for the NGRIP record. The sudden increase of temperature at the start of the MIS 5c period is delayed with around 1.5 ka in the NALPS record when compared to the NGRIP record. This could potentially suggest that climate at lower latitudes shows a slower response to changes in solar insolation. This would then also imply that in the PNG-01 record, the abrupt increase of temperature at the start of the MIS 5c stage should be situated between around 105 (NGRIP) and 103 ka (NALPS) because the Père Noël cave is situated north of the Alps and south of Greenland.

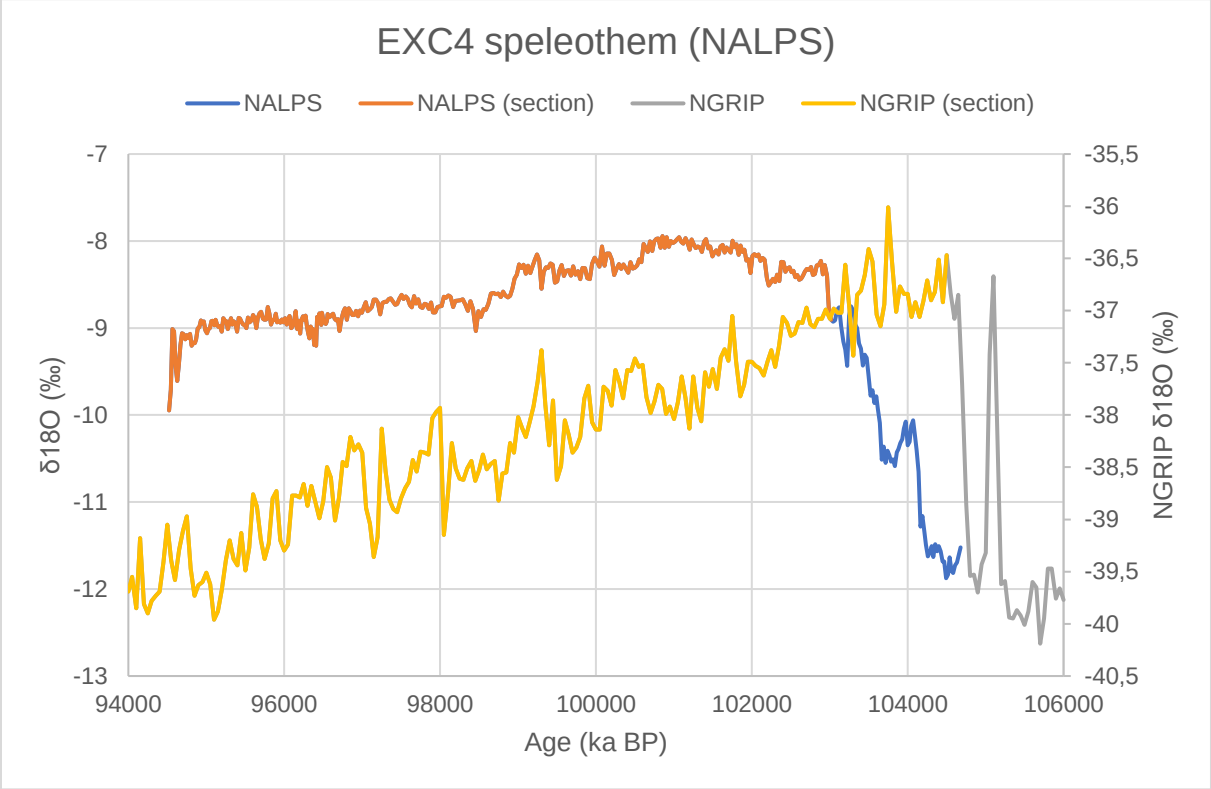

Figure 31 - EXC4 speleothem (NALPS) compared to NGRIP (Original data: Boch et al., 2011; NGRIP Members, 2004)

2.4.3 Summary of paleoclimatic situation

A multitude of different paleoclimatic records were studied in the previous paragraphs. Each record stores the climatic change in a unique and different way. This explains why correlations between different records are far from straightforward and remain one

of the most difficult aspects of paleoclimatic research. Although the large-scale trends can be more or less found in all proxies, a closer look at the different curves shows distinct differences. Explaining these differences is not always simple and the reality is that even today the exact sequence of events and feedback mechanisms leading towards the abrupt changes in climate seen in the last interglacial period, remains unclear.

Nevertheless, a good description of the climatic conditions during the MIS 5c period, which more or less corresponds with the timeframe of PNG-01 speleothem formation, is possible, based on the proxies discussed on the previous pages. In short, the MIS 5c period is the oldest interstadial of the last glacial period on earth, depending on the record, this warmer period is also referred to as the Brørup or the Saint Germain I interstadial. It was a period marked by a decrease in solar insolation, which appears to be linked with a decrease in relative sea-level. The start of this period is defined by a rapid and positive temperature shift of around 10-11°C, which was then followed by a relatively minor decrease in temperature over a period of around 10 ka, a trend which can be observed in both the ice core and speleothem records. The marine cores and pollen records on the other hand, point more towards a rather stable and relatively warm climate, which allowed for an expansion of the (boreal) forests. In reality, it is most likely a combination of both.

3 MATERIALS AND METHODS

3.1 INTRODUCTION

In the previous section of this thesis, the different proxies used for speleothem paleoclimate reconstructions were discussed. This section includes an elaborate description of the different analytical methods that were applied to obtain the different proxy records from the PNG-01 stalagmite. The first step of constructing proxy time series is constructing an accurate age-depth model. For this, thirteen samples were taken along the growth axis of the speleothem and radiometrically dated. Afterwards, a macro-morphological description of the stalagmite was carried out. For the proxy time-series, 197 samples were retrieved for stable isotope ratio measurements ($\delta^{18}O$ and $\delta^{13}C$). In addition, 94 of these samples were also analysed for their trace element concentration to increase the number of proxies for paleoclimate reconstructions.

Figure 32 – The PNG-01 speleothem, orange tape was used to indicate distances from the top (dft) of the stalagmite. The left side of the image shows the polished slabs, the right side the core half

The PNG-01 sample (figure 32) consists of a 1015 mm long core that was retrieved from the Gibraltar speleothem located in the Père Noël Cave. The core was cut in half using a diamond saw: one half is used for scientific analysis while the other halve is archived in the collection of the Royal Belgian Institute of Natural Sciences (RBINS). From the core halve, a ca. 10 mm thick slab was cut and polished with sandpaper (figure 32). A distance scale was created on the slabs with distances expressed as 'distance from top' (dft) in mm.

3.2 U/TH-DATING

In August 2016, 13 samples, labelled G-1 to G-13 (table 2), were taken at strategic places along the growth axis of the PNG-01 speleothem. The main target here was to take enough samples to construct an age model of good quality for two main reasons: 1) proxy time-series need to be as accurate as possible and 2) in temperate climate areas, speleothem growth is an indicator of warm/wet climate conditions and therefore speleothem growth is by itself an important paleoclimate proxy. However, U/Th-ages are expensive and destructive (they require 100 to 500 mg of sample material that cannot be recovered after analysis) and therefore the amount should be limited. Keeping this in mind, samples were taken at depths of specific interest, e.g. top and bottom of the speleothem and discontinuities that might represent a hiatus.

Sample ID	Empty vial (g)	Vial + sample (g)	Sample (g)	dft (mm)
G-1	0,93603	1,15029	0,21426	3
G-2	0,95088	1,17758	0,22670	96
G-3	0,95032	1,21964	0,26932	100
G-4	0,94217	1,18160	0,23943	198
G-5	0,94972	1,20935	0,25963	310
G-6	0,94616	1,25756	0,31140	316
G-7	0,94187	1,20757	0,26570	329
G-8	0,95470	1,19075	0,23605	393
G-9	0,94559	1,25626	0,31067	498
G-10	0,94962	1,17142	0,22180	602
G-11	0,95059	1,19851	0,24792	713
G-12	0,93841	1,21746	0,27905	816
G-13	0,93710	1,18344	0,24634	883

Table 2- Overview of the samples collected for U/Th-analysis, dft stands for distance from top and marks the stratigraphic position of each sample

The samples were collected with a mechanical drill, which used tungsten carbide drill bits with a diameter of 1 mm. In between the collection of two samples, all equipment was thoroughly cleaned with ethanol and Kimtech tissues. Samples were collected by drilling slots along the internal growth layers. Thickness of these slots was mostly limited to 2,5 mm (see figure 34). The amount of milled calcite powder collected for every sample can be found in table 2.

The milled calcite powder was collected in Eppendorf® containers, sealed with Parafilm® and put in Ziploc® bags and shipped to the University of Minnesota (Minneapolis, USA) for U-Th dating (figure 33). All consumables such as the Eppendorf® vials, pipet tips etc. used for U-Th and trace element sample collection were additionally cleaned with 2M HNO_3 before use. The specifics of the U-Th dating can be found in section 2.2.4. Results were obtained in December 2016. The provided U-Th dates were then used to construct an age-depth model for the PNG-01 stalagmite.

Figure 33 - Sealed samples ready for shipment to the university of Minnesota (Minneapolis, USA)

3.3 AGE-DEPTH MODELLING

The relationship between the position of a proxy data point along the growth axis of a speleothem and the corresponding age is given by an age-depth model. The main objective of constructing an age-depth model is constructing proxy time series for the entire length of the paleoclimate archive based on a limited number of dated depths. Constructing an age-depth model is not always straightforward due to complications with the age dataset such as age inversions and outliers. However, several algorithms have been developed that allow to minimize the effects of these issues.

3.3.1 Algorithms

Commonly used age-depth modelling algorithms for reconstructing speleothem time series are COPRA (Breitenbach et al., 2012), MOD-AGE (Hercman and Pawlak, 2012), OxCal (Bronk Ramsey, 2008) and StalAge (Scholz and Hoffmann, 2011). Each of these algorithms has their own specific advantages and disadvantages. For example, COPRA transfers errors of the ages to the proxy time series, but uses a rather complicated MatLab procedure. MOD-AGE efficiently deals with hiatuses, but the software is again not very user-friendly. OxCal takes into account the error distribution of the individual ages, but was originally designed for 14C age models and calibration. Finally, StalAge has some problems with data points at the limits of the dataset, but is completely open source, user-friendly and deals efficiently with the most common problems observed in speleothems like outliers or age inversions. Because StalAge provides even the non-expert user with an algorithm that has several advantages over the existing methods, this algorithm is preferred for this thesis study.

3.3.2 StalAge

StalAge was specifically programmed to detect and account for outliers and age inversions, it uses stratigraphic information to improve the model, a monotonicity constraint and provides 95%-confidence limits for the uncertainties of the age model. Another benefit of StalAge over the existing methods is that it has no adjustable free parameters, which means that it is easier to reproduce and compare results between different studies. The algorithm itself is written in the open source statistical software R. Starting from the raw data and moving towards the final age model, the algorithm processes the data in three major steps. First, major outliers are identified, after which they can be deleted or the error of the age can be enlarged. Secondly, the age data is screened for minor outliers and age inversions. Finally, the age-depth model and the corresponding 95%-confidence limits are calculated by a Monte-Carlo simulation using 300 iterations. In this final step, the age-depth model is again tested for age inversions (Scholz and Hoffmann, 2011).

According to Scholz and Hoffmann (2011), the StalAge algorithm relies on two basic assumptions:

1. An age model should be **monotonic**. Because speleothems grow from the bottom up and post-depositional redistribution does not occur, the assumption

is made that younger layers are always on top of the older ones even though re-dissolution of calcite and re-mobilisation of U-series isotopes is not entirely impossible. Also, inaccuracy of the U-series ages is possible due to detrital contamination or mistakes made during sample preparation.

2. The **simplest age-distance relationship** (a straight line) is used to avoid over-interpretation of the data.

Of course, also StalAge has it flaws, however, in Scholz and Hoffmann (2011) the performance of the algorithm was tested with synthetic and natural datasets and in all cases, StalAge generally produced appropriate error limits even for uncertain input data. One major disadvantage is the occurrence of substantial changes in growth rate in the boundary areas of a speleothem sample (Scholz and Hoffman, 2011), in other words growth rates at the borders of the final age model should be treated with caution. Another often used algorithm, which is not discussed here, is OxCal. It has several of the same benefits as StalAge, but because StalAge was specifically developed for speleothem research, it requires less fine-tuning and manual input of 'expert-data' which makes the chance of making mistakes due to a lack of experience with the algorithm smaller (Scholz et al., 2012).

3.4 SCANNING THE PNG-01 STALAGMITE

High-resolution digital scans (with a resolution of 2400 dpi) were made of all the eight different sections making up the complete PNG-01 stalagmite. Afterwards, the scans of the stalagmite were loaded into Affinity Designer, a graphical editor comparable with Adobe Illustrator. The background was carefully removed and the individual scans were connected with each other to create a good representation of how the original, unbroken, speleothem would have looked like (see figure 40). These scans enabled a detailed morphological description of the speleothem, which is discussed in chapter 4.

3.5 STABLE ISOTOPE AND TRACE ELEMENT MEASUREMENTS

3.5.1 Sample collecting

To allow for direct correlation between the stable isotope and trace element results, both analyses were carried out on subsets of the same powder. These samples were collected in a similar way as the samples for the U-Th dating. A total of 197 samples were collected at regular intervals of ca. 5 mm. Stable isotope analysis was carried out

on each of the 197 samples and trace elements were analysed on 94 samples. The lower resolution of the trace elements is due to the time-consuming chemistry process prior the ICP-MS analysis. Because the amount of sample material necessary for these two types of analyses is much lower than for the U/Th-age determination, drilling a small hole with a 1 mm diameter tungsten carbide drill bit in the stalagmite at one location yielded enough sample material for both analyses. Wherever possible, coarse crystalline sections in the calcite were avoided because this reduced the chance of collecting material belonging to a different growth layer. This was done by sampling from the same growth layer, but at a different location as can be seen figure 34.

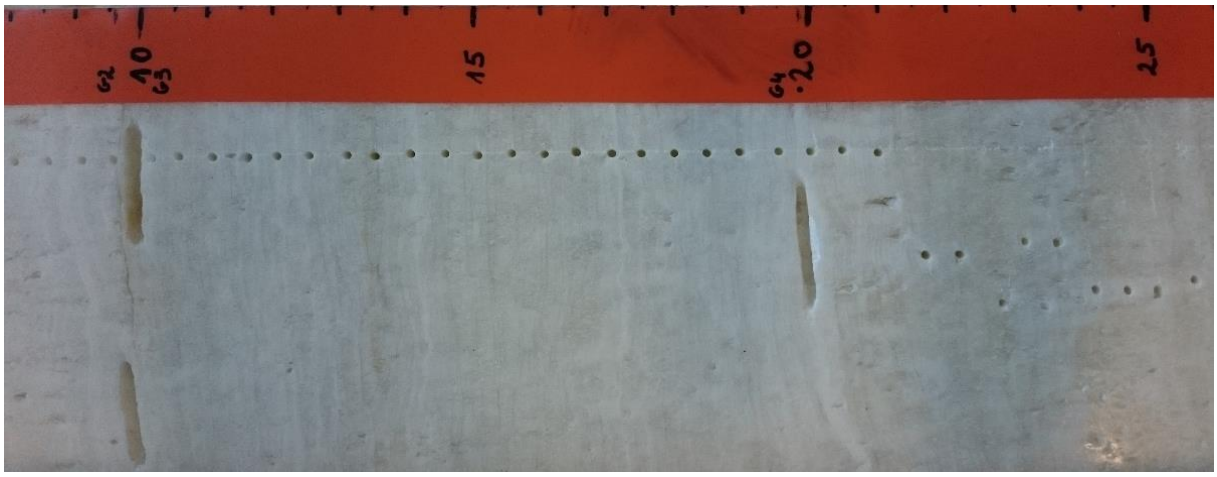

Figure 34 – Trajectory of the sample locations for stable isotope and trace element analysis (small holes) and U-Th dating (large slots) in the youngest section of the PNG-01 stalagmite

After collecting the sample material into sterilized (2M HNO_3) Eppendorf® vials, all samples were carefully numbered and stored in an oven with a constant temperature of 50°C to avoid contamination prior the analysis.

3.5.2 Stable isotopes of oxygen and carbon: Isotope Ratio Mass Spectrometry (IRMS)

The $\delta^{13}C$ and $\delta^{18}O$ stable isotope measurements were carried out at the stable isotope facilities at the Vrije Universiteit Brussel on a Perspective isotopic ratio mass spectrometer (Nu Instruments, UK) coupled to a 'nu carb' automated carbonate device (figure 35). The analyte, in this case CO_2, is introduced into the IRMS through a Dual Inlet system. The state-of-the-art IRMS setup only requires small samples of calcium carbonate, typically between 15 to 150 µg. The nu carb automated carbonate device can hold up to 50 samples and the carbonate preparation procedure is fully automated. Nevertheless, it is important to understand the crucial steps carried out in this process.

Firstly, the selected glass sample vial is brought to vacuum conditions by pumping out all air, after which a controlled amount of phosphoric acid (103%) is injected in the vial. Following reaction occurs, generating the CO_2 gas to be analysed:

$$CaCO_3 + 2H_3PO_4 \rightarrow Ca_3(PO_4)_2 + 3H_2O + 3CO_2$$

Due to the vacuum conditions, both CO_2 and H_2O are in the gas phase. Before the gas phase is transferred cryogenically (cooled with liquid nitrogen) to the dual inlet, it passes a water trap. The water trap temperature is maintained at -80 °C, removing all the water from the gas phase. Within the dual inlet, the sample gas is balanced with a reference gas and hereafter both gasses are alternatingly introduced into the spectrometer and measured. When all vials are analysed, the results are stored in an Excel-file (Nu Instruments, 2017).

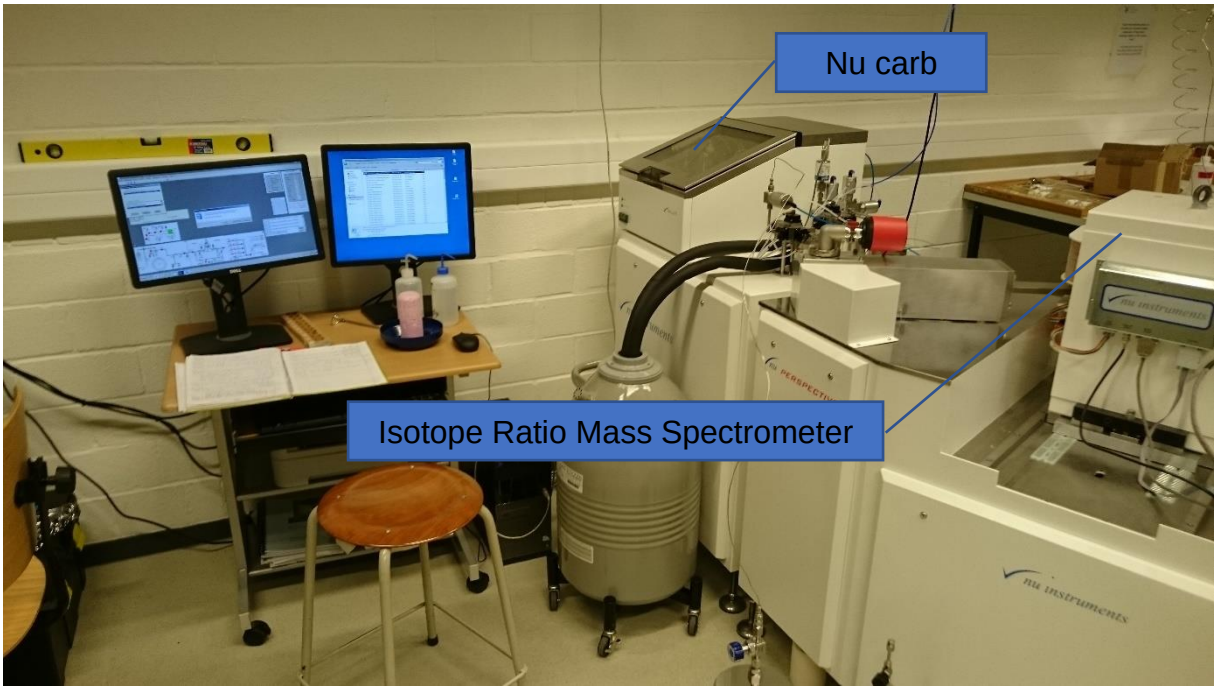

Figure 35 - Nu carb automated carbonate device coupled to the Isotope Ratio Mass Spectrometer (AMGC lab at the VUB)

In this study, each batch contained 42 vials consisting out of 32 samples and 10 vials of reference material. Only 42 positions were used because this takes 24h, enabling a fluent workflow. The in-house reference material, MAR-2 (2), was made of Marbella limestone and calibrated against NBS-19 (Friedman et al., 1982). Reported $\delta^{13}C$ and $\delta^{18}O$ values are 3,41‰ ± 0,10‰ and 0,13‰ ± 0,20‰ respectively (De Winter et al., 2016). Duplicates (28) were measured to detect for potential problems in the measurement routine. The raw data was corrected as follows:

1. **Quality** of the data was **assessed** by checking if the initial sample beam of the mass spectrometer was between the minimum and maximum reference beam and by looking at the amount of sample 'chops'. If too much sample material was inside the vials, pressure of the CO_2 gas became too high for the mass spectrometer and some gas had to be removed, impacting the quality of the measurements. Every sample with more than 1 'chop' was measured again.
2. **Linear correction** of the oxygen and carbon isotope values for the instrumental drift occurring during the measurements of one batch of samples.
3. Final **correction** of the measurements by comparing the measured values of the MAR2(2) **standards** with the reference values. If for example the standards from one batch showed on average values 0,1‰ higher than the reference value, 0,1‰ was subtracted from all stable isotope results.

3.5.3 Trace elements: high resolution inductively coupled plasma mass spectrometry (HR-ICP-MS)

To ensure a multiproxy approach in this study, trace element abundances were measured using high resolution inductively coupled plasma mass spectrometry (HR-ICP-MS), Thermo Element 2 in AMGC laboratory). Trace elements of interest are Sr, Ba, Mg, U, Pb, Y and Zn. A total of 94 samples, that were already analysed for their $\delta^{13}C$ and $\delta^{18}O$ concentrations, were measured. Initially, the goal was to analyse all 197 samples, but the number of samples was limited to 94 because of the time-consuming sample preparation prior the measurement and because only limited time slots were available at the HR-ICP-MS facility. Almost all samples with an odd number were measured, to ensure trace element records of the entire archive.

First, approximately 4 to 5 mg (average weight of all samples was 4,42 mg) of carbonate powder was transferred with utmost care from the original Eppendorf® vials into Savillex Teflon® containers (figure 37). These containers resist high temperatures and strong acids and are crucial when conducting trace elemental analysis. Before use, the Savillex Teflon® containers were cleaned consecutively with HCl and two HNO_3-HF solutions to minimize the possibility of contamination. At each cleaning step, the containers were left overnight at 100°C on a hotplate. Weighing was done on a Sartorius Cubis® ultramicro balance with a readability of 0,0001 mg (figure 36).

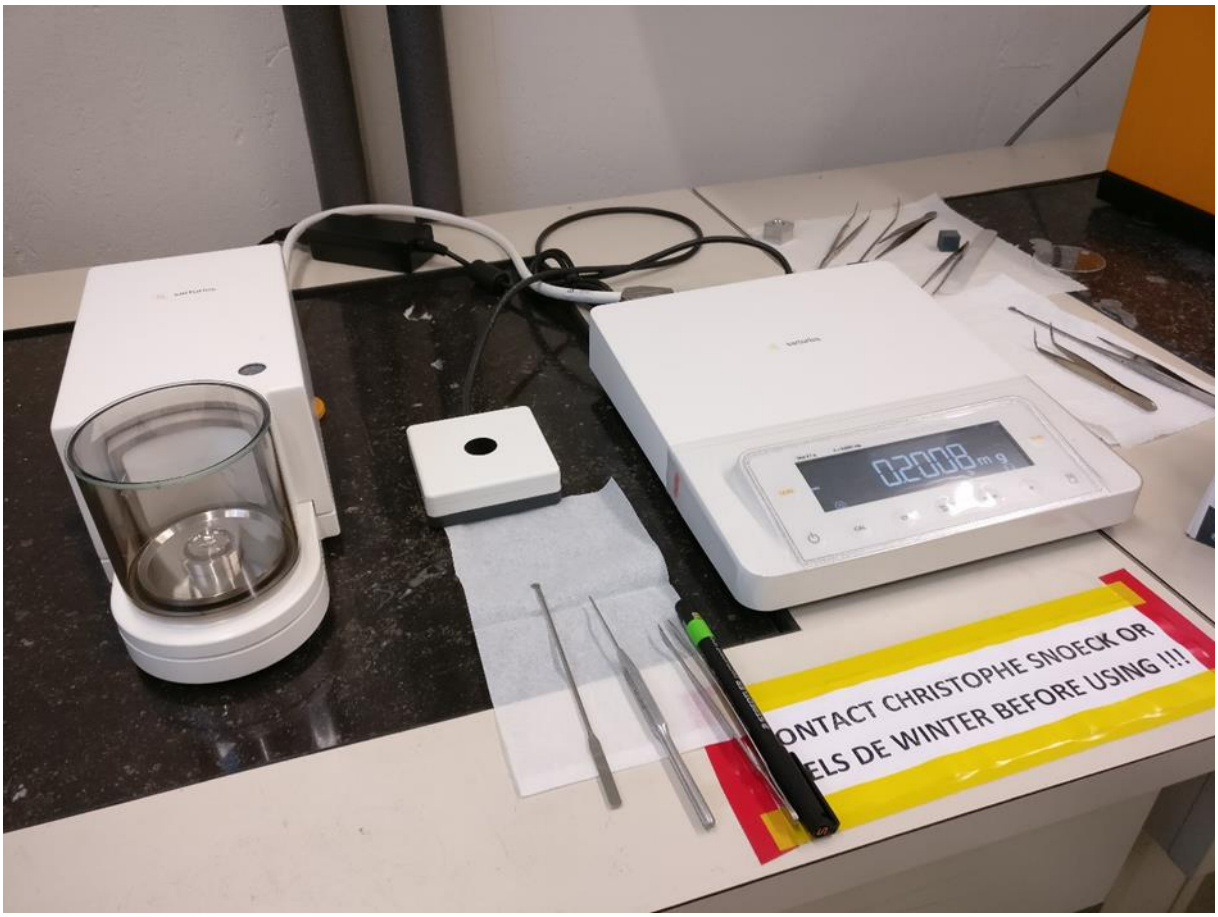

Figure 36 - Sartorius Cubis® ultramicro balance used to measure trace element sample weights

Next, all weighed samples were digested using 1,5 ml 14M subboiled HNO_3. Digestion with strong acids ensures a complete solution of the samples and a decomposition of the matrix. Before adding the acid, 0,5 mL of Milli-Q, H_2O was added to the samples to avoid sample loss by splashing during the intense digestion reaction. Digestion of $CaCO_3$ with HNO_3 occurs by the following reaction:

$$2HNO_3 + CaCO3 \rightarrow H_2O + CO_2 + Ca(NO_3)_2$$

Then, the containers were closed and placed on a hot plate at 96°C to increase the reaction rate. After 1 hour and 30 minutes, the lids of the containers were removed and the solution was left to evaporate overnight (figure 37). Within each batch, two procedural blanks were included to check if any contamination occurred during the sample preparation. Additionally, two ISO certified carbonate reference materials (CRM782 and CRM513) and two SARM (Service d'Analyse des Roches et des Minéraux, Paris) reference materials (BE-N and PM-S) were included within each batch.

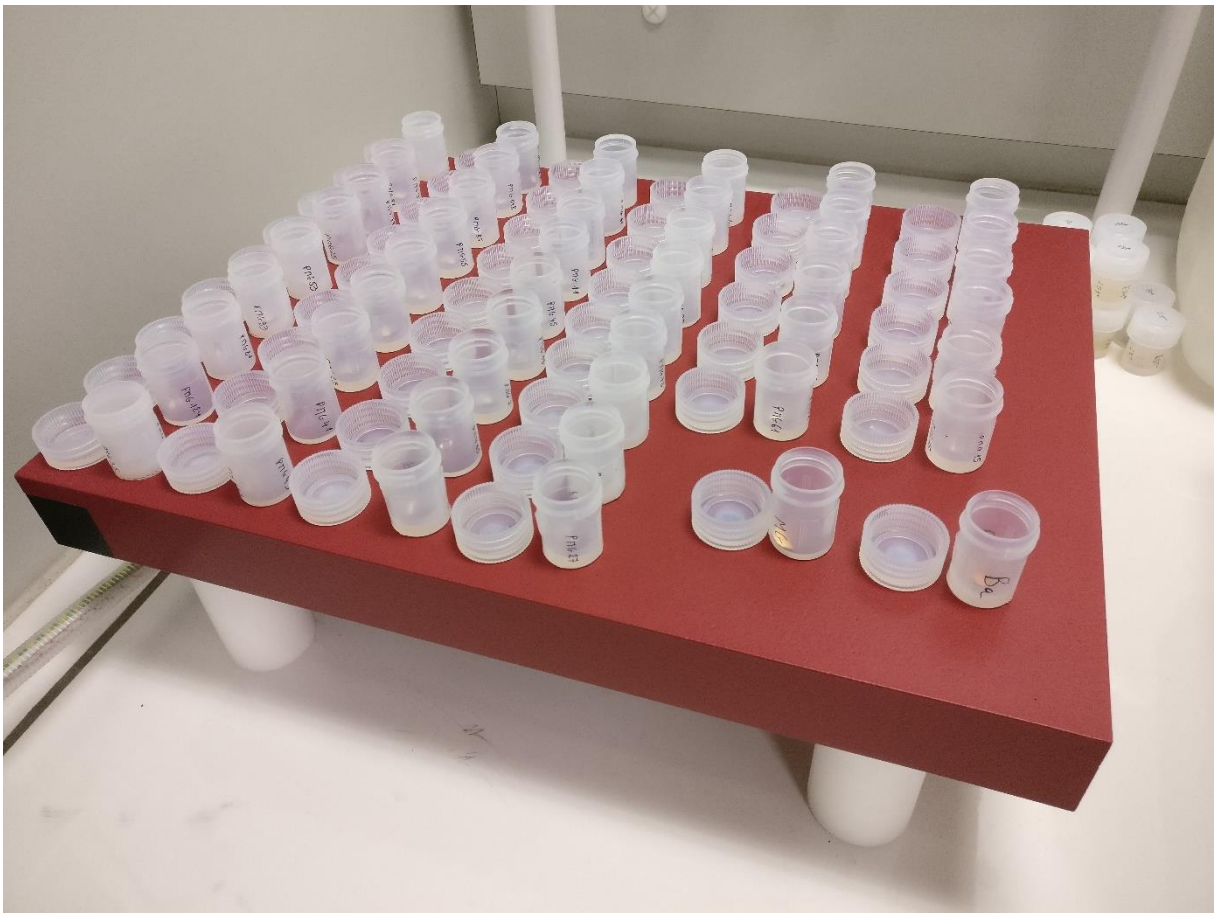

Figure 37 - One of the hot plates after evaporating the liquid fraction from the Savillex containers

Before analysis, all samples were again dissolved with 5 mL 10% subboiled HNO_3. Then, 2 mL of the sample solution was transferred in a 15 mL sterile centrifuge tube and diluted with 1,9 mL 3% subboiled HNO_3. Lastly, 0,1 mL 500 ng g-1 Indium spike was added, which can be used to correct for instrumental drift. The total dilution factor was 2000. The BE-N and PM-S reference materials were diluted with a factor 10 000. The dilution of the speleothem carbonate was a compromise between a solution of which the concentration of trace elements of interest is above the limit of detection and a solution of which the Ca^{2+} is not too high because this would clog the cones of the mass spectrometer and hereby decrease the sensitivity.

The actual measurements were performed with an Element 2 (Thermo Finnigan, Germany) HR-ICP-MS (figure 38). Samples and standards were analysed at high resolution (^{27}Al, ^{53}Cr, ^{55}Mn, ^{57}Fe, ^{63}Cu, ^{66}Zn, ^{75}As, ^{85}Rb, ^{86}Sr, ^{88}Sr, ^{89}Y, ^{111}Cd, ^{115}In, ^{137}Ba, ^{146}Nd, ^{208}Pb, ^{238}U) and medium resolution (^{25}Mg, ^{29}Si, ^{31}P, ^{34}S, ^{43}Ca, ^{44}Ca, ^{115}In). Blanks of 10% subboiled HNO_3 were measured every 3 samples to check the

sensitivity of the analysis. Set-up, follow-up and maintenance of the HR-ICP-MS was carried out by Prof. Steven Goderis.

For the data processing of the raw data, all measurements were loaded into Microsoft Excel. Processing of the raw trace element data is a five-step process:

1. Correcting for **instrumental drift**; this correction is based on the assumption that the measured In-spike should be constant in all samples. The raw data is multiplied by the average measured In-value of all samples in that specific batch and then divided by the measured In-value of the sample which is being corrected.
2. Average signal of the **blanks** was **subtracted** from all measurements.
3. Incorporation of the **sample weights** which are necessary for step 4.
4. Calculation of the **preliminary results** by comparing the measured values of the standards with their reference values. Therefore, first the measured values of the standards were corrected with every other standard measured in that batch. The standard which delivered results which deviated the least from the reference values for the standards was selected and used to correct all the other samples in that batch.
5. The **limit of detection** (LOD) was calculated based on this arbitrary formula:

$$\frac{3 * standard\ deviation\ of\ the\ blanks * reference\ value\ of\ the\ standard}{\sqrt{10} * measurement\ of\ the\ standard}$$

   and all measurements below the LOD were discarded from the dataset. The remaining results are the final results and are presented in the Results and Discussion section (chapter 4).

The principle of ICP-MS measurements is explained by Figure 39. Liquid samples are pumped to the nebulizer and atomized into an aerosol, which is transported via the spray chamber to the injector located inside the torch. A plasma (> 6000°C) is generated in the torch, which ionises the elements from the sample. The produced ions are then extracted from the plasma into the mass spectrometer region which is held at vacuum. Afterwards, ions are focused by a series of ion lenses into the quadrupole mass analyser in which ions are separated based on their mass/charge ratio and finally measured by a detector (Jens Laboratory, 2017).

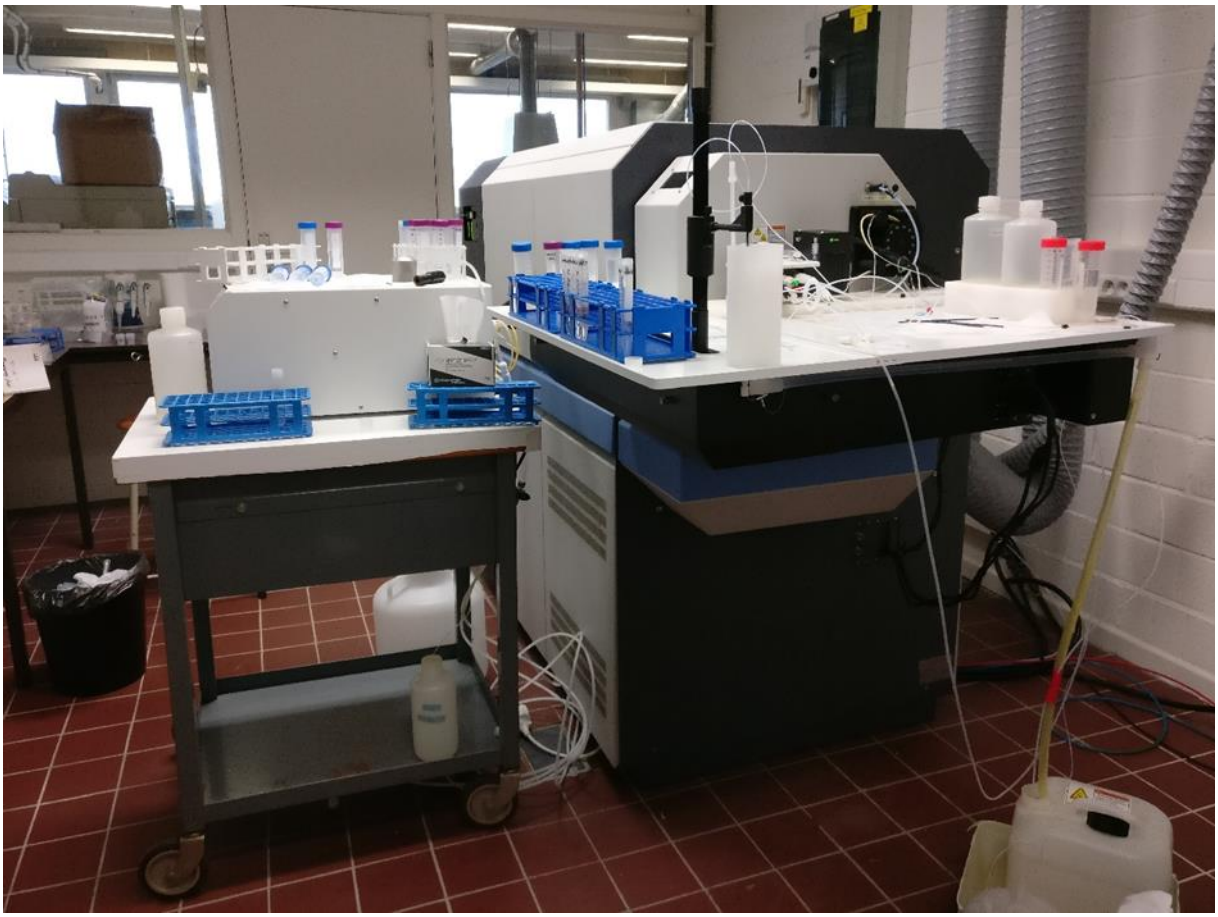

Figure 38 – Element 2 (Thermo Finnigan, Germany) HR-ICP-MS, AMGC laboratory at the Vrije Universiteit Brussel

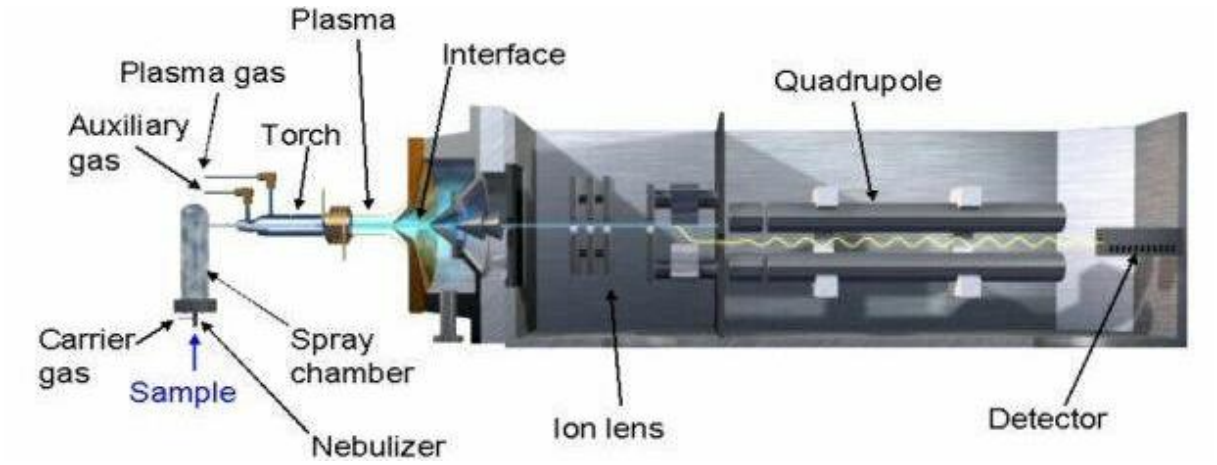

Figure 39 - Schematic figure of the main components of an ICP-MS (Jens Laboratory, 2017)

4 RESULTS AND DISCUSSION

In this section, the results and findings of all analyses and measurements discussed in the previous section will be examined. Results and discussions will be dealt with separately. Because the discussion uses the figures and graphs obtained in the results sections, the decision was made to divide this section based on the different analyses: 1) morphologic description of the speleothem, 2) age-modelling and determination of growth speed, 3) stable isotope analyses and 4) trace element measurements. Every subsection will start with an overview of the obtained results and is then followed by a discussion. At the end of this section, a more 'holistic' discussion will incorporate the findings of all used methods, correlate these with each other and with other proxies covering the same timeframe.

4.1 MORPHOLOGY OF THE PNG-01 SPELEOTHEM

4.1.1 Observations

Due to the nature of the coring process of speleothems, the speleothem is broken up into several pieces. In this case, the PNG-01 stalagmite is spit in 8 different sections, which are labelled from top to bottom (i.e. youngest to oldest): A, A-B, B, C, D, E, F and G, respectively. A brief description of these different sections (which are visualised and labelled in figure 40) is presented here. All distances are expressed in mm as 'distance from top' (dft).

- **Section A (0 to 310 mm dft)** is quite uniform, almost white and characterized by fine but clear laminations. Some laminations are more translucent, giving them a darker appearance while others are wider, uniform and almost perfectly white. One of these wider laminations was used to drill a sample for the U/Th-dating. In the bottom of this section (230 to 270 mm dft), crystal size increases (up to 1 mm) and some small inter-crystal porosity is observed.
- **Section A-B (310 to 370 mm dft)**: the top of this shorter section is similar to the more crystaline part of section A, but at the bottom of this section the crystal sizes are even larger and some large cavities are present. In the middle part of this section, there are three distinct and dense horizons. From 340 mm dft onwards, laminations remain visible, but are not as straight (they have a wavy-like appearance) as the ones in the younger part of the speleothem.

- **Section B (370 to 590 mm dft):** the upper half and the bottom part of section B are the most crystalline parts of the speleothem (crystal size up to 2-3 mm), which is also indicated by the large number of cavities observed. This made sample collecting in this part of the speleothem harder because it was not always easy to follow one specific growth layer.
- **Section C (590 to 610 mm dft)**: this short section is characterized by a thick transparent and coarse crystalline layer of around 5 mm between the finer calcite material.
- **Section D (610 to 650 mm dft)**: the crystals become more elongated/fibrous in this section (up to 1-2 mm). There are still laminations visible, but these are harder to discriminate in the more fibrous sections.
- **Section E (650 to 830 mm dft)**: a very regular and uniform section with clear, fine and regular laminations in the whole section. Small colour variations between the laminations makes them visible.
- **Section F (850 to 870 mm dft)**: is nearly identical as section E: it contains very fine and almost white calcite material with visible laminations.
- **Section G (870 to 1015 mm dft)**: like section E and F, this section is quite uniform. However, at its bottom the crystal size increases up to 2 mm. In these section crystals are elongated, but not as large or well developed as in section B. Lamination is still visible, but in comparison with for example section A, the transition between different layers is more ‘gradual’.

Overall, the most important observation in the record of speleothem morphology is the variation between more regulary laminated or layered sections like section A and E to denser and coarser crystalline parts observed in sections A-B, B, C and G. These more crystalline sections are coloured red on the overview of the complete speleothem on figure 40. Main colour changes are between the darker, compact and sometimes translucent calcite and the coarser white calcite. Laminations are visible throughout the stalagmite core (albeit less clear in the more crystalline sections) and are parallel orientend. In the youngest section of the speleothem the laminations are separated by darker, almost translucent, calcite.

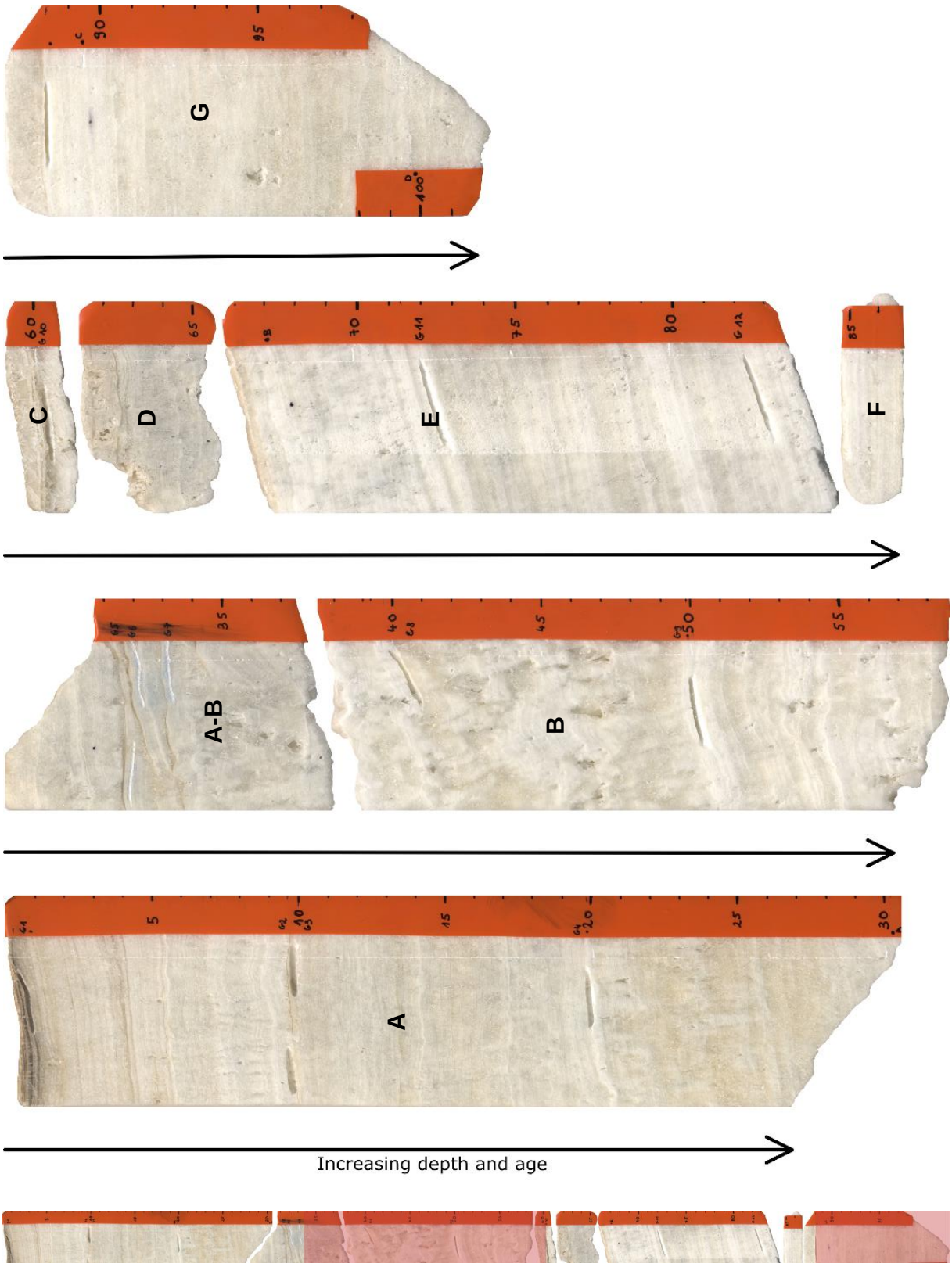

Figure 40 – Chronological overview of the different sections making up the PNG-01 speleothem combined with a reconstruction of the original, unbroken, speleothem on which the coarse crystalline sections are indicated in red

4.1.2 Discussion

Changes in the speleothem crystal morphology reflect variations in parent water flow, drip rate and rate of CO_2 outgassing (Fairchild et al., 2006) and thus also in a way the paleoclimatic conditions at time of formation. The changes between the more layered and the more crystalline parts in the speleothem probably indicate variations in the amount of water available for speleothem formation: the coarser sections most likely represent wetter periods while the other sections are probably deposited under drier conditions. Changes in the macroscopic morphology of the speleothem can be correlated with the results of the geochemical methods discussed on the following pages. Transition towards wetter or drier climates are visible in the speleothem morphology, more specifically: porous, white calcite is said to be associated with increasing growth rates during wetter periods, more translucent calcite points to drier climates with decreasing growth rates (Genty, et al., 2001).

However, to really assess changes in crystallography, macroscopic description of the speleothem morphology should be expanded with microscopic analysis of thin sections. This allows to closely study the build-up of the layering and to distinguish between the different fabric types and how these can be reflected in the different factors discussed above. Problem is that this technique is quite time consuming and many thin sections are required. If additional research is carried out on this speleothem, thin section analysis could be one of the first techniques carried out to further enhance the quality of the paleoclimatic reconstruction. Comparing the different parts of the speleothem, for example the more layered parts and the sections with coarse crystals, could deliver valuable extra information.

Finally, noticeable and translucent horizons or discontinuities, like for example the three horizons in section A-B, could possibly represent phases of growth interruption. That is the reason why samples for the U/Th-ages were taken above and below these discontinuities to check if they really can be linked with hiatuses (see 4.2.1).

4.2 AGE-DEPTH MODELLING AND DETERMINATION OF GROWTH RATES

Based on the U/Th defined ages and the respective depths of the samples, an age-depth model was calculated using the StalAge-algorithm. This age-depth model allows to connect the depth of all samples with an age and estimates the variation in growth

rate throughout the formation of the speleothem. In this section, these different aspects are presented and discussed.

4.2.1 U/Th-ages and age model

Table 3 gives an overview of U/Th defined ages and the respective errors for all analysed samples. The corrected ^{230}Th-ages assume an initial ^{230}Th/^{232}Th-ratio of 4,4 ± 2,2*10^{-6} and are the values for material in secular equilibrium with a bulk earth ^{232}Th/^{238}U-ratio of 3,8. Errors are arbitrarily assumed to be 50%. Note that the ages below are expressed in years before present (BP) with the present defined as the year 1950. Sample G-7 was immediately identified as an outlier, an age of 17 ka simply does not fit with all the other measurements and cannot be explained by any known process in speleothem formation. The reason for this discrepant age is unknown, but potentially some kind of contamination occurred during sample preparation. Aside from this major outlier, several age inversions are present in the age dataset. However, the StalAge algorithm is specifically designed to cope with outliers and age inversions. Age inversions are ignored because of the monotonicity constraint built into StalAge.

Sample ID	Dft (mm)	^{230}Th-age (yrs BP)	Standard error
G-1	3	92745	± 442
G-2	96	97184	± 349
G-3	100	94807	± 303
G-4	198	101059	± 303
G-5	310	97189	± 430
G-6	316	96987	± 315
G-7	329	17216	± 199
G-8	393	97157	± 275
G-9	498	99786	± 308
G-10	602	97477	± 296
G-11	713	102775	± 358
G-12	816	102806	± 374
G-13	883	101426	± 308

Table 3 – U/Th defined ages and their respective errors (ages and errors are rounded)

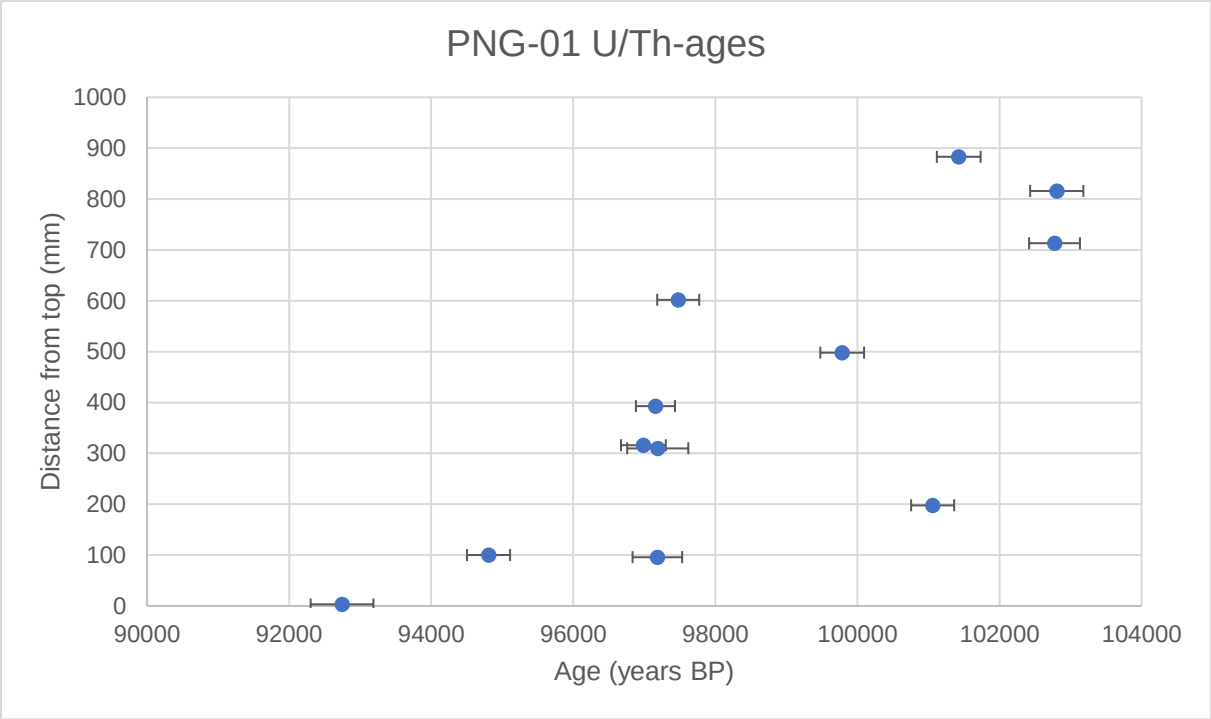

Figure 41 - Overview of the U/Th-ages and their respective errors (sample G-7 was removed from the dataset)

With exception of sample G-7, all ages (see figure 41) were used as input for age model constructed with the StalAge algorithm. Input for the algorithm is limited to two text files; one file contains the depths, ages and errors of the U/Th-ages and a second file consists of the depths for which the correspondent ages should be calculated (in this case these are the depths of the 197 samples collected for the stable isotope measurements). After pointing the script towards the location of these two files, the script guides the user through the different steps and only asks for user-input at certain points. More details can be found in the 'Materials and methods'-section (chapter 3), but in this case 3 of the 12 ages used as input were considered as outliers and were removed, error bars on other ages were increased to fit the model. The final age model can be seen on figure 42. The zone defined by the two grey lines defines the error on the age model. As discussed in the methods section, the error of the model increases significantly at the outer limits of the model.

According to this age model, speleothem formation started at 103,6 ka (upper and lower limit of the model are 106,1 and 102,6 ka respectively) and stopped at 93,8 ka BP (94,6 and 90,8 ka for the upper and lower limit), which suggests a period of speleothem growth of around 9,8 ka. According to this model, the speleothem forms continuously with no indication of hiatuses although, the growth rate has fluctuated over time.

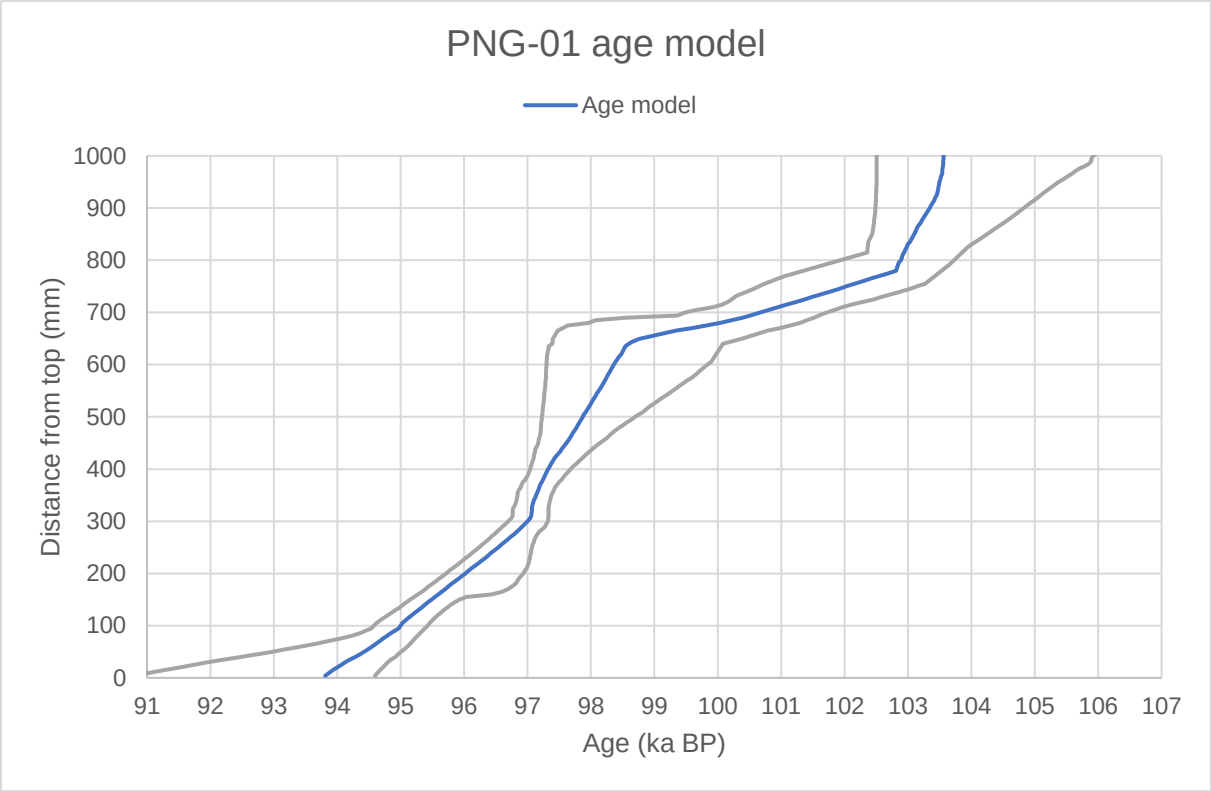

Figure 42 – PNG-01 age model based on 9 U/Th-ages, with error shown in grey

4.2.2 Growth rates

Looking at the age model 4 periods with distinctive differences in growth rates can be identified. An overview of these different periods and their corresponding growth rates is given in table 4.

Section	Dft (mm)	Ages (ka)	Growth rate (mm/yr)
1	1015 - 790	103,6 – 102,8	0,281
2	790 – 630	102,8 – 98,5	0,0372
3	630 – 310	98,5 – 97,1	0,229
4	310 – 0	97,1 – 93,8	0,0939

Table 4 – Growth rate variation in the PNG-01 speleothem

On average the growth rate is 0,104 mm/year, but growth rate in the oldest section of the speleothem is larger at 0,281 mm/year and is more than 7 times higher than in the section with the slowest growth, which corresponds to 0,0372 mm/year. There are two periods with faster speleothem growth, which are then in both cases followed by a period of significantly slower growth. This is also illustrated in figure 43, which displays the variation in growth rate through time and was constructed by calculating growth rates over subsections of 7 measurements.

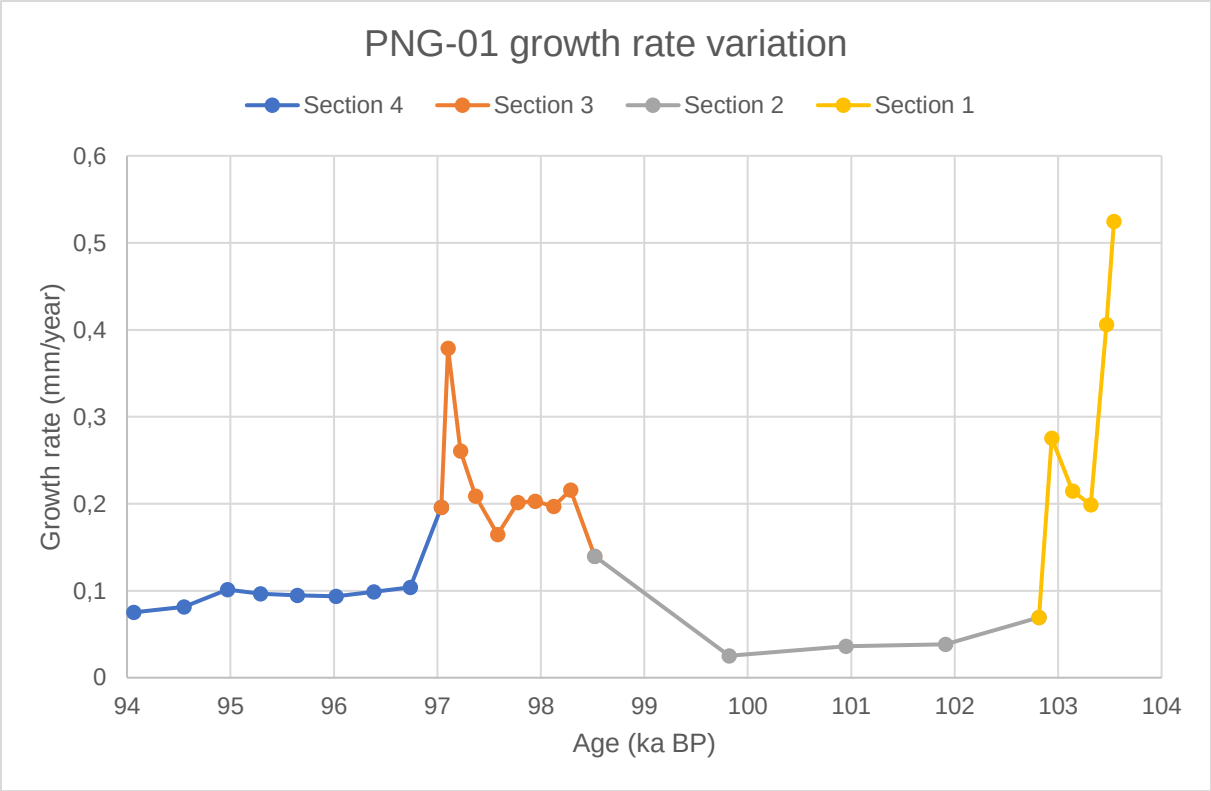

Figure 43 – PNG-01 growth rate variation through time, sections described in table 4 are indicated

4.2.3 Discussion

Variation in speleothem growth rate can be used as a proxy for the climatic conditions on the surface above the cave (Fairchild and Baker, 2012; Verheyden et al., 2014). The age model seems to suggest a transition from climatic conditions favourable for speleothem growth at the start of speleothem formation towards a climate less favourable for speleothem growth for the next 3000 to 4000 years. This transition could indicate a drier climate because the presence of liquid water is essential for speleothem growth (speleothem formation stops during glacial periods). This pattern seems to repeat itself time during the PNG-01 timeframe. However, the danger here lies in the possible over-interpretation of this age model. An age model is only a model of the reality and the errors on the model are quite large. The differences in growth rate could have been less outspoken and correlate with more stable climatic conditions. Also, the start and end date of speleothem formation have large potential errors. Taking the upper limit for the start age and the lower limit for the end of speleothem formation, the speleothem could even span a period of up to 15,3 ka, which is almost the double of the calculated timespan if the other extreme limits are used (8 ka).

To conclude, this variation in growth rates cannot provide strong evidence for climatic variation due to the large uncertainties, but like the speleothem morphology it can be used in convergence with the interpretation of the stable isotope and trace element measurements. The only way to improve this age model and reduce the amount of involved uncertainty is by increasing the number of U/Th-ages, which is another point for improvement if further research on this speleothem is to be carried out.

4.3 STABLE ISOTOPE MEASUREMENTS

Stable isotope measurements form the foundation for the paleoclimatic reconstruction in this thesis. Stable isotopes can be measured at high resolution and are by far the most studied proxy in speleothem records. This makes that the link between climate and the variation in the $\delta^{13}C$ and $\delta^{18}O$ signal is generally quite well understood. However, every speleothem has its own unique characteristics so there is no one size fits all solution for the interpretation of these records. This section gives an overview of the stable isotope results and a discussion of the results.

4.3.1 Results

Results of all 197 measurements for both $\delta^{13}C$ and $\delta^{18}O$ were linked with the age model described in the previous section to create the records visible in figure 44. Table 5 gives an overview of the statistical parameters of both the $\delta^{13}C$ and $\delta^{18}O$ record. Note that all isotopic values are expressed in ‰ VPDB. In section 7.2 a complete overview of all the measurements can be found.

	Mean (‰)	Maximum (‰)	Minimum (‰)	Range (‰)	Avg. std. error
$\delta^{13}C$	-6,92	-3,12	-9,68	6,55	± 0,0287
$\delta^{18}O$	-5,65	-4,32	-7,36	3,04	± 0,0739

Table 5 – Overview of the statistical parameters of the $\delta^{13}C$ and $\delta^{18}O$ records

The range of the $\delta^{13}C$ record is more than two times the range of the $\delta^{18}O$ record, which shows the greatest variability of this record. The amplitude of change in the oxygen record may be lower, but seems to correlate quite well with the variation observed in the carbon record at least in the younger section between 93,8 and 101 ka. In the older parts of the speleothem, the correlation appears less strong. Correlation between these records can be visualised by plotting these two records against each other (see figure 45). Correlation can also be tested analytically with the Pearson correlation coefficient, which is the coefficient of the covariance of two variables divided

by the product of their standard deviations. The result is a value between -1 and +1, which expresses the strength and direction of linear relationships between pairs of continuous variables; a value of +1 signifies a perfect positive correlation and a value 0 indicates no correlation at all (Sedgwick 2012).

The Pearson correlation between the $\delta^{13}C$ and $\delta^{18}O$ record is 0,776, indicating a good positive correlation between the two records. However, if the complete dataset of measurements is divided in two groups, one group containing all the measurements between 93,8 and 101 ka (blue on the figure 45) and one group containing the older measurements up to 103,6 ka (red coloured on the figure 45), it becomes evident that the good correlation between the two records originates from the excellent correlation in the younger section of the speleothem. The Pearson correlation coefficient for the younger subgroup is 0,908 while the same coefficient for the group of older measurements is only 0,0796 indicating almost no correlation in this part of the speleothem. Also, note that due to the variation in growth speed, the temporal resolution of these stable isotope records is not constant.

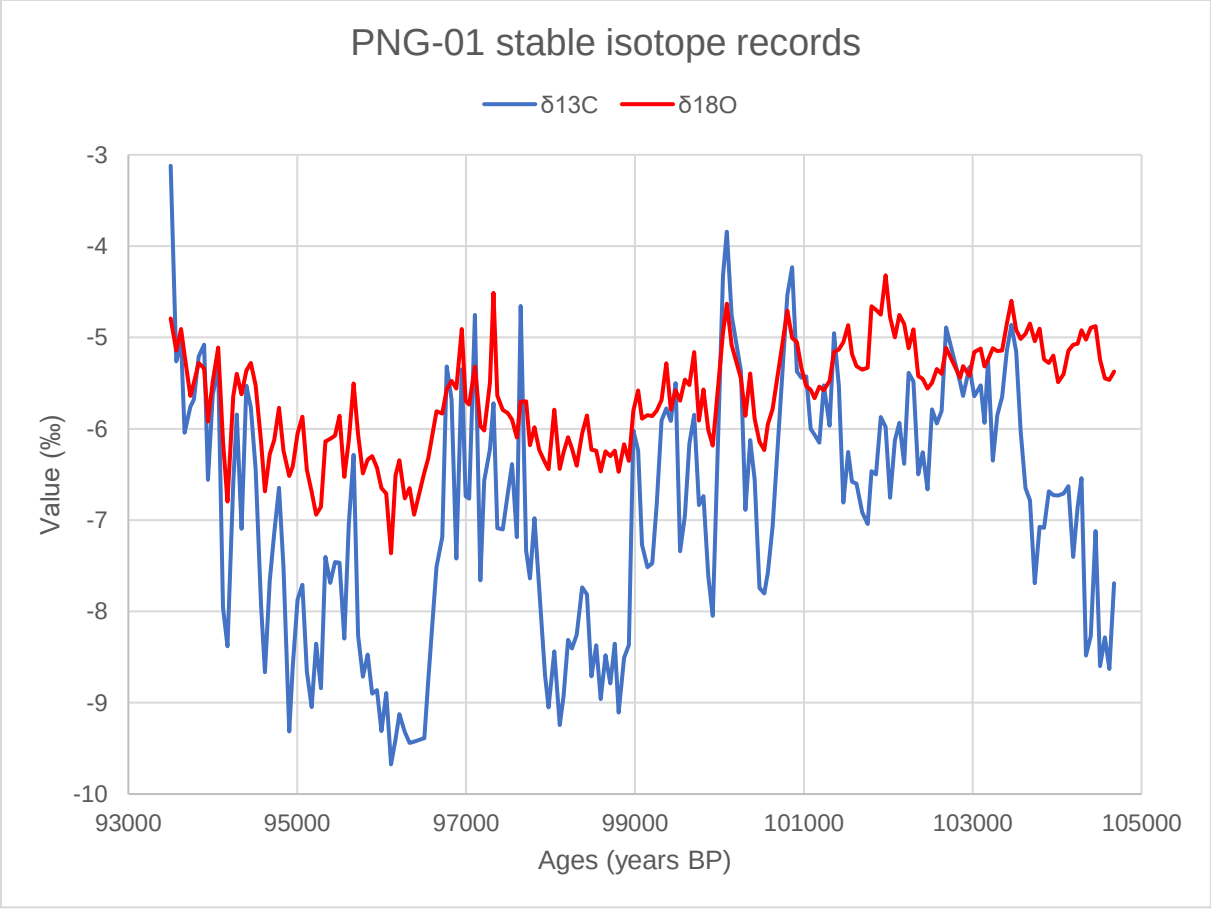

Figure 44 - Stable isotope record of the PNG-01 speleothem (raw data)

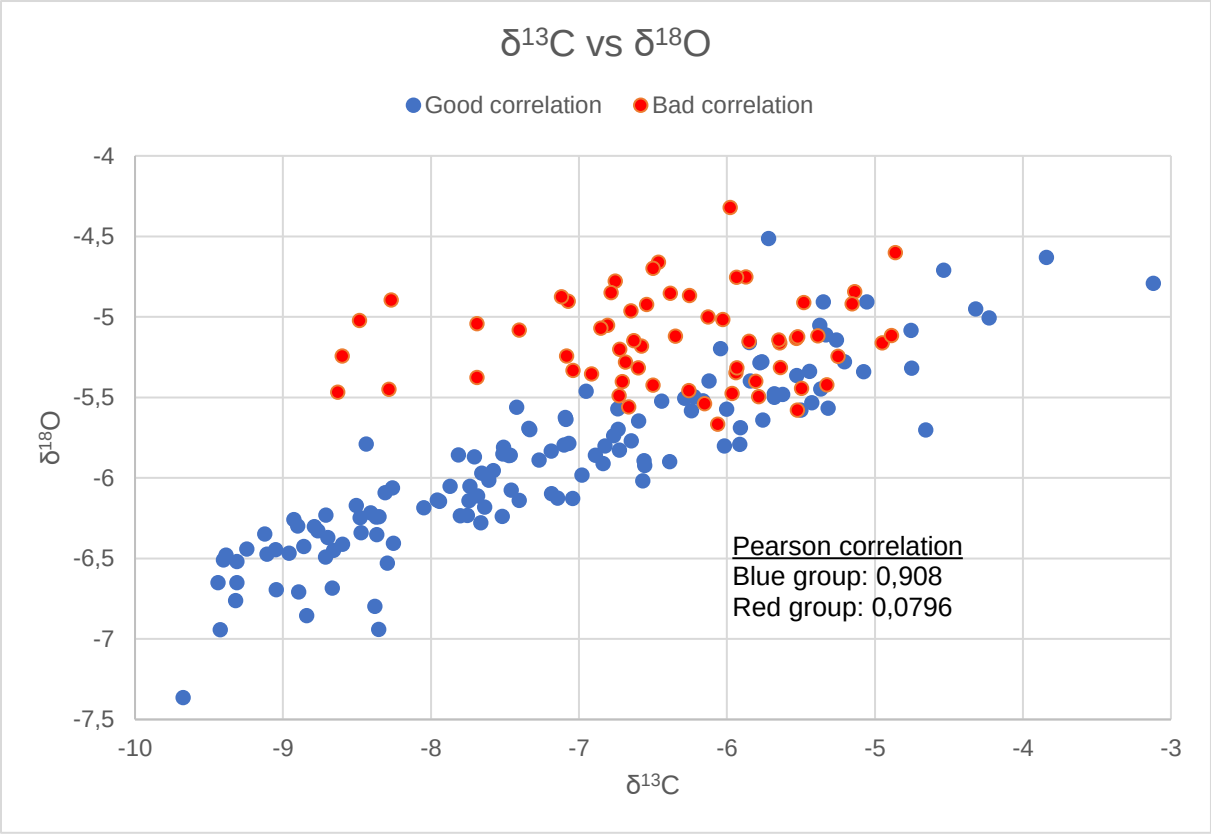

Figure 45 – Correlation between δ13C and δ18O record; the dataset was divided in a group of stable isotope measurements with good (blue group, 93,8-101 ka) and a group with bad correlation (red group, 101-103,6 ka)

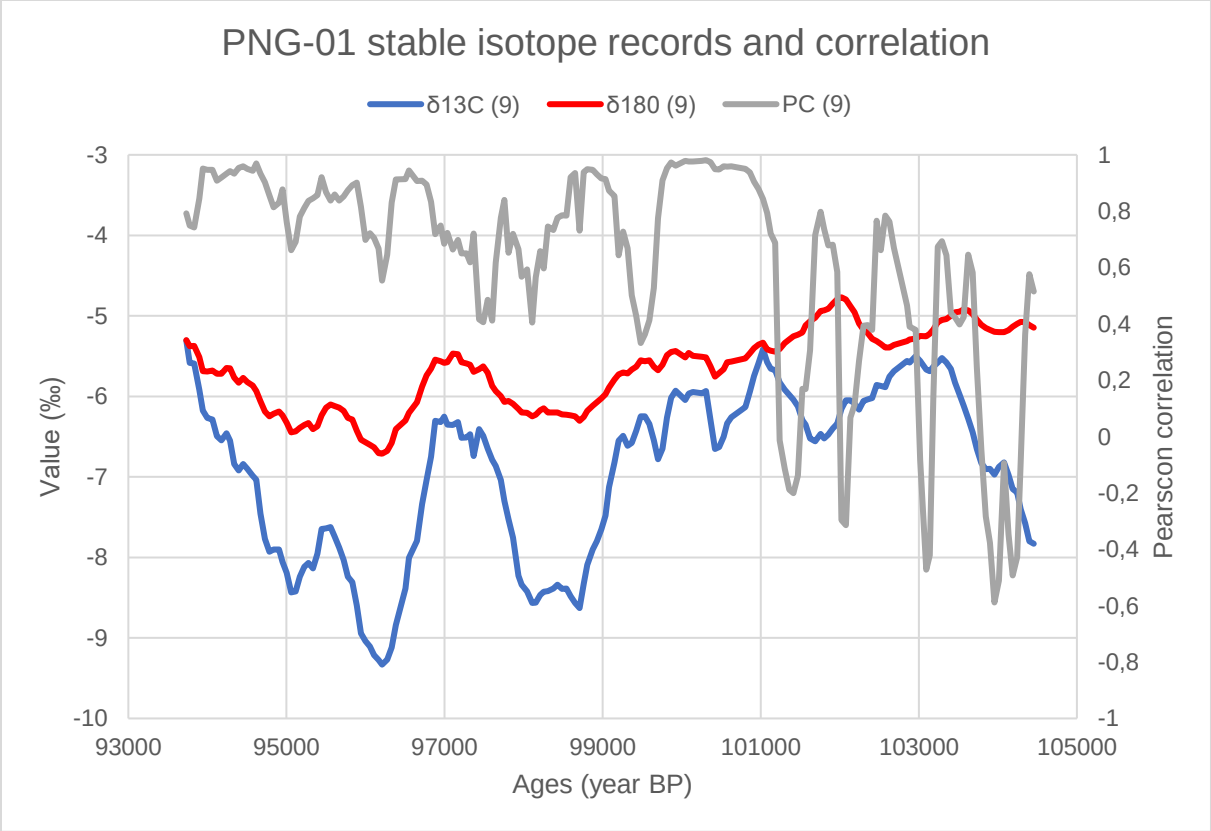

Figure 46 – PNG-01 stable isotope records and their correlation through time

Finally, small-scale fluctuations in the stable isotope records make it hard to describe the larger-scale trends stored in these records. A moving average function, which can be compared with a window that moves over the measurements and calculates the average over a set number of measurements, smooths out these smaller fluctuations and was applied to both records in figure 46. In this case, averages were calculated for subsets of 9 measurements. The moving Pearson correlation is also indicated on the same figure. In a similar fashion to the moving average, the moving correlation shows how the correlation between the two stable isotope records varies through time (window size was again set to 9).

4.3.2 Discussion

Before interpreting the stable isotope signals, it is important to assess if the stalagmite is deposited in isotopic equilibrium. This can be determined by looking at the covariation between the $\delta^{13}C$ and $\delta^{18}O$ signal, one of the so-called 'Hendy'-tests (see the section on speleothems). Isotopic equilibrium can be assumed only if there is no covariation between isotopic signals from the same growth layers. In this case, kinetic fractionation is an important process altering the isotopic signals because the $\delta^{13}C$ and $\delta^{18}O$ signals show strong covariation, especially in the part between 93,8 and 101 ka. In the older part of the speleothem, the correlation is much less pronounced and it is possible that in the period between 101 and 103,6 ka, the stalagmite indeed deposited in isotopic equilibrium. However, this should be tested further by taking additional samples from one growth layer and check if $\delta^{13}C$ varies while $\delta^{18}O$ values remain constant.

Nevertheless, it is prudent to assume that most of the speleothem is influenced by kinetic fractionation processes making it hard to interpret the variation in the stable isotope signals in function of temperature change. Assuming the presence of kinetic fractionation, both evapotranspiration and prior calcite precipitation are linked to climatic parameters and can result in positive covariation between $\delta^{13}C$ and $\delta^{18}O$. However, the results of the trace element measurements will come into play because they help to understand which processes really influenced the stable isotope signals. Therefore, the stable isotope signals will be discussed more in-depth together with the results of the trace element measurements discussed in the next section.

4.4 TRACE ELEMENT MEASUREMENTS

As discussed in previous sections, variations in the trace elements stored in the calcite growth layers can possible indicate which processes influenced or altered the stable isotope signals. In this section, the results of the 94 trace elements measurements are presented and briefly discussed.

4.4.1 Results

Figure 47 shows the different measured trace elements records; the host-rock derived elements Ba, Mg, Sr and U and the soil-derived elements Pb, Y and Zn. Other elements like Cu and Cd are not shown because the link between the variation of these elements and the paleoclimate signal is unclear at this point. In the future, more in-depth knowledge of the behaviour of these elements could potentially further increase the quality of paleoclimatic reconstructions based on speleothems. Besides the trace element measurements also the variation in growth rate and the stable isotope signals were plotted on the figure to make correlation between these different records more straightforward. Note that only measurements above the calculated detection limit for each element were used. All element concentrations are expressed in ppm. In section 7.3 a complete overview of all measurements can be found.

An overview of the statistical parameters of the studied trace elements can be found in table 6. Due to the high Ca concentration in the samples, the HR-ICP-MS slowly 'clogged' over time, increasing the detection limit and decreasing the quality of the measurements. Because samples were measured in a completely random order, these measurements of somewhat 'lower quality' are spread over the entire dataset and not influencing one specific section. Precision of the measurements was obtained by calculating the standard deviation on the 6 measurements of the CRM782 standard.

	Sr (ppm)	Ba (ppm)	Mg (ppm)	U (ppm)	Zn (ppm)	Pb (ppm)	Y (ppm)	Ca (ppm)
Mean	73,759	41,112	3649,155	0,059	2,514	0,210	0,007	865430,057
Maximum	121,467	86,843	6210,053	0,099	11,445	1,113	0,052	1088620,802
Minimum	19,838	18,392	1583,692	0,018	0,283	0,038	0,001	443379,521
Range	101,628	68,450	4626,361	0,081	11,162	1,076	0,051	645241,281
Precision (± σ)	13%	8%	22%	17%	9%	16%	14%	20%

Table 6 - Overview of the statistical parameters of the Sr, Ba, Mg, U, Z, Pb, Y and Ca records (rounded values)

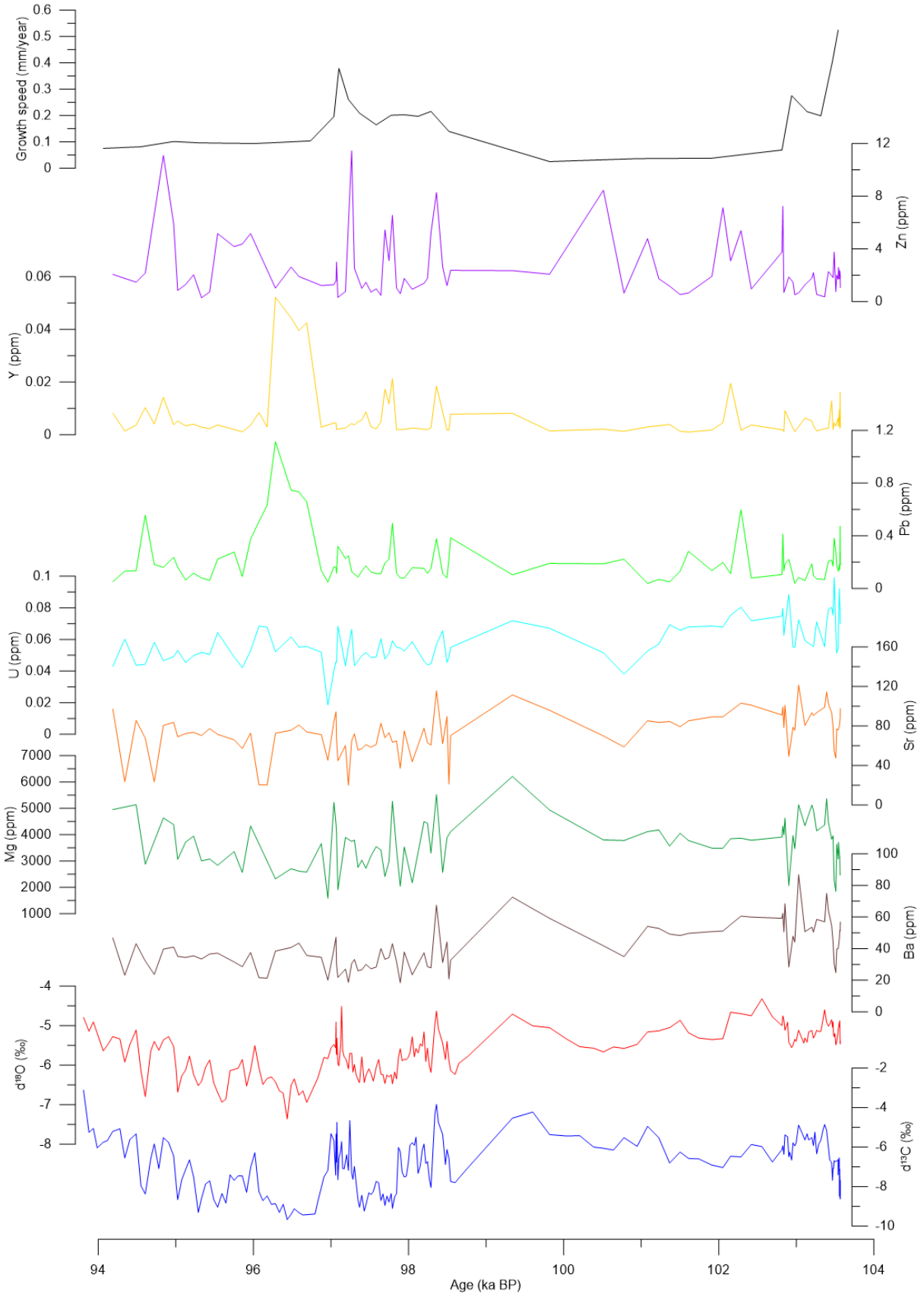

Figure 47 - Overview of measured trace elements combined with the stable isotope record and growth rate variation of the PNG-01 stalagmite, growth rate variation explains the changes in temporal resolution observed in the records (Figure made with Grapher developed by Golden Software)

Ranges of all trace element measurements are quite high, indicating large variability of trace element incorporation during the formation of the PNG-01 stalagmite. Precision on the measurements of most elements is around or a significantly below 20%. The Y-measurements should be treated carefully because the average value (0,007 ppm) is close to the calculated limit of detection (0,45 ppb).

	Ca	Mg	Sr	Ba	U	Pb	Y	Zn
Ca	1							
Mg	0,783	1						
Sr	0,731	0,829	1					
Ba	0,601	0,685	0,910	1				
U	0,007	-0,023	0,246	0,441	1			
Pb	-0,142	-0,263	-0,123	-0,083	0,159	1		
Y	0,022	-0,061	0,088	0,035	-0,004	0,733	1	
Zn	0,224	0,280	0,197	0,127	0,022	0,112	0,125	1

Table 7 - Pearson correlation coefficients for all studied trace elements (rounded values)

Like for the stable isotope measurements, correlation between different trace element records can provide valuable extra information (see table 7). For example, the correlation between the host-rock derived elements, Sr, Ba, Mg and U is expected to be quite high. Looking at the table above, this seems to be case (the greener the values, the stronger the positive correlations - the darker the red, the more negatively correlated the values). Pearson correlations between Sr, Ba, Mg are all over 0,6, only U has lower correlations with the other three host-rock derived elements. Correlation between the soil-derived elements is much weaker, only Pb and Y have a relatively high correlation coefficient of 0,733.

Variations of the 1000 Sr/Ca and the 1000 Mg/Ca-ratios, the oxygen and carbon isotope records and growth rate variation of the PNG-01 stalagmite are displayed on figure 48. The red marked areas on the stalagmite correspond with periods of higher growth rate and relate to their respective start and end dates on the growth variation curve. Table 8 contains the most important statistical parameters for these two new variables.

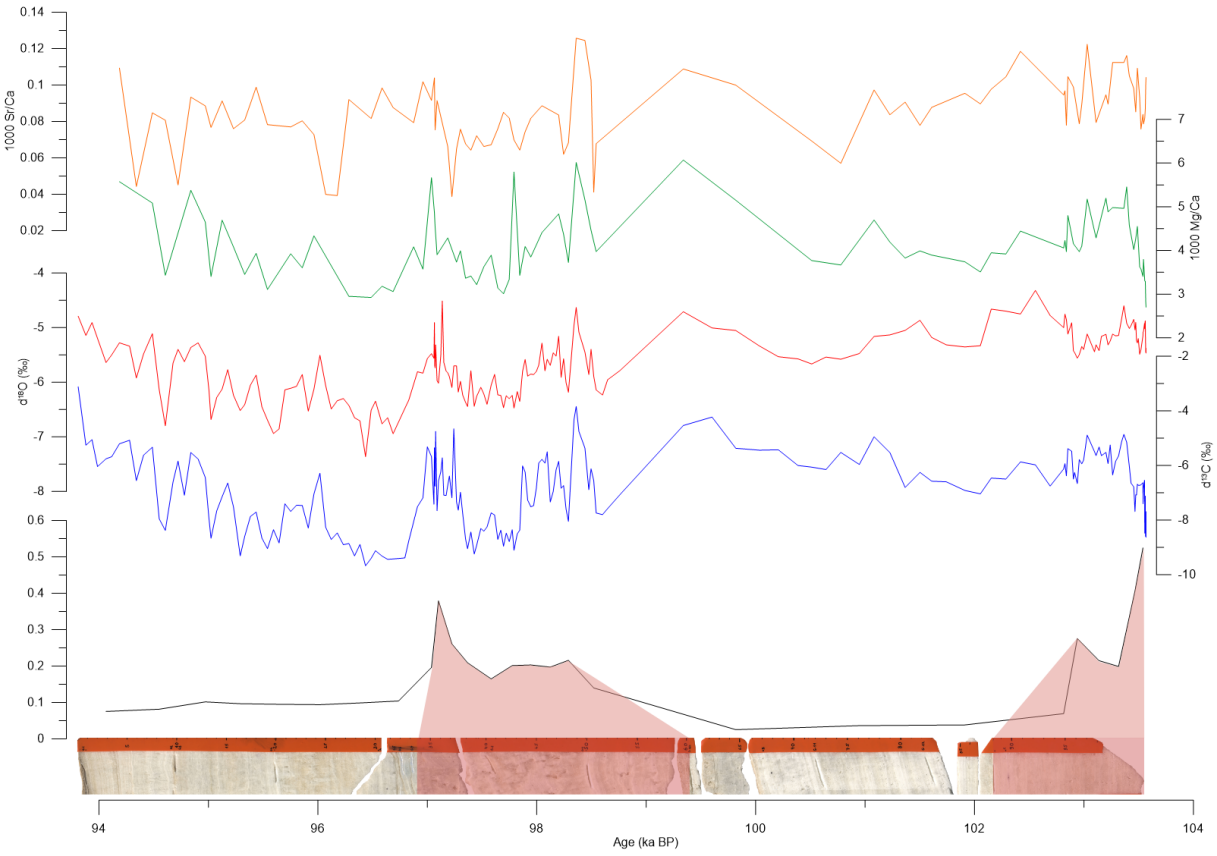

Figure 48 - PNG-01 1000 Sr/Ca and 1000 Mg/Ca-ratios combined with the stable isotope records and the variation of growth rate through time (Figure made with Grapher)

	1000 Sr/Ca	1000 Mg/Ca
Mean	0,085	4,098
Maximum	0,126	6,069
Minimum	0,039	2,701
Range	0,087	3,368

Table 8 – Statistical parameters of the 1000 Sr/Ca and 1000 Mg/Ca ratios (rounded values)

Using ratios of these two elements instead of absolute values, is the only way to correctly compare them with each other and compare the results of this thesis study with other similar studies. However, because the Ca concentrations in the samples are rather constant and much higher than the concentrations of the other elements, using the absolute values of the trace elements to compare them with each other, will not have a large influence on the interpretations and can be justified here. In other words, in a pure low-Mg calcite like the PNG-01 speleothem (the Mg/Ca-ratio varies between around 0,3 and 0,6%), variations in Mg/Ca and Sr/Ca-ratios are caused by changes in the Mg and Sr content and reflect changes in water residence time linked to changes in water excess (Verheyden et al., 2001).

Finally, also for these new variables correlation coefficients were determined (see table 9), but this time also correlations with the stable isotope records were calculated. Correlation between the Sr/Ca and Mg/Ca-ratios is quite good with a coefficient of 0,707. However, correlations between the trace element ratios and the stable isotope records are less strong, but also not negligible because coefficients are every time above 0,4. Choosing which coefficient corresponds with a 'good' correlation is of course an arbitrary decision.

	1000Sr/Ca	1000Mg/Ca	δ13C	δ18O
1000Sr/Ca	1			
1000Mg/Ca	0,707	1		
δ13C	0,431	0,480	1	
δ18O	0,511	0,419	0,804	1

Table 9 - Pearson correlation coefficients (rounded values)

4.4.2 Discussion

As discussed in the section on speleothems, host-rock derived elements like Sr, Ba and Mg can be used as a proxy for effective precipitation, with higher values corresponding to drier periods. Peaks in the soil-derived elements like Y, Zn and Pb on the other hand can possibly be linked to periods of higher infiltration.

Aside from the expected positive correlation between the host-rock derived elements Sr, Ba and Mg it is difficult to really observe large scale trends in the different trace element records. There appear to be some events of higher infiltration when looking at the records of Zn, Pb and Y, but sometimes these events correspond with peaks in the other trace elements and stable isotope records (e.g. around 98,5 ka) while other times peaks in Pb and Y, for example at around 96,4 ka, are not reflected in the records of the host-rock derived elements. This illustrates the complexity of using trace element records to reconstruct paleoclimate. Only by correlating these measurements with all the other proxies stored in the speleothem, valid hypotheses about the paleoclimate during the formation of the speleothem can be constructed, this aspect is discussed in the next section.

4.5 Correlation between the different PNG-01 proxies

The good positive correlation between the oxygen and carbon stable isotope records is a sign of kinetic fractionation processes influencing the stable isotope signals. This is almost certain the case in the younger section of the speleothem up to 101 ka, but

in the older section between 101 and 103,6 ka the correlation between the records is less pronounced and almost zero, which could potentially point towards more isotopic equilibrium conditions. However, isotopic equilibrium in speleothem deposition is quite rare and more research is necessary to potentially confirm this. The most likely hypothesis is that during the formation of the PNG-01 speleothem, the influence of kinetic effects on the calcite deposition increased over time.

One of the important processes, which can explain positive covariation between the oxygen and carbon isotope record is prior calcite precipitation (PCP). Calcite precipitation in the host rock prior to reaching the cave because of CO_2 degassing, influences the signature of drip waters forming speleothems. Aside from elevated $\delta^{13}C$ and $\delta^{18}O$ values, PCP also increases the Mg/Ca and Sr/Ca-ratios (Fairchild and Treble, 2009; Genty et al., 2003; Verheyden et al. 2000). Positive covariation between the stable isotope records and these ratios can thus point to the presence of PCP. In this case, these correlations exist, many peaks observed in the stable isotope record correspond with peaks in the Mg/Ca and Sr/Ca-ratios. Unfortunately, this is not always the case. This is also reflected in the corresponding Pearson correlation coefficients, which are in all four occasions above 0,4. This points to the presence of a correlation albeit not a strong one. PCP cannot explain all variation observed in the different records, but most likely PCP is one of the important processes controlling the observed signals. This hypothesis is likely because Verheyden et al. (2000) also attributed long-term change in the Mg/Ca and Sr/Ca ratios from a younger Holocene stalagmite from the same Père Noël cave to changes in PCP. When residence times are higher, the chance of PCP is also higher because the calcite saturation of the percolating waters increases. In this way, PCP can be linked with changes in water residence time which are linked to changes in water excess (Verheyden et al., 2000).

For the PNG-01, this would imply that the Sr/Ca and Mg/Ca ratios can be interpreted as reflecting changes in water excess or effective precipitation (rainfall minus evaporation), with higher values corresponding to periods with less water excess. In other words, higher values of these ratios and of the stable isotope signals could reflect drier climatic conditions, with less water recharge. Peaks in the concentration in soil derived elements like Pb, Y and Zn can, on an annual scale, point towards periods of higher infiltration during wetter periods.

Changes in climatic conditions should also be reflected in the speleothem morphology and variation in growth rate. **Growth rate** of the PNG-01 stalagmite is relatively high (between ± 0,2 and ± 0,6 mm/year) in the oldest section between 103,6 and 103 ka, but from around 103 ka onwards, growth rate of the stalagmite is much lower (± 0,05 mm/year). Around 99,9 ka the growth rate starts to increase again and around 97,1 ka the growth rate reaches peak values (± 0,5 mm/year). Afterwards, it decreases relatively fast and remains low (± 0,8 mm/year) until the end of speleothem formation. This indicates that conditions for speleothem growth were most favourable in the oldest section of the speleothem and between around 99 and 97 ka. These periods of increasing growth rate also seem to correspond with the observed changes in speleothem **morphology** as can be seen on figure 40 and figure 48, where the red coloured sections, which are the sections recognizable by larger growth layers and crystal sizes, on the speleothem relate to their respective start and end dates on the curve of growth rate variation. Because liquid water is necessary for the formation of speleothems, periods with slower speleothem formation point to drier climatic conditions.

Bringing all of this together, the different proxies stored in the PNG-01 stalagmite likely reflects the following paleoclimatic conditions between 103,6 and 93,8 ka:

- At around **103,6 ka,** presence of favourable conditions for speleothem growth (relatively wet) potentially triggered the start of speleothem formation.
- Slower growth rate after **103** ka and up **to** around **100 ka** could be an indication of a transition to drier climatic conditions, which is also reflected by the relatively high stable isotope values in this section
- After around **100 ka** both the stable isotope and the Sr/Ca and Mg/Ca-ratios show relatively low values **until** around **97 ka** that could imply that this period was characterized by wetter conditions. In the same period, soil-derived elements (Pb, Y and Zn) possibly also show some periods of peak infiltration, which is expected under a generally wetter climate. Observed growth rate in this period also fits with the interpretation of a wetter period.
- In the youngest section of the speleothem (around **97 to 93,8 ka**), growth rate decreases and the stable isotope values show a gradual increase, which could be an indication for a gradual trend towards a return to drier climatic conditions with less water recharge. The Mg/Ca and Sr/Ca-ratios are also higher in this

section, but in contrast with the Mg/Ca-ratio, the Sr/Ca-ratio does not seem to reflect a similar trend and is, aside from some strong peaks, rather constant. Strong peaks in Pb and Y at around 96,5 ka, possible indicating higher infiltration, correspond with the lowest stable isotope values in this section, which shows that the start of this period was dominated by a relatively wet climate.

These interpretations must be considered as preliminary and should be seen as pointers for further research. For example, due to the variation in growth rate, the temporal resolution of the different records varies and becomes rather low in the two sections possibly corresponding with drier climates, which could give a distorted image. This aspect could be improved by refining both the ages and the resolution of the proxy analyses.

4.6 COMPARISON WITH OTHER PALEOCLIMATE PROXIES

4.6.1 Introduction

In this part of the discussion, the observed trends in the PNG-01 stalagmite are compared with other, well studied climate proxies. Therefore, an overview figure was made (figure 49), which contains, aside from the PNG-01 stable isotope records, variation in growth rate and morphology, four different paleoclimatic records already discussed in the section about the climate during the early Weichselian; the ELSA greyscale stack from the Eifel region (Sirocko et al., 2005), the NGRIP ice core record from Greenland (NGRIP Members, 2004), the NALPSL EXC4 speleothem record from the northern Alps (Boch et al., 2011), and finally the benthic marine core MD95-2042 from the Iberian margin (Shackleton et al., 2000). For the NGRIP record, the GICC05modelext timescale (Centre for Ice and Climate, 2017) was used and all ages were converted to ages BP.

The last section covers the volcanic activity in the Eifel region and the possible link with the PNG-01 record. Similar to the ELSA greyscale stack, the ELSA tephra stack is a record of the tephra layers in this region, which are linked with different maar eruptions. Correlating the PNG-01 record with these eruptions could potentially improve the PNG-01 age model, and although interesting, this aspect fell outside the scope of a 1 year MS thesis.

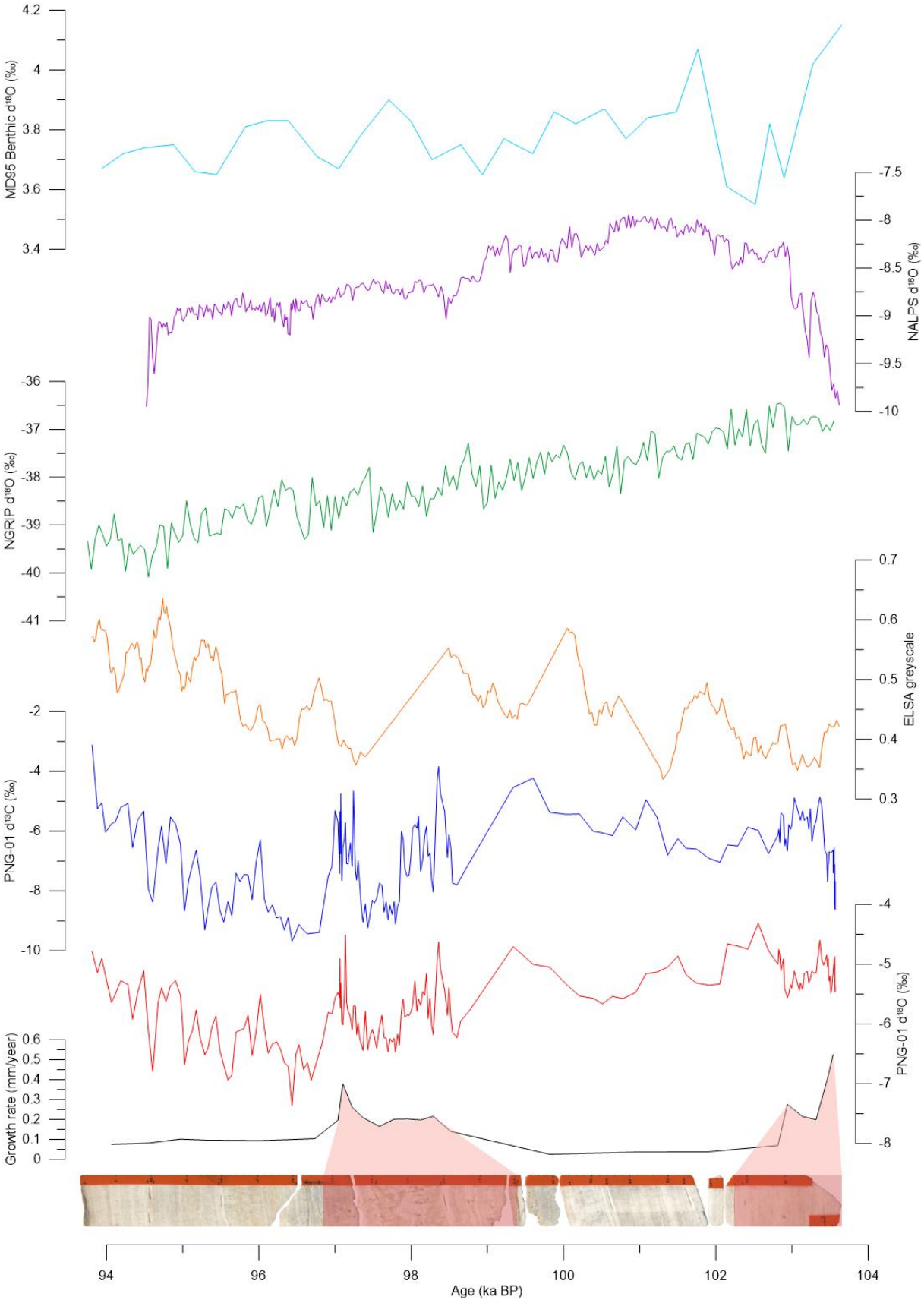

Figure 49 – Comparison between the PNG-01 stable isotope record, variation in growth rate and stalagmite morphology and other paleoclimate proxies: the ELSA greyscale stack as recorder of vegetation change, the NGRIP ice core and NALPS speleothem records as proxies for paleotemperature and the benthic signal in the MD95 marine core as proxy for changes in continental ice volume

4.6.2 NGRIP and NALPS

The NGRIP ice core and NALPS speleothem record are said to be mainly reflecting changes in atmospheric temperature and in this way, they both suggest a decrease in temperature over the timeframe of the PNG-01 stalagmite formation (from the warm NGRIP Greenland Interstadial 23 towards the colder Greenland Stadial 23), a trend that is difficult to compare with PNG-01 proxies because the PNG-01 proxies mainly reflect changes in water excess. However, aside from the possible wetter period between 100 and 97 ka, the trend towards more influence of kinetic fractionation seems to correlate with drier and thus possibly also colder climatic conditions in the younger sections of the speleothem.

Looking more specifically to the NALPS record, there appears to be a discontinuity in the trend at around 99 ka, the NALPS $\delta^{18}O$-values decrease with around 0,5‰ over a period of around 1000 year. At around the same time, growth rate of the PNG-01 stalagmite starts to increase. Are these two events, a decrease in temperature in the NALPS record and an increase in effective rainfall observed in the PNG-01 record, somehow linked to each other? The first section of the NALPS also shows an increase of the $\delta^{18}O$ signature with approximately 3‰, is this increase in temperature correlated with the start of the PNG-01 stalagmite formation? These are only two possible questions that can only be answered when more research is carried out.

Comparison with the distant NALPS and NGRIP records is thus far from straightforward and only some very careful comparisons can be made. Comparison with the more proximal ELSA greyscale stack from the Eifel region could potentially be more interesting. As a refresher, values closer to one represent lighter coloured sediments with less organic material and higher values are thus interpreted as drier periods. Visually, the ELSA stack and the stable isotope records seem to correlate with each other. Especially the trend towards drier conditions in the youngest section of the PNG-01 speleothem seems to be also well reflected in the ELSA stack. Moreover, the wetter period between around 100 and 97 ka detected in the PNG-01 core, corresponds quite nicely with a shift to a wetter climate with more production of organic matter observed in the Eifel maar deposits (Sirocko et al., 2005). This good correlation validates the hypotheses proposed a few pages ago (section 4.5) that the period between 100 and 97 ka was wet and was followed a climate which become gradually drier. In the older half of the PNG-01 speleothem (above 99 ka), the correlation with

the ELSA stack is clearly less strong. However, even in the older section of the speleothem there appear to be some similarities between the ELSA curve and the $\delta^{13}C$ signal, which is influenced by vegetation shifts on the surface if a speleothem is deposited in isotopic equilibrium. Differences in the exact ages of some of these peaks could be the result of errors in the PNG-01 age model, or in the other datasets discussed here. Further work is needed to refine this part.

4.6.3 Benthic marine core

Finally, the benthic $\delta^{18}O$ record from the MD95-2042 core can be compared with the measurements presented in this thesis. In theory, this record reflects changes in continental ice volume. However, due to the low resolution of this record at the scale of interest, correlations are quite difficult. One possible interpretation here could be that from around 101,5 ka the benthic $\delta^{18}O$ signal slowly decreases, which would indicate a gradual build-up of continental ice volume. If that was the case, this could correlate with the observed cooling trend in the NALPS and NGRIP records and the shift towards a drier climate potentially observed in the ELSA stack and PNG-01 records.

4.6.4 Volcanic activity in the Eifel region

Förster and Sirocko (2015) created similarly to the ELSA greyscale stack a stack of all tephra layers in the Eifel region for the last 500 000 years, the ELSA tephra stack. In total, 91 individual tephra layers were identified. They observed that many eruptions were clustered near the timings of global climate transitions, for example around the Eemian to Weichselian transition. Between around 115 ka and 100 ka, a cluster of different maars erupted, for example the well-known Dümpelmaar Plinian eruption at 106 ka and a phreatomagmatic eruption at 104 ka. These maar eruptions were followed by the eruption of three Strombolian-type tephra layers at 95 ka, 90 ka and 85 ka (Förster and Sirocko, 2015).

Volcanic eruption can influence regional and global climate, because volcanic ashes released into the atmosphere cause temporary cooling by reducing the amount of solar radiation reaching the surface of the earth. However, eruptions should be a of sufficient magnitude to cause a real impact and ideally should also be situated at lower latitudes (Kelly et al., 1996). The Strombolian-type eruption at around 95 ka most likely did not have a large impact on the regional climate, which would imply that the different paleoclimatic proxies in the PNG-01 speleothem were probably not really influenced

by this eruption. It is also difficult to pinpoint the exact location of this eruption on the age model of the PNG-01 speleothem due to the relatively large error on the model.

However, events of volcanic ash fall can be identified inside speleothems, for example by a principal component analysis of trace elements in a speleothem as described in Jamieson et al. (2015). A higher resolution record of the trace element variation in the PNG-01 speleothem could potentially reveal if ash of this 95 ka eruption reached the area above the cave and subsequently influenced the trace elemental signature. This could further enhance the quality of the age model. The same is true for the stronger phreatomagmatic eruption at 104 ka. Because this eruption took place close to the start of speleothem formation (around 103,6 ka) and because the error of the age model increases at the boundaries, it is possible that evidence for this eruption can be found inside the PNG-01 speleothem. Potentially, the 104 ka and 106 ka eruptions are somehow linked to the change in climatic conditions, which triggered the start of PNG-01 formation, but completely understanding the complex series of feedback mechanisms influencing each other and creating the change in climate at that time will require more research. The present work on the PNG-01 core opens interesting future perspectives for correlation with the Eiffel ash record.

4.7 COMPARISON WITH SIMILAR STUDIES

4.7.1 Han-9 stalagmite

Vansteenberge et al. (2016) reconstructed the paleoclimate in continental northwestern Europe during the Eemian and early Weichselian (between 125 and 97 ka) based on stable isotope measurements on the Han-9 speleothem from the Han-sur-Lesse cave system, the same cave system of which the Père Noël cave is part of. Table 10 compares some statistic parameters of the stable isotope records of both the PNG-01 and Han-9 speleothem.

	Mean (‰)	Maximum (‰)	Minimum (‰)	Range (‰)
$\delta^{13}C$ PNG-01	-6,92	-3,12	-9,68	6,55
$\delta^{13}C$ Han-9	-7,53	-3,58	-10,30	6,72
$\delta^{18}O$ PNG-01	-5,65	-4,32	-7,36	3,04
$\delta^{18}O$ Han-9	-5,91	-5,04	-7,02	1,98

Table 10 – Comparison of the statistical parameters of the Han-9 and PNG-01 speleothem (Han-9 data from Vansteenberge et al., 2016)

Both speleothems appear to contain very similar isotopic records, only the range of $\delta^{13}C$ signal is clearly higher in the Han-9 records. This could of course be somewhat expected given the fact that they formed in close proximity of each other and they cover partially the same timeframe. Nevertheless, this similarity indicates the quality of the stable isotope measurements.

In contrast with the PNG-01 speleothem, the Han-9 speleothem experienced two hiatuses during the formation of the speleothem. The second hiatus (between 106,6 and 103 ka) was interpreted to have an affinity with the cold GS24 period, the last stadial period before the GI23 period, which corresponds with the formation of the PNG-01 speleothem. Keeping in mind that the age model used in this thesis has large uncertainties on the outer limits, a difference of only 0,6 ka between the start of PNG-01 speleothem formation and the continuation of the Han-9 speleothem formation is quite interesting and strengthens the hypothesis that the GI23 warmer climate created the favourable conditions responsible for the start of PNG-01 speleothem formation. The transition from GI23 to the colder GS23 probably coincides with the end of speleothem formation.

4.7.2 Present-day and recent deposits in the Père Noël cave

Table 11 compares the isotopic signature of present-day calcite deposited in the Père Noël cave with the PNG-01 values. Although there is a timespan of around 100 000 years between the deposition of the calcite, their isotopic signatures are nevertheless very similar. On average, the present-day values are a bit higher, but the differences are limited. Because prior calcite precipitation was interpreted to be an import process influencing the present-day and Holocene deposits (Verheyden et al., 2001; Verheyden et al., 2008), both the more recent and the PNG-01 values are representing hydrological change. This would imply that on average the climate was wetter during the MIS 5c equivalent timeframe than in the Holocene.

	PNG-01 (‰)	**Range (‰)**	**Present-day (‰)**	**Range (‰)**
$\delta^{13}C$	-9,68 to -3,12	6,55	-9,0 to -2,6	6,4
$\delta^{18}O$	-7,36 to -4,32	3,04	-6,0 to -3,8	2,2

Table 11 - Comparison between the isotopic signature of present-day calcite and the PNG-01 speleothem, both deposited in the Père Noël cave (present-day values are from Verheyden et al., 2008)

If this was the cause, the average growth rate of more recent speleothems should also be lower and this seems to be the case. Verheyden et al. (2014) describe a Holocene stalagmite from the same Père Noël cave, which is deposited between 12,9 and 1,8 ka and has a total length of 640 mm. This indicates an average growth rate of 0,058 mm/year. The average growth rate of the PNG-01 speleothem is 0,104 mm/year (1015 mm was deposited in 9758 years according to the age model), although this average is influenced by the substantially wetter period between around 100 ka and 97 ka. This strengthens the hypothesis that on average the climate above the Père Noël cave and in continental Belgium was wetter during the formation of the PNG-01 speleothem than it is today and probably was during most of the Holocene.

If speleothems are deposited in isotopic equilibrium, the expected $\delta^{13}C$ values for C3 and C4 type of vegetation are between -14 to -6‰ and -6 to +2‰ respectively (see 2.2.5.1.1). Based on presence of C3 vegetation in the area above the cave, the fact that $\delta^{13}C$ signals of the Père Noël cave are influenced by kinetic fractionation processes and that the $\delta^{13}C$ values of today are even higher than they were during PNG-01 formation, it is safe to assume that the processes influencing the isotopic signals in the Père Noël cave today are similar to the processes of 100 000 years ago.

4.8 SUMMARY

Based on a multitude of different proxies (morphology, growth rate, stable isotopes and trace element measurements) recovered from the PNG-01 stalagmite from the Père Noël cave, a potential reconstruction of the paleoclimatic of Belgium during the MIS 5c equivalent timeframe or more specifically from around 103,6 to 93,8 ka, was made.

Unfortunately, due to the influence of kinetic fractionation processes, the carbon and oxygen stable isotope signals could not be interpreted in function of temperature, but were together with the trace element measurements used to assess alternating wet and dry paleoclimate over time. The start of the PNG-01 speleothem formation is possibly linked with the transition from Greenland Stadial 24 to Greenland Interstadial 23, which created favourable conditions for speleothem formation. Most of the speleothem was, aside from a wetter period between around 100 and 97 ka, most likely deposited during drier conditions, which is for example reflected in the variation of the speleothem growth rates but also in the speleothem morphology.

Finally, the youngest section of the speleothem likely reflects a rather gradual shift towards the even drier conditions linked with GS23 (visible in both the PNG-01 stable isotope records and the ELSA greyscale stack), which probably stopped formation of the PNG-01 formation.

5 CONCLUSION

Did the continental climate in Belgium during the early Weichselian experience similar climatic change as observed in other paleoclimatic proxies?

Based on the research conducted on the PNG-01 stalagmite, the main question of this thesis can be answered with both yes and no. According to the proxy used for correlation, the correlation can be rather good (e.g. ELSA greyscale stack), or rather weak (e.g. NGRIP). Of course, this short 'yes and no' answer hides some of the finer details, which can be extracted from the PNG-01 proxies (see section 4.8).

The climate during the formation of the PNG-01 speleothem shows some distinct periods (at the start of speleothem formation and between 100 and 97 ka) of increased growth rate, which are most likely linked to a higher availability of water. In the drier periods, speleothem formation was slow but probably not interrupted. These changes in water availability reflected in the speleothem morphology, the stable isotope records and the trace element values, give further confidence to this conclusion.

Did the PNG-01 stalagmite precipitate in isotopic equilibrium? Are the stable isotope and trace element signals mainly controlled by temperature or by effective precipitation?

Based on the very good correlation between the oxygen and carbon stable isotope records in the youngest section of the speleothem between 93,8 and 101 ka, kinetic processes probably altered the stable isotope signals. In the older section of the speleothem, correlation is less strong, but most likely the complete speleothem was influenced by kinetic fractionation processes of which the influence got stronger towards the younger sections of the speleothem. This points towards a drier climate with less recharge, a trend which can also be observed in the speleothem morphology and the variation in growth rate. Only if a speleothem is deposited in isotopic equilibrium, the stable isotope trends can possibly be used as a proxy for paleotemperatures. This is not the case here, so the signals are mostly controlled by effective precipitation.

How do the results of this study compare with other research?

At first sight, only the ELSA greyscale stack from the Eifel maars seems to correlate with the PNG-01 stable isotope proxies. Both the ELSA stack and the PNG-01 proxy records mainly reflect alternating wet or dry paleoclimates. The NGRIP ice core record and the NALPS speleothem record reflect mainly changes in atmospheric temperature, and although the decreasing trend in temperature observed in these records cannot directly be found in the PNG-01 records, the start and end date of speleothem formation correlate quite well with the transition towards GI23 and GS23 respectively.

Closing thoughts

Paleoclimate reconstructions based on speleothem proxies are far from straightforward. If no isotopic equilibrium can be assumed, which is almost always the case, interpreting the stable isotope signals remains complex. Many processes can influence the variations observed in the records and although the study of trace elements helps with the interpretation of the stable isotope signals, a lot of additional research is still required to fully understand which processes control the availability of the different trace elements. Correlating all the possible proxies stored in the speleothem is essential for good and valid paleoclimatic reconstructions.

There is room for improvement in the study of PNG-01 speleothem. For example, thin sections are essential to better understand the macroscopic morphological changes observed in the speleothem. Also, the resolution of the stable isotope and the trace element records should be increased, most importantly in the section with slow growth rates. Having already an estimation of the growth rate variation would allow to construct a model which calculates the inter-sample distances that would deliver records with a constant temporal resolution. Higher resolution trace element records could potentially also reveal if the PNG-01 speleothem was influenced by the volcanic eruptions in the Eifel region. Also, direct measurements of the $\delta^{18}O$-signal stored in fluid inclusions of the speleothem could aid with the interpretation of the oxygen stable isotope record. Finally, other techniques, for example cathodoluminescence on thin samples, could possibly expose some extra information stored inside the speleothem.

---

6 REFERENCES

BAKER, A., ITO, E., SMART, P. L., McEWAN, R. F. 1997. Elevated and variable values of ^{13}C in speleothems in a British cave system. *Chemical Geology* **136**, 263-270.

BELL, M., WALKER, M. J. C. 2005. *Late Quaternary Environmental Change - Physical and Human Perspective*. Pearson Education Limited, New York, 348p.

BERGER, A., LOUTRE, M. F. 1991. Insolation values for the climate of the last 10 million years. *Quaternary Science Reviews* **10**, 297-317.

BOCH, R., CHENG, H., SPÖTL, C., EDWARDS, R. L., WANG, X., HAUSELMANN, P. 2011. NALPS: a precisely dated European climate record 120-60 ka. *Climate of the Past* **7**, 1247-1259.

BOND, G. C., SHOWERS, W., ELLIOT, M., EVANS, M., LOTTI, R., HAJDAS, I., BONANI, G., JOHNSON, S. 1999. The North Atlantic's 1-2 kyr Climate Rhythm: Relation to Heinrich Events, Dansgaard/Oeschger Cycles and the Little Ice Age. *Mechanisms of Global Climate Change at Millenial Time Scales Geophysical Monograph* **112**, 35-58.

BORSATO, A., FRISIA, S., FAIRCHILD, I. J., SOMOGYI, A., SUSINI, J. 2007. Trace element distribution in annual stalagmite laminae mapped by micrometer-resolution X-ray fluorescence: Implications for incorporation of environmentally significant species. *Geochimicia et Cosmochimica* Acta **71**, 1494-1512.

BREITENBACH, S. F. M., REHFELD, K., GOSWAMI, B., BALDINI, J. U. L., RIDLEY, H. E., KENNETT, D. J., PRUFER, K. M., AQUINO, V. V., ASMERON, Y., POLYAK, V. J., CHENG, H., KURTHS, J., MARWAN, N. 2012. Constructing Proxy Records from Age models (COPRA). *Climate of the Past* **8**, 1765-1779.

BRONK RAMSEY, C. 2008. Deposition models for chronological records. *Quaternary Science Reviews* **27**, 42-60.

CENTER FOR ICE AND CLIMATE, 2017. Data, ice samples and software, http://www.iceandclimate.nbi.ku.dk/data/.

CHAPMAN, M., SHACKLETON, N. J., DUPLESSY, J-C. 2000. Sea surface temperature variability during the last glacial–interglacial cycle: assessing the magnitude and pattern of climate change in the North Atlantic. *Palaeogeography, Palaeoclimatology, Palaeoecology* **157**, 1–25.

CHENG, H., EDWARDS, R. L., BROECKER, W. S., DENTON, G. H., KONG, X., WANG, Y., ZHANG, R., WANG, X. 2009. Ice Age Terminations. *Science* **326**, 248-252.

DANSGAARD, W. 1964. Stable isotopes in precipitation. *Tellus XVI (1964)* **4**, 436-468.

DE BEAULIEU, J. L., REILLE, M. 1992. The last climatic cycle at la Grande Pile (Vosges, France), a new pollen profile. *Quaternary Science Reviews* **11**, 431-438.

DE WINTER, N., SNOECK, C., CLAEYS, P. 2016. Seasonal Cyclicity in Trace Elements and Stable Isotopes of Modern Horse Enamel. *PLosONE* **11**, 1-29.

EMILIANI, C. 1955. Pleistocene Temperatures. *Journal of Geology* **63**, 538-578.

FAIRCHILD, I. J., BAKER, A. 2012. Speleothem Science: From Process to Past Environments. Wiley-Blackwell, 450p.

FAIRCHILD, I. J., BORSATO, A., TOOTH, A. F., FRISIA, S., HAWKESWORTH, C. J., HUANG, Y., McDERMOTT, F., SPIRO, B. 2000. Controls on trace element (Sr-Mg) compositions of carbonate cave waters: implications for speleothem climatic records. *Chemical Geology* **166**, 208-232.

FAIRCHILD, I. J., FRISIA, S., BORSATO, A., TOOTH, A.F. 2006. Geochemical Sediments and Landscapes (Chapter 7 – Speleothems). Blackwells, Oxford, 21p.

FAIRCHILD, I. J., TREBLE, P. 2009. Trace elements in speleothems as recorders of environmental change. *Quaternary Science Reviews* **28**, 449-468.

FÖRSTER, M. W., SIROCKO, F. 2015. Volcanic activity in the Eifel during the last 500,000 years: The ELSA-Tephra-Stack. *Global and Planetary Change* **142**, 100-107.

FRIEDMAN, I., O'NEILL, J., CEBULA, G. 1982. Two New Carbonate Stable-Isotope Standards. *Geostandards Newsletter* **6**, 11-12.

FRISIA, S., BORSATO, A. 2010. Karst. *Developments in Sedimentology* **61**, 269-318.

GASCOYNE, M. 1983. Trace-element partition coefficients in the calcite-water system and their paleoclimatic significance in cave studies. *Journal of Hydrology* **61**, 213-222.

GENTY, D., BLAMART, D., OUAHDI, R., GILMOUR, M., BAKER, A., JOUZEL, J., VAN-EXTER, S. 2003. Precise dating of Dansgaard-Oeschger climate oscillations in western Europe from stalagmite data. *Nature* **421**, 833-837.

GENTY, D., DEFLANDRE, G. 1998. Drip flow variations under a stalacticte of the Père Noël cave (Belgium). Evidence of seasonal variations and air pressure constraints. *Journal of Hydrology* **208**, 208-232.

GENTY, D., QUINIF, Y. 1996. Annually laminated sequences in the internal structure of some Belgian stalagmites – importance for paleoclimatology. *Journal of Sedimentary Research* **66**, 275-288.

GOVIN, A. ET AL. 2015. Sequence of events from the onset to the demise of the Last Interglacial: Evaluating strengths and limitations of chronologies used in climatic archives. *Quaternary Science Reviews* **129**, 1-36.

GRIMES, K. G. 1999. The Water Below: An introduction to karst hydrology and the hydrological setting of the Australian karsts. *Proceedings of the 13th Australasian Conference on Cave and Karst Management*, 24-31.

HELMENS, K. F. 2014. The Last Interglacial-Glacial cycle (MIS 5-2) re-examined based on long proxy records from central and northern Europe. *Quaternary Science Reviews* **86**, 115-143.

HENDY, C. H. 1971. The isotopic geochemistry of speleothems – I. The calculation of the effects of different modes of formation on the isotopic composition of speleothems and their applicability as paleoclimatic indicators. *Geochimica et Cosmochimica* Acta **35**, 801-824.

HERCMAN, H., PAWLAK, J. 2012. MOD-AGE: An age-depth model construction algorithm. *Quaternary Geochronology* **12**, 1-10.

HOEFS, J. 2015. *Stable Isotope Geochemistry*. Springer, Switzerland, 402p.

ICS 2017. International Chronostratigraphic Chart v2016/12, http://www.stratigraphy.org/ICSchart/ChronostratChart2016-12.pdf.

IMBRIE, J., HAYS, J. D., MARTINSON, D. G., SHACKLETON, N. J. 1984. The orbital theory of Pleistocene climate: Support from a revised chronology of the marine delta 18O record. *Milankovitch and Climate* **1**, 269-305.

IPCC 2013. Fifth Assessment Report, https://www.ipcc.ch/pdf/assessment-report/ar5/wg1/WG1AR5_SPM_FINAL.pdf.

JAMIESON, R. A., BALDINI, J. U. L., FRAPPIER, A. B., MÜLLER, W. 2015. Volcanic ash fall events identified using principal component analysis of a high-resolution speleothem trace element dataset. *Earth and Planetary Science Letters* **426**, 36-45.

JENS LABORATORY 2017. ICP-MS, http://eecelabs.seas.wustl.edu/ICP-MS.aspx.

KELLY, P. M., JONES, P. D., PENGQUN, J. 1996. The spatial response of the climate system to explosive volcanic eruptions. *International Journal of Climatology* **15**, 537-550.

KENDALLL, C., McDONNELL, J. J. 1998. *Isotope Tracers in Catchment Hydrology*. Elsevier Science B.V., Amsterdam, 839p.

KMI 2017. Climate statistics for Rochefort, http://www.kmi.be/resources/climateCity/pdf/climate_INS91114_ROCHEFORT_nl.pdf.

KÖHLER, P., BINTANJA, R., FISCHER, H., FORTUNAT, J., KNUTTI, R., LOHMANN, G., MASSON-DELMOTTE, V. 2009. What caused Earth's temperature variations during the last 800,000 years? Data-based evidence on radiative forcing and constraints on climate sensitivity. *Quaternary Science Reviews* **29**, 129-145.

KRÜGER, Y., MARTI, D., STAUB, R. H., FRENZ, M. 2011. Liquid-vapour homogenisation of fluid inclusions in stalagmites: Evaluation of a new thermometer for paleoclimate research. *Chemical Geology* **289**, 39-47.

LACHNIET, M. S. 2009. Climatic and environmental controls on speleothem oxygen-isotope values. *Quaternary Science Reviews* **28**, 412-432.

LAMBECK, K., ESAT, T. M., POTTER, E. 2002. Links between climate and sea levels for the past three million years. *Nature* **419**, 199-2016.

LISIECKI, L. E., RAYMO, M. E. 2005. A Pliocene-Pleistocene stack of 57 globally distributed benthic d18O records. *Palaeoceanography* **20**, PA1003.

MANGERUD, J., GYLLENCREUTZ, R., LOHNE, O., SVENDSEN, J. I. 2011. Glacial History of Norway. *Developments in Quaternary Science* **15**, 279-298.

MARTINSON, D. G., PISIAS, N. G., HAYS, J. D., IMBRIE, J., MOORE, T. C., SHACKLETON, N. J. 1987. Age Dating and the Orbital Theory of the Ice Ages: Development of a High-Resolution 0 to 300,000-Year Chronostratigraphy. *Quaternary Research* **27**, 1-29.

McDERMOTT, F. 2004. Paleo-climate reconstruction from stable isotope variations in speleothems: a review. *Quaternary Science Reviews* **23**, 901-918.

MICKLER, P. J., STERN, L. A., BANNER, J. L. 2006. Large kinetic isotope effects in modern speleothems. *Geological Society of America Bulletin* **118**, 65-81.

NEEM Members. 2012. Eemian interglacial reconstructed from a Greenland folded ice core. *Nature* **493**, 489-494.

NGRIP Members, 2004. High-resolution record of Northern Hemisphere climate extending into the last interglacial period. *Nature* **431**, 147-151.

NU INSTRUMENTS 2017. Nu Perspective IRMS – Application Note AN20, http://www.nu-ins.com/wp-content/uploads/Application-Note-20.pdf.

OPPO, D. W., McMANUS, J. F., CULLEN, J. L. 2006. Evolution and demise of the Last Interglacial warmth in the subpolar North Atlantic. *Quaternary Science Reviews* **25**, 3268-3277.

OXFORD DICTIONARIES, 2017. Weichsel. https://en.oxforddictionaries.com/definition/Weichsel.

PEEL, M. C., FINLAYSON, B. L., MCMAHON, T. A. 2007. Updated world map of the Köppen-Geiger climate classification. *Hydrology and Earth System Sciences* **11**, 1633-1644.

POULAN, A., ROCHEZ, G., BONNIVER, I., HALLET, V. 2015. Stalactite drip-water monitoring and tracer tests approach to assess hydrogeologic behaviour of karst vadose zone: case study of Han-sur-Lesse (Belgium). *Environmental Earth Sciences* **74**, 7685-7697.

RIEBEEK, H. 2005. Paleoclimatology: The Ice Core Record, https://earthobservatory.nasa.gov/Features/Paleoclimatology_IceCores/.

ROBERTS, M. S., SMART, P. L., BAKER, A. 1998. Annual trace element variation in a Holocene speleothem. *Earth and Planetary Science Letters* **154**, 237-246.

SCHOLZ, D., HOFFMANN, D. L. 2011. StalAge - An algorithm designed for construction of speleothem age models. *Quaternary Geochronology* **6**, 369-382.

SCHOLZ, D., HOFFMANN, D. L., HELLSTROM, J., RAMSEY, C. B. 2012. A comparison of different methods for speleothem age modelling. *Quaternary Geochronology* **14**, 94-104.

SCHURGERS, G., MIKOLAJEWICZ, U., GRÖGER, M. 2007. The effect of land surface changes on Eemian climate. *Climate Dynamics* **4**, 357-373.

SCIENCEBLOGS, 2017. Carbon isotopes, http://scienceblogs.com/startswithabang/files/2012/06/carbon-950x537.jpg.

SEDGWICK, P. 2012. Pearson's correlation coefficient. *British Medical Journal* **345**, 1-2.

SHACKLETON, N. 1967. Oxygen Isotope Analyses and Pleistocene Temperatures Re-assessed. *Nature* **25**, 15-17.

SHACKLETON, N. 1969. The Last Interglacial in the Marine and Terrestrial Records. *Proceedings of The Royal Society* **174**, 135-154.

SHACKLETON, N. J., HALL, M. A., VINCENT, E. 2000. Phase relationships between millennial-scale events 64,00-24,000 years ago. *Paleoceanography* **15**, 565-569.

SHACKLETON, N. J., SANCHEZ-GONI, M. F. et al. 2003. Marine Isotope Substage 5e and the Eemian Interglacial. *Global and Planetary Change* **36**, 151-155.

SINTUBIN, M., 2004. De Geologische Geschiedenis van België [CD-ROM]. Acco.

SINTUBIN, M., DEBACKER, T. N., VAN BAELEN, H., 2009. Early Paleozoic orogenic events north of the Rheic suture (Brabant, Ardenne): A review. C. R. *Geosciences* **341**, 156-173.

SIROCKO, F. 2016. The ELSA – Stacks (Eifel-Laminated-Sediment-Archive): An introduction. *Global and Planetary Change* **142**, 96-99.

SIROCKO, F., SEELOS, K., SCHABER, K., REIN, B., DREHER, F., DIEHL, M., LEHNE, R., JÄGER, K., KRBETSCHEK, M, DEGERING, D. 2005. A late Eemian aridity pulse in central Europe during the last glacial inception. *Nature* **436**, 833-836.

STOCKER, T. F., JOHNSEN, S. J. 2003. A minimum thermodynamic model for the bipolar seesaw. *Paleoceanography* **18**.

TZEDAKIS, P. C., FROGLEY, M. R., HEATON, T. H. E. 2003. Last Interglacial conditions in southern Europe: evidence from Ioannina, northwest Greece. *Global and Planetary Change* **36**, 157-170.

VAN RAMPELBERGH, M. 2014. Speleothems as tools to reconstruct paleoclimates in temperate (Belgium) and semi-arid (Socotra, Yemen) regions during the Mid- to Late Holocene. Ph.D. dissertation, Vrije Universiteit Brussel.

VANSTEENBERGE, S., VERHEYDEN, S., CHENG, H., EDWARDS, R. L., KEPPENS, E., CLAEYS, P. 2016. Paleoclimate in continental northwestern Europe during the Eemian and early Weichselian (125–97ka): insights from a Belgian speleothem. *Climate of the Past* **12**, 1445-1458.

VERHEYDEN, S. & DELABY, S. 2012. The Belgian Karst. Unpublished work. CSARI, Geological Survey of Belgium, Royal Belgian Institute of natural Sciences and University of Mons, Belgium.

VERHEYDEN, S., GENTY, D., DEFLANDRE, G., QUINIF, Y., KEPPENS, E. 2008. Monitoring climatological, hydrological and geochemical parameters in the Père Noël cave (Belgium): implication for the interpretation of speleothem isotopic and geochemical time-series. *International Journal of Speleology* **37** (3), 221-234.

VERHEYDEN, S., KEPPENS, E., FAIRCHILD, I. J., McDERMOTT, F., WEIS, D. 2000. Mg, Sr and Sr isotope geochemistry of a Belgian Holocene speleothem: implications for paleoclimate reconstructions. *Chemical Geology* **169**, 131-144.

VERHEYDEN, S., KEPPENS, E., QUINIF, Y., CHENG, H. J., EDWARDS, L. R. 2014. Late-glacial and Holocene climate reconstruction as inferred from a stalagmite - Grotte du Père Noël, Han-sur-Lesse, Belgium. *Geologica Belgica* **17**/1, 83-89.

WILLIAMS, P. W. 2008. The role of the epikarst in karst and cave hydrogeology: a review. *International Journal of Speleology* **37**, 1-10.

WOHLFARTH, B. 2013. A review of Early Weichselian climate (MIS 5d-a) in Europe (Technical Report TR-13-03). Svensk Kärnbränslehantering AB, Stockholm, 70p.

WOILLARD, G. M. 1978. Grande Pile Peat Bog: A Continuous Pollen Record for the Last 140,000 Years. *Quaternary Research* **9**, 1-21.

7.1 U/TH AGES

^{230}Th dating results. The error is 2σ error.

Sample Number	^{238}U (ppb)	^{232}Th (ppt)	^{230}Th / ^{232}Th (atomic x10^{-6})	δ^{234}U* (measured)	^{230}Th / ^{238}U (activity)	^{230}Th Age (yr) (uncorrected)	^{230}Th Age (yr) (corrected)	$\delta^{234}U_{Initial}$** (corrected)	^{230}Th Age (yr BP)*** (corrected)
G-1	40,2 ±0,1	1173 ±23	557 ±11	636,6 ±1,6	0,9858 ±0,0018	93275 ±296	**92810 ±442**	827 ±2	**92745 ±442**
G-2	54,1 ±0,1	184 ±4	4890 ±99	632,4 ±2,4	1,0113 ±0,0018	97303 ±347	**97249 ±349**	832 ±3	**97184 ±349**
G-3	54,9 ±0,1	134 ±3	6730 ±137	632,8 ±2,1	0,9949 ±0,0016	94911 ±302	**94872 ±303**	827 ±3	**94807 ±303**
G-4	59,5 ±0,1	102 ±2	10017 ±208	633,3 ±1,9	1,0380 ±0,0015	101151 ±302	**101124 ±303**	842 ±3	**101059 ±303**
G-5	61,4 ±0,1	1554 ±31	662 ±13	637,3 ±1,9	1,0170 ±0,0018	97656 ±324	**97254 ±430**	839 ±3	**97189 ±430**
G-6	56,9 ±0,1	133 ±3	7121 ±145	634,9 ±2,0	1,0115 ±0,0017	97089 ±314	**97052 ±315**	835 ±3	**96987 ±315**
G-7	49,7 ±0,1	5 ±1	42702 ±4321	639,1 ±2,1	0,2425 ±0,0026	17283 ±199	**17281 ±199**	671 ±2	**17216 ±199**
G-8	52,3 ±0,1	134 ±3	6505 ±133	638,7 ±1,6	1,0152 ±0,0015	97262 ±274	**97222 ±275**	840 ±2	**97157 ±275**
G-9	53,3 ±0,1	93 ±2	9827 ±202	641,9 ±2,0	1,0353 ±0,0016	99878 ±308	**99851 ±308**	851 ±3	**99786 ±308**
G-10	54,3 ±0,1	67 ±1	13676 ±298	653,4 ±1,9	1,0271 ±0,0016	97562 ±295	**97542 ±296**	860 ±3	**97477 ±296**
G-11	70,7 ±0,1	144 ±3	8656 ±177	659,4 ±2,3	1,0674 ±0,0018	102871 ±357	**102840 ±358**	881 ±3	**102775 ±358**
G-12	65,5 ±0,1	56 ±1	20562 ±444	648,0 ±2,5	1,0597 ±0,0018	102885 ±374	**102871 ±374**	866 ±4	**102806 ±374**
G-13	71,2 ±0,1	147 ±3	8485 ±173	663,4 ±1,8	1,0611 ±0,0017	101523 ±307	**101491 ±308**	883 ±3	**101426 ±308**

U decay constants: $\lambda_{238} = 1.55125 \times 10^{-10}$ (Jaffey et al., 1971) and $\lambda_{234} = 2.82206 \times 10^{-6}$ (Cheng et al., 2013). Th decay constant: $\lambda_{230} = 9.1705 \times 10^{-6}$ (Cheng et al., 2013).

*$\delta^{234}U = ([^{234}U/^{238}U]_{activity} - 1) \times 1000$. ** $\delta^{234}U_{initial}$ was calculated based on ^{230}Th age (T), i.e., $\delta^{234}U_{initial} = \delta^{234}U_{measured} \times e^{\lambda_{234} T}$.

Corrected ^{230}Th ages assume the initial $^{230}Th/^{232}Th$ atomic ratio of 4.4 ±2.2 x10^{-6}. Those are the values for a material at secular equilibrium, with the bulk earth $^{232}Th/^{238}U$ value of 3.8. The errors are arbitrarily assumed to be 50%.

***B.P. stands for "Before Present" where the "Present" is defined as the year 1950 A.D.

7.2 STABLE ISOTOPE MEASUREMENTS

Sample	Dft (mm)	Age (yrs BP)	$\delta^{13}C$ (‰)	Std. error	$\delta^{18}O$ (‰)	Std. error
1	4	93501,21	-3,12035	0,016283	-4,79055	0,090975
2	10	93567,52	-5,26045	0,046746	-5,14345	0,098876
3	15	93622,78	-5,05575	0,016067	-4,90615	0,090694
4	19	93666,99	-6,04385	0,029566	-5,19605	0,09466
5	25	93733,3	-5,75802	0,026205	-5,639	0,049062
6	29	93777,51	-5,68022	0,026033	-5,498	0,048571
7	34	93832,77	-5,20815	0,016283	-5,27775	0,090694
8	40	93899,08	-5,07842	0,025898	-5,339	0,048663
9	44	93943,29	-6,55762	0,026205	-5,922	0,050677
10	49	93998,55	-5,62482	0,026033	-5,481	0,048909
11	55	94064,86	-5,33255	0,016067	-5,11035	0,090975
12	60	94120,12	-7,95865	0,016886	-6,13725	0,090623
13	65	94175,38	-8,38025	0,023086	-6,7968	0,056604
14	71	94241,69	-6,59715	0,023344	-5,645	0,056604
15	75	94285,9	-5,84205	0,025079	-5,3982	0,056602
16	80	94341,16	-7,09395	0,023194	-5,6234	0,056603
17	85	94396,42	-5,52865	0,023086	-5,363	0,056603
18	90	94451,68	-5,76555	0,023194	-5,2782	0,056613
19	95	94506,94	-6,44245	0,023536	-5,5234	0,056644
20	101	94573,25	-7,94235	0,023194	-6,1446	0,056602
21	105	94617,46	-8,66725	0,027458	-6,6838	0,056603
22	110	94672,72	-7,66515	0,023194	-6,278	0,056602
23	115	94727,98	-7,14505	0,023344	-6,1252	0,056601
24	120	94783,24	-6,64695	0,02302	-5,7694	0,056601
25	125	94838,5	-7,51855	0,016283	-6,23835	0,090562
26	131	94904,81	-9,31265	0,016283	-6,51825	0,090623
27	135	94949,02	-8,59875	0,016283	-6,41015	0,090562
28	140	95004,28	-7,87085	0,016283	-6,05205	0,090446
29	145	95059,54	-7,70795	0,033899	-5,86895	0,094369
30	150	95114,8	-8,66005	0,016067	-6,44885	0,093303
31	155	95170,06	-9,04715	0,016283	-6,69275	0,090512
32	160	95225,32	-8,35325	0,016067	-6,93965	0,090562
33	165	95280,58	-8,84075	0,024312	-6,85433	0,105193
34	170	95335,84	-7,40525	0,024557	-6,13863	0,105227
35	175	95391,1	-7,68675	0,024414	-6,10993	0,108815
36	180	95446,36	-7,45925	0,031418	-6,07523	0,105269
37	185	95501,62	-7,46575	0,02474	-5,85753	0,108317
38	190	95556,88	-8,29625	0,024414	-6,52883	0,105227
39	195	95612,14	-7,04375	0,024557	-6,12613	0,105193
40	200	95667,4	-6,28625	0,024312	-5,50543	0,105322
41	205	95722,66	-8,26175	0,024557	-6,06133	0,105227
42	210	95777,92	-8,71425	0,024414	-6,48963	0,106361

43	215	95833,18	-8,47275	0,02522	-6,33893	0,105322
44	220	95888,44	-8,90225	0,02474	-6,29823	0,106361
45	225	95943,7	-8,86075	0,024557	-6,42553	0,105322
46	230	95998,96	-9,31225	0,024414	-6,64983	0,105322
47	235	96054,22	-8,89475	0,04094	-6,70813	0,10668
48	240	96109,48	-9,67525	0,024414	-7,36343	0,108082
49	245	96164,74	-9,40275	0,02522	-6,50933	0,107637
50	249	96208,95	-9,12425	0,024961	-6,34663	0,105322
51	255	96275,26	-9,32175	0,024414	-6,76193	0,105193
52	260	96330,52	-9,43925	0,024414	-6,64923	0,106215
53	265	96385,78	-9,42475	0,02474	-6,94253	0,107427
55	276	96507,35	-9,38675	0,024414	-6,47813	0,105269
56	280	96551,56	-8,76625	0,024961	-6,32743	0,107227
58	289	96651,03	-7,51115	0,06748	-5,80785	0,052466
59	295	96717,34	-7,18805	0,067428	-5,83335	0,052466
60	300	96772,6	-5,31795	0,067391	-5,56585	0,052533
61	305	96827,86	-5,67985	0,067391	-5,47635	0,052533
62	310	96883,12	-7,42175	0,067391	-5,56085	0,052618
63	316	96949,43	-5,35065	0,069012	-4,90635	0,052419
64	320	96993,64	-6,73655	0,067428	-5,69785	0,052466
65	324	97037,85	-6,76625	0,067428	-5,73635	0,052618
66	330	97104,16	-4,75315	0,06748	-5,31685	0,052533
67	336	97170,47	-7,65805	0,067391	-5,97035	0,052533
68	340	97214,68	-6,56995	0,06748	-6,01785	0,052533
69	346	97280,99	-6,22285	0,067391	-5,49535	0,054219
70	350	97325,2	-5,72075	0,067391	-4,51185	0,052419
71	354	97369,41	-7,08865	0,067428	-5,63635	0,052466
72	360	97435,72	-7,10125	0,016067	-5,79565	0,090473
73	365	97490,98	-6,72825	0,06796	-5,82735	0,053969
74	370	97546,24	-6,38815	0,0681	-5,89885	0,052533
75	375	97601,5	-7,18605	0,067369	-6,09635	0,052533
76	379	97645,71	-4,65695	0,06748	-5,70185	0,073107
77	385	97712,02	-7,33385	0,067628	-5,70035	0,052533
78	389	97756,23	-7,63875	0,067428	-6,17985	0,052419
79	394	97811,49	-6,98065	0,067428	-5,98235	0,052419
80	399	97866,75	-7,75615	0,016557	-6,23275	0,090777
81	405	97933,06	-8,69725	0,067391	-6,36935	0,052533
82	409	97977,27	-9,05115	0,067391	-6,44485	0,052618
83	415	98043,58	-8,43825	0,017267	-5,78965	0,093816
84	421	98109,89	-9,24495	0,067391	-6,44085	0,052618
85	425	98154,1	-8,92685	0,06748	-6,25735	0,052618
86	430	98209,36	-8,31075	0,067428	-6,09185	0,052618
87	434	98253,57	-8,40765	0,067428	-6,21635	0,052533
88	439	98308,83	-8,25455	0,069474	-6,40485	0,052466
89	445	98375,14	-7,73835	0,01591	-6,05155	0,09087

90	450	98430,4	-7,81545	0,01591	-5,85545	0,090473
91	455	98485,66	-8,71155	0,016067	-6,23035	0,090446
92	460	98540,92	-8,37165	0,016067	-6,24125	0,090623
93	465	98596,18	-8,95975	0,016067	-6,46615	0,090473
94	470	98651,44	-8,47985	0,016283	-6,24705	0,090777
95	475	98706,7	-8,78995	0,017696	-6,30095	0,093303
96	480	98761,96	-8,35205	0,036581	-6,23985	0,090512
97	484	98806,17	-9,10835	0,01591	-6,47255	0,09283
98	490	98872,48	-8,50645	0,01591	-6,17045	0,090512
99	495	98927,74	-8,36755	0,016067	-6,35135	0,090473
100	500	98983	-6,01765	0,027077	-5,80125	0,093303
101	505	99038,26	-6,24075	0,037485	-5,58215	0,096605
102	509	99082,47	-7,27085	0,016067	-5,88805	0,090562
103	515	99148,78	-7,51595	0,016067	-5,84995	0,090473
104	520	99204,04	-7,47305	0,016067	-5,85985	0,090562
105	525	99259,3	-6,82415	0,016886	-5,80175	0,090623
106	530	99314,56	-5,91113	0,012619	-5,68755	0,078471
107	535	99369,82	-5,77863	0,012419	-5,28325	0,07849
108	540	99425,08	-5,91513	0,029652	-5,78995	0,081226
109	545	99480,34	-5,50063	0,012619	-5,57865	0,078522
110	550	99535,6	-7,34013	0,012619	-5,69135	0,078522
111	555	99590,86	-6,95163	0,012419	-5,46005	0,078693
112	560	99646,12	-6,16313	0,012619	-5,52075	0,078693
113	565	99701,38	-5,84863	0,012619	-5,15845	0,078693
114	570	99756,64	-6,83713	0,012619	-5,91055	0,078623
115	575	99811,9	-6,73763	0,012419	-5,56925	0,078522
116	580	99867,16	-7,60913	0,012419	-6,01295	0,07849
117	585	99922,42	-8,04863	0,012419	-6,18465	0,078566
118	596	100044	-4,32113	0,012419	-4,95035	0,078522
119	600	100088,2	-3,84163	0,012419	-4,63005	0,078522
120	605	100143,5	-4,75713	0,012619	-5,08375	0,078522
121	615	100254	-5,36663	0,012619	-5,44745	0,078522
122	620	100309,2	-6,88913	0,012419	-5,85855	0,078623
123	625	100364,5	-6,12263	0,012298	-5,39625	0,078566
124	630	100419,8	-6,56013	0,012619	-5,89195	0,078776
125	635	100475	-7,74363	0,012298	-6,14065	0,078566
126	640	100530,3	-7,80313	0,012419	-6,23335	0,078566
127	644	100574,5	-7,57963	0,012419	-5,95405	0,078522
128	649	100629,7	-7,07013	0,012893	-5,78575	0,078522
129	665	100806,6	-4,53763	0,012619	-4,70845	0,07849
130	670	100861,8	-4,23013	0,012619	-5,00555	0,078566
131	675	100917,1	-5,37263	0,015819	-5,05225	0,078522
132	680	100972,4	-5,44213	0,012619	-5,33695	0,07849
133	685	101027,6	-5,42763	0,012893	-5,53265	0,07849
134	690	101082,9	-6,00313	0,012419	-5,57235	0,078471

135	694	101127,1	-6,06363	0,012619	-5,66505	0,078522
136	699	101182,3	-6,15213	0,012619	-5,53875	0,078566
137	704	101237,6	-5,52463	0,012419	-5,57845	0,078566
138	710	101303,9	-5,96602	0,025898	-5,474	0,048776
139	715	101359,2	-4,95292	0,026729	-5,16061	0,07116
140	720	101414,4	-5,53162	0,026635	-5,13311	0,07116
141	725	101469,7	-6,80832	0,026729	-5,05061	0,071209
142	730	101525	-6,25502	0,026579	-4,86611	0,07116
143	734	101569,2	-6,57872	0,026729	-5,17961	0,071272
144	739	101624,4	-6,60042	0,026635	-5,31511	0,07135
145	745	101690,7	-6,91612	0,026635	-5,35361	0,07116
146	751	101757,1	-7,04182	0,02686	-5,33111	0,071125
147	755	101801,3	-6,46452	0,026635	-4,66061	0,071125
148	760	101856,5	-6,50062	0,026635	-4,69811	0,071272
149	765	101911,8	-5,87232	0,026729	-4,75061	0,071272
150	770	101967	-5,98002	0,026579	-4,31911	0,07116
151	775	102022,3	-6,75672	0,026729	-4,77761	0,071125
152	780	102077,6	-6,12942	0,026729	-5,00011	0,07116
153	785	102132,8	-5,93512	0,026729	-4,75261	0,071209
154	790	102188,1	-6,38282	0,026635	-4,85211	0,07116
155	795	102243,3	-5,38652	0,026729	-5,11761	0,071209
156	800	102298,6	-5,48122	0,026635	-4,91111	0,073101
157	805	102353,9	-6,49992	0,026729	-5,42261	0,07135
158	810	102409,1	-6,25802	0,026729	-5,45611	0,07116
159	815	102464,4	-6,66472	0,026729	-5,55861	0,07135
160	820	102519,6	-5,78642	0,02686	-5,49511	0,07116
161	825	102574,9	-5,94112	0,02686	-5,34461	0,071441
162	830	102630,2	-5,80682	0,02686	-5,40011	0,071125
163	835	102685,4	-4,88852	0,026635	-5,11561	0,071272
164	850	102851,2	-5,49722	0,027027	-5,44211	0,071272
165	853	102884,4	-5,63992	0,033859	-5,31461	0,074423
166	860	102961,7	-5,32662	0,027027	-5,42011	0,071209
167	865	103017	-5,64332	0,026635	-5,16061	0,071209
168	872	103094,3	-5,52342	0,026729	-5,12211	0,075038
169	876	103138,6	-5,93412	0,026729	-5,31661	0,07116
170	880	103182,8	-5,25082	0,026579	-5,24411	0,07116
171	885	103238	-6,34952	0,026579	-5,11861	0,071209
172	890	103293,3	-5,85222	0,02686	-5,15011	0,071209
173	895	103348,5	-5,65092	0,026729	-5,14361	0,071209
174	900	103403,8	-5,13762	0,026729	-4,84311	0,07116
175	905	103459,1	-4,86232	0,026729	-4,59961	0,082072
176	910	103514,3	-5,15502	0,026635	-4,91911	0,071125
177	915	103569,6	-6,02972	0,026579	-5,01561	0,075702
178	920	103624,8	-6,65022	0,026205	-4,962	0,048663
179	925	103680,1	-6,78442	0,025898	-4,848	0,048571

180	930	103735,4	-7,68962	0,026033	-5,042	0,049235
181	935	103790,6	-7,07282	0,025898	-4,903	0,048909
182	940	103845,9	-7,08402	0,025898	-5,242	0,049235
183	945	103901,1	-6,68622	0,027252	-5,28	0,051304
184	950	103956,4	-6,72542	0,026033	-5,2	0,048909
185	955	104011,7	-6,73062	0,025898	-5,488	0,048663
186	961	104078	-6,70882	0,026033	-5,402	0,049062
187	966	104133,2	-6,63042	0,025898	-5,147	0,048663
188	971	104188,5	-7,40462	0,025898	-5,081	0,049428
189	976	104243,8	-6,85382	0,026205	-5,07	0,049062
190	980	104288	-6,54302	0,026033	-4,923	0,049235
191	985	104343,2	-8,48322	0,025898	-5,022	0,048776
192	990	104398,5	-8,27042	0,026205	-4,895	0,049235
193	995	104453,7	-7,11962	0,025898	-4,875	0,049062
194	1000	104509	-8,60082	0,026033	-5,243	0,049062
195	1005	104564,3	-8,28402	0,026033	-5,449	0,048909
196	1010	104619,5	-8,63162	0,026033	-5,466	0,049235
197	1015	104674,8	-7,69082	0,026205	-5,375	0,049062

7.3 TRACE ELEMENT MEASUREMENTS

Sample	Sr [ppm]	Ba [ppm]	Mg [ppm]	U [ppm]	Zn [ppm]	Pb [ppm]	Y [ppm]	Ca [ppm]
7	97,19	46,79	4951,88	0,04	2,06	0,05	0,01	888475,54
9	23,47	23,14		0,06		0,13	0,00	529999,24
11	85,66	43,13	5138,05	0,04	1,46	0,13	0,00	1010598,12
13	67,63	32,19	2875,86	0,04	2,15	0,56	0,01	838270,01
15	23,30	23,64		0,06		0,18	0,00	516265,56
17	80,53	39,67	4635,29	0,05	11,08	0,16	0,01	862132,71
19	83,55	41,02	4385,01	0,05	5,92	0,24	0,00	943255,29
21	69,00	35,10	3059,70	0,05	0,84	0,16	0,01	899271,00
23	72,30	34,44	3716,67	0,05	1,29	0,06	0,00	791849,61
25	73,48	35,48	3944,65	0,05	2,03	0,12	0,00	966541,08
27	70,30	33,42	3002,77	0,05	0,28	0,08	0,00	869941,79
29	77,28	36,60	3075,07	0,05	0,73	0,06	0,00	781863,67
31	71,49	37,13	2837,73	0,06	5,15	0,22	0,00	913476,48
35	65,91	31,55	3358,75	0,05	4,17	0,28	0,00	855971,28
37	57,18	28,57	2563,32	0,04	4,36	0,09	0,00	711342,49
39	72,73	37,59	4329,91	0,05	5,15	0,37	0,00	998856,89
41	20,50	21,61		0,07		0,51	0,01	513016,72
43	20,22	21,35		0,07		0,63	0,00	514474,21
45	72,52	38,44	2322,69	0,05	1,02	1,11	0,05	787638,52
49	75,63	40,75	2709,58	0,06	2,61	0,75	0,04	926603,21
51	80,88	43,52	2613,22	0,06	1,90	0,73	0,04	821745,24
53	73,93	35,69	2579,47	0,06		0,66	0,04	843331,91

57	71,16	34,53	3661,34	0,05	1,21	0,13	0,00	896765,88
59	45,15	20,02	1583,69	0,02		0,05		443379,52
61	84,49	39,59	5227,06	0,04	1,28	0,17	0,00	922521,00
63	94,29	47,25	4414,01	0,05	1,57	0,16	0,00	906863,49
65	68,03	30,56	4094,17	0,05	2,99	0,11	0,00	902767,72
67	44,70	21,73	1906,56	0,07	0,31	0,32	0,00	488593,20
73	60,18	27,09	3896,72	0,04	0,76	0,23	0,00	908867,96
75	19,84	18,67		0,06		0,25	0,00	512444,51
77	64,99	30,61	3743,19	0,07	11,45	0,13	0,00	1002621,67
79	72,00	33,14	3792,03	0,04	2,52	0,11	0,00	949996,69
81	55,45	26,04	2754,15	0,05		0,09	0,00	818909,11
83	57,07	26,61	3034,13	0,05	1,00	0,13	0,01	888488,82
85	61,07	30,01	2722,50	0,05	1,46	0,17	0,01	846114,85
85	61,69	30,88	3026,53	0,06	1,23	0,19	0,01	954789,01
87	58,43	27,28	3198,53	0,05	0,71	0,12	0,00	881881,18
89	61,26	28,33	3546,42	0,05	0,96	0,11	0,00	911219,25
91	82,72	40,08	3418,72	0,06	0,46	0,11	0,00	1088620,80
93	68,05	33,25	2407,19	0,05	5,44	0,19	0,02	799962,25
95	73,21	34,38	2984,31	0,05	3,10	0,22	0,01	893909,47
97	63,51	43,10	5268,42	0,06	6,55	0,49	0,02	909156,79
99	64,71	31,73	3452,27	0,06	1,03	0,12	0,00	1006821,55
101	36,98	18,39	2034,51	0,05	0,59	0,08		497261,13
103	75,05	37,86	3533,99	0,05	1,75	0,08	0,00	918009,66
107	43,66	23,41	2171,99	0,06	0,93	0,16	0,00	492491,78
113	77,72	37,41	4496,25	0,05	1,37	0,15		929794,46
115	62,85	28,58	4431,42	0,04	1,76	0,11	0,00	1014342,40
117	60,56	27,86	3301,26	0,04	5,21	0,15	0,00	886366,44
119	115,50	67,54	5523,95	0,06	8,28	0,38	0,02	918552,15
121	61,97	31,20	2566,76	0,07	2,62	0,11		497735,13
123	89,47	44,25	3885,23	0,05	1,20	0,08	0,00	870828,65
124	21,11	20,79		0,05		0,22	0,00	512736,89
125	70,24	32,75	4114,38	0,05	2,37	0,38	0,01	1035513,88
129	111,36	72,57	6210,05	0,07	2,34	0,10	0,01	1023244,82
131	95,82	59,16	4935,01	0,07	2,07	0,19	0,00	958379,17
135	69,87	41,81	3801,07	0,05	8,45	0,19	0,00	1008602,92
137	58,74	34,93	3776,14	0,04	0,64	0,22	0,00	1029602,75
139	85,26	54,08	4114,85	0,05	4,77	0,04	0,00	876080,40
140	83,50	52,78	4180,14	0,06	1,73	0,07		997484,65
141	84,48	49,20	3566,71	0,07	1,16	0,05	0,00	932119,65
142	79,14	48,29	4054,40	0,07	0,53	0,13	0,00	1016228,25
143	85,16	49,65	3777,52	0,07	0,65	0,28	0,00	970257,65
145	89,12	50,75	3490,13	0,07	1,91	0,13	0,00	933056,83
146	89,20	51,12	3488,29	0,07	7,12	0,20	0,00	994745,90
147	95,23	55,19	3845,66	0,08	3,08	0,11	0,02	974398,64
148	103,05	60,58	3864,02	0,08	5,38	0,60	0,00	986022,74

149	101,02	59,96	3787,25	0,07	0,95	0,08	0,00	852368,17
152	91,05	59,19	3907,93	0,07	3,75	0,10	0,00	962973,28
153	99,15	62,35	4328,66	0,08	7,22	0,41	0,00	1023614,23
154	78,23	50,53	3988,47	0,06	0,67	0,13	0,00	1003928,29
155	100,91	68,45	4627,82	0,07		0,19	0,01	964301,93
157	49,08	28,30	2060,68	0,09	1,86	0,22		496009,53
160	78,65	47,94	3968,20	0,06	1,47	0,09	0,00	999030,13
161	75,58	44,12	3464,94	0,05	0,51	0,04	0,00	845605,36
163	121,47	86,84	5136,16	0,07	0,65	0,08	0,00	992296,83
165	80,44	50,70	4341,93	0,06	1,26	0,06	0,01	1012733,38
168	93,39	53,58	5125,56	0,06	1,77	0,19	0,01	986366,81
169	90,49	50,40	4935,88	0,06	2,20	0,10	0,00	1010682,93
171	93,47	58,48	4143,37	0,07	0,54	0,07	0,00	831745,96
175	98,92	56,99	4367,48	0,06	0,35	0,07	0,00	880070,28
176	114,37	74,99	5366,91	0,07	1,39	0,14	0,00	983976,19
177	102,36	64,06	4455,62	0,08	2,27	0,21	0,00	973782,71
179	93,34	54,58	3824,27	0,08		0,22	0,01	951248,59
181	79,01	44,55	3958,99	0,08	1,82	0,17	0,00	926826,79
183	54,44	30,26	2267,13	0,10	3,75	0,38	0,00	498155,90
185	47,36	24,76	1842,92	0,07	0,74	0,28	0,00	508551,51
186	77,02	39,75	3633,26	0,05	2,00	0,17	0,00	1016095,07
187	75,80	40,00	3073,10	0,05	1,67	0,14	0,01	902849,34
189	76,89	41,45	3710,34	0,07	2,58	0,13	0,00	977490,35
191	80,01	46,79	3229,08	0,09	1,72	0,18	0,01	978357,64
193	83,90	51,76	3185,04	0,08	2,35	0,14	0,00	966666,34
195	87,66	51,06	2469,46	0,08	2,04	0,47	0,02	874421,98
197	97,64	56,88	2529,91	0,07	1,05	0,18	0,00	936803,66

AFDELING GEOLOGIE
Celestijnenlaan 200E bus 2408
3000 LEUVEN, BELGIË
tel. + 32 16 32 64 60
fax + 32 16 32 29 80
www.kuleuven.be